Technische Universität München
TUM School of Medicine and Health

# Cancer-derived Prostaglandin E2 impairs local effector differentiation through attenuation of IL-2 responsiveness in tumor-infiltrating stem-like TCF1$^{+}$CD8$^{+}$ T cells

Sebastian Benjamin Lacher

Vollständiger Abdruck der von der TUM School of Medicine and Health der Technischen Universität München zur Erlangung eines

Doctor of Philosophy (Ph.D.)

genehmigten Dissertation.

Vorsitz: Prof. Dr. Maximilian Reichert

Betreuer: TUM Junior Fellow Dr. Jan Böttcher

Prüfende der Dissertation:

1. Prof. Dr. Percy Knolle
2. Prof. Dr. Dietmar Zehn
3. Prof. Dr. Anne Krug

Die Dissertation wurde am 13.02.2024 bei der TUM School of Medicine and Health der Technischen Universität München eingereicht und durch die TUM School of Medicine and Health am 18.07.2024 angenommen.

## Acknowledgments

My special thanks go to Dr. Jan Böttcher for his exceptional guidance and support during my time as a Ph.D. student. I appreciate all the inspiring and constructive ideas he provided to advance the progress of this project. Moreover, I am deeply thankful for his open-door policy, willingness to make time whenever needed, and commitment to fostering a collaborative and enriching research environment. Additionally, I would like to express my gratitude to Prof. Dr. Percy Knolle and Prof. Dr. Dietmar Zehn, my mentors, whose valuable discussions, expertise, and ideas contributed to this work.

I am very grateful for the entire Institute of Molecular Immunology, where I experienced abundant support and encouragement in the laboratory and during coffee breaks. Working within AG Böttcher has been an immense privilege. The teamwork, support, and guidance from every lab member have made a lasting impression, and I am sincerely thankful for the valuable contributions of each team member. I am grateful for the true friendships that I have developed with every lab mate. Special thanks are extended to Hannah Wintersteller and Jennifer Hsiao for their invaluable contribution in proofreading this thesis.

Special thanks go to my family for supporting me throughout my academic journey. They have consistently provided encouragement and offered renewed strength every day. They always listened and supported me through challenging times. Sylvia, Klaus, Sabrina, and Anna thank you for being my family; I would not have come this far without you.

I extend heartfelt gratitude to Tobias, who became a family member and stood by me every single day since then. Even in challenging times, he offered uplifting words, cheering sports activities, and a good laugh whenever I needed it.

Finally, I would like to express my special gratitude to my mother Sylvia. She has been there for me all my life, supported me, and given me courage and comfort. I could always rely on her and be sure that she would be by my side. Mom, I will never forget you. You will stay in my memories.

# Table of contents

## Zusammenfassung

$CD8^+$ T-Zellen spielen eine entscheidende Rolle in der Immunantwort gegen Krebs, indem sie nach Aktivierung durch antigen-präsentierende Immunzellen im Lymphknoten als stammzellähnliche $TCF1^+CD8^+$ T-Zellen in den Tumor wandern. Dort können sie sich in cytotoxische Effektor-$CD8^+$ T-Zellen differenzieren und expandieren, die direkt an der Eliminierung von Tumorzellen beteiligt sind. Doch die genaue Regulation der Differenzierung und Expansion von stammzellähnlichen $TCF1^+CD8^+$ T-Zellen sowie die Faktoren, die diese Schritte beeinflussen, sind bislang noch nicht vollständig verstanden und benötigen weitere umfassende Forschung.

Viele humane und murine Tumore produzieren das bioaktive Lipid Prostaglandin E2 ($PGE_2$). $PGE_2$ besitzt eine immunsuppressive Wirkung auf verschiedene Immunzellen, was es zu einem potenziell bedeutsamen Faktor für die Regulation von T-Zellantworten innerhalb des Tumormilieus macht.

In dieser Arbeit wurde die Auswirkung von tumorsekretiertem $PGE_2$ auf die anti-tumorale Immunantwort durch stammzellähnliche $TCF1^+CD8^+$ T-Zellen untersucht. Dabei wurde festgestellt, dass $PGE_2$ in Tumoren zu einer Verringerung von intratumoralen $CD8^+$ T-Zellen führte, was wiederum das Tumorwachstum begünstigte. Ein T-Zell-spezifischer Knockout der beiden $PGE_2$-Rezeptoren (EP), EP2 und EP4, zeigte, dass es direkt auf $CD8^+$ T-Zellen wirkte und ihre lokale Expansion hemmte. Einzelzell-RNA- und Einzelzell-T-Zellrezeptor-Sequenzierung von tumorinfiltrierenden $CD8^+$ T-Zellen enthüllte, dass $PGE_2$ die Differenzierung und die darauffolgende klonale Expansion von stammzellähnlichen $TCF1^+CD8^+$ T-Zellen direkt im Tumor behinderte. $PGE_2$ verringerte die Sensitivität gegenüber IL-2 und unterdrückte nachfolgend den mTORC1 Signalweg in $CD8^+$ T Zellen, was mit einem gezielten Knockout von EP2 und EP4 gerettet werden konnte.

Diese Ergebnisse zeigen einen bisher unbekannten Kontrollpunkt in der Immunantwort gegen Krebs auf, der überwunden werden muss, um wirksame $CD8^+$ T-Zellantworten im Tumor zu generieren. Dieser neu entdeckte Kontrollpunkt in der anti-Krebs-Immunantwort stellt einen vielversprechenden Ansatzpunkt für zukünftige T-Zell-gerichtete Therapien dar.

## Abstract

$CD8^+$ T cells play a crucial role in the immune response against cancer by migrating into the tumor as stem-like $TCF1^+CD8^+$ T cells after activation by antigen-presenting immune cells in lymph nodes. At the tumor, they can differentiate and expand into cytotoxic effector $CD8^+$ T cells capable of directly eliminating tumor cells. However, the precise regulation of the differentiation and expansion of stem-like $TCF1^+CD8^+$ T cells, as well as the factors influencing these steps, are not yet fully understood and require further comprehensive research.

Many human and murine tumors secrete the bioactive lipid Prostaglandin E2 ($PGE_2$), which mediates an immunosuppressive effect on various immune cells. This makes $PGE_2$ a potentially significant factor in the regulation of T cell responses within the tumor.

In this study, the impact of tumor-derived $PGE_2$ on the antitumoral immune response mediated by stem-like $TCF1^+CD8^+$ T cells was investigated. It was observed that $PGE_2$ in tumors led to a reduction in intratumoral $CD8^+$ T cell numbers, subsequently promoting tumor growth. A T cell-specific knockout of the two $PGE_2$ receptors (EP), EP2 and EP4, revealed that $PGE_2$ directly affected $CD8^+$ T cells and inhibited their local expansion. Single-cell RNA and single-cell T cell receptor sequencing of tumor-infiltrating $CD8^+$ T cells revealed that $PGE_2$ hindered the differentiation and subsequent clonal expansion of stem-like $TCF1^+CD8^+$ T cells directly within the tumor. $PGE_2$ reduced sensitivity to IL-2 and subsequently suppressed the mTORC1 signaling pathway in $CD8^+$ T cells, a response that could be rescued with a targeted knockout of EP2 and EP4.

These findings reveal a previously unidentified checkpoint in the anti-cancer immune response that must be overcome to generate effective $CD8^+$ T cell responses within the tumor. This newly discovered checkpoint holds promise as a target for future T cell-targeted therapies.

# 1 Introduction

## 1.1 The immune system

The immune system is outstanding in safeguarding the body against a range of threats, including pathogens, parasites, allergenic or toxic proteins, and abnormal cells with the potential to develop into cancer. It comprises two main components: Innate immunity and adaptive immunity[1].

The innate immune system acts as the body's primary barrier against invading pathogens, employing physical barriers like the skin and mucous membranes to prevent pathogen entry. Moreover, chemical barriers such as the skin pH, stomach acid, defensins, and the complement system contribute further to the body's defense mechanisms[2,3]. The cellular compartment of the innate immune system, including phagocytic cells like neutrophils, monocytes, macrophages, and dendritic cells (DCs), is crucial for eliminating pathogens through phagocytosis. DCs also serve as essential mediators between the innate and adaptive immune systems by presenting antigens to lymphocytes via their major histocompatibility complexes (MHCs)[1]. Another cell type that plays a pivotal role in the early cell-mediated immune responses is natural (NK) killer cells, which recognize and eliminate both virus-infected and cancerous cells[4].

In contrast to innate immunity, the adaptive immune system consists of B and T lymphocytes, which recognize a vast range of antigens using their B cell receptors (BCRs) and T cell receptors (TCRs) on their cell surface, respectively[3]. B cells play a crucial role by generating antibodies that bind to antigens, thereby neutralizing pathogens and contributing to humoral immunity[1,3]. T lymphocytes, on the other hand, are further categorized into $CD4^+$ and $CD8^+$ T cells. $CD4^+$ T cells regulate and coordinate immune responses, while $CD8^+$ T cells are specialized in eliminating infected and abnormal cells[1,5]. Upon encountering their specific antigen with their BCRs and TCRs, B and T cells initiate rapid divisions, resulting in the generation of a substantial population of identical clones. This phenomenon, known as clonal expansion, is accompanied by the formation of a specialized subset of long-lived memory cells. These memory cells persist in the body, facilitating a

quicker and more potent immune response upon subsequent encounters with the same pathogen[1].

In general, the innate immune system recognizes common structures, such as lipopolysaccharides, double-stranded RNA, and peptidoglycans, that are shared among numerous infectious agents[1,6]. In contrast, the adaptive immune system provides specific, targeted responses against pathogens by using their specific BCRs and TCRs. While the innate immune response is activated immediately, the adaptive immune response typically takes several days as lymphocytes undergo clonal expansion and differentiation.

### 1.1.1 The development of T lymphocytes

T cells originate in the bone marrow and then travel through the bloodstream to reach the thymus, where they undergo various selection procedures[7,8]. In the thymic cortex, all T cells undergo positive selection, transitioning from a double negative ($CD4^-CD8^-$) to a double positive ($CD4^+CD8^+$) state characterized by the expression of the coreceptors, CD4 and CD8, on their surface[1,8]. Concurrently, the mature $\alpha\beta$-TCR is generated via somatic V(D)J recombination. To ensure that T cells recognize antigens presented on MHCs, cortical thymic epithelial cells (cTECs) present self-antigens on MHC class I and II molecules to T cells. T cells that recognize peptide-loaded MHC I or MHC II molecules receive survival signals and downregulate CD4 or CD8, respectively[8]. Conversely, T cells that do not strongly recognize MHC molecules undergo apoptosis, which is termed as 'death by neglect'. Following positive selection in the cortex, T cells migrate to the thymus medulla, where they encounter medullary thymic epithelial cells (mTECs). mTECs present a diverse repertoire of self-antigens from various parts of the body on their MHC I molecules, facilitated by the autoimmune regulator (AIRE) transcription factor[1]. Thymic dendritic cells phagocytose mTECs, leading to the presentation of self-antigens on MHC II molecules. T cells that interact too strongly with self-peptide complexes on either MHC I or II receive apoptotic signals, resulting in the release of only mature naive T cells from the thymus into the bloodstream[1,7,8].

### 1.1.2 CD8+ T cell priming and activation

CD8+ T cells are key players in immune surveillance, directly eliminating cancerous cells or cells displaying foreign antigens. During the initiation of antigen-specific CD8+ T cell responses, naive CD8+ T cells are activated within secondary lymphoid organs such as the spleen or draining lymph nodes, a process called T cell 'priming' that is mediated by antigen-presenting cells (APCs)[1]. One key APC population is DCs, which participate in immune surveillance as immature DCs in peripheral tissues like the skin or mucosal surfaces[9]. Acting as sentinels, DCs survey the periphery to take up pathogens and antigens from the surroundings. Upon antigen capture and activation, they can migrate to the nearest secondary lymphoid organ, presenting antigen fragments on their MHC I and II molecules to prime naive CD8+ and CD4+ T cells, respectively[10,11].

Notably, effective activation of naive T cells requires additional signals beyond antigen-presentation. This may encompass costimulatory molecules like CD80 and CD86 from the B7 family, which are present on activated APCs and can activate the costimulatory molecule CD28 on T cells[5]. Other costimulatory signals include molecules such as CD40L, OX40, 4-1BB, inducible T cell costimulator (ICOS), and CD27. These molecules can contribute to T cell priming or later activation and differentiation stages of CD8+ T cells[12]. Following T cell activation, inhibitory receptors such as programmed cell death protein 1 (PD-1), T cell immunoglobulin and mucin domain-containing protein 3 (TIM-3), lymphocyte-activation gene 3 (LAG-3), 2B4, and T cell immunoreceptor with immunoglobulin and ITIM domain (TIGIT) can be upregulated in CD8+ T cells, mediating a dampening effect on their activation status[1,12]. Whether a CD8+ T cell is in an active or inactive state depends on the interplay between positive (costimulatory) and negative (coinhibitory) signals within the costimulatory pathway.

In addition, soluble mediators, in particular cytokines, can modulate the activation and differentiation of CD8+ T cells[1]. For instance, cytokines such as interleukin 2 (IL-2), IL-7, IL-9, IL-15, and IL-21 can serve as promoters of growth and survival. Conversely, transforming growth factor beta (TGF-β) and IL-10 are

recognized for their inhibitory role in the function and proliferation of $CD8^+$ T cells[13,14].

Recent advances in cancer immunology research have now uncovered an additional signal that complements the traditional 3 signals regulating T cell activation. It has been proposed that factors such as nutrients, metabolites, oxygen levels, and environmental signals, including tumor-derived factors, may contribute to shaping T cell responses within the tumor microenvironment (TME)[15,16]. In this context, both tumor-infiltrating cells and the tumor cells themselves can modify the local nutritional environment[14]. These alterations can metabolically inhibit T cell functions and may contribute to increased T cell exhaustion[17,18]. Under normal circumstances, T cells adjust their nutrient consumption and metabolism during differentiation to fulfill their energy requirements[14,18]. As a result, these adjustments are accompanied by changes in gene expression through epigenetic and post-translational protein adaptations, resulting in a modified status of T cell activation[18]. This underscores the notion that additional factors and conditions within the TME also play a significant role in determining the fate of T cells.

### 1.1.3 Effector $CD8^+$ T cell functions

$CD8^+$ T cell-mediated cytotoxicity is a highly antigen-specific process that begins with the binding of the TCR to the cognate MHC I complex on the target cell. This initial interaction triggers the formation of the immunological synapse, characterized by the accumulation of supramolecular activation complex (SMAC) proteins at the interface between the $CD8^+$ T cell and the APC. SMAC acts like a 'sealing ring', ensuring that cytolytic molecules are directed specifically toward the target cell and not the surrounding vicinity[19].

After the establishment of the immunological synapse, the $CD8^+$ T cell releases intracellular granules that contain 3 calcium-dependent cytotoxic components: Perforin, granzymes, and granulysin. Subsequently, perforin integrates into the target cell membrane. This integration facilitates the formation of pores, enabling the entry of cytotoxic granules[1]. Granzymes play a crucial role in initiating diverse pathways involved in cytotoxicity. For instance, granzyme A

and K can induce pore formation and trigger the release of inflammatory cytokines[20]. Granzyme F and C can cause ruptures in the cellular membrane, leading to cell death, while granzyme M disrupts microtubule structures, resulting in morphological changes in the target cell. In contrast, granzyme B (GzmB) can induce apoptosis by activating the caspase-mediated apoptotic pathway[20]. Moreover, in human cytotoxic $CD8^+$ T cells, granulysin, which is absent in mice, exhibits cytolytic activity against target cells and acts as a chemoattractant for T cells, monocytes, and NK cells. Furthermore, granulysin possesses pro-inflammatory properties, leading to the expression of cytokines in certain tumor cell lines and monocytes[21].

In addition to the release of cytotoxic granules, $CD8^+$ T cells play a role in eliminating infected or cancerous cells by expressing Fas ligand (FasL). FasL is a member of the tumor necrosis factor (TNF) family and is expressed on the surface of activated NK and cytotoxic $CD8^+$ T cells. Through binding to Fas on the target cell surface, FasL initiates a signaling cascade that triggers apoptosis. The interaction between FasL and Fas results in the formation of a receptor trimer. The death domains (DDs) within Fas, play a pivotal role in mediating the apoptotic signal within the target cell by recruiting procaspases, which then can activate apoptosis-initiating caspases such as caspase 3, 6, and 7, resulting in mitochondrial damage and ultimately in cell death[22].

Besides being directly involved in cytotoxicity, $CD8^+$ T cells also mediate immunoregulatory functions by secreting cytokines and chemokines. The most important cytokines released by $CD8^+$ T cells are Interferon-gamma (IFN$\gamma$), TNF-alpha (TNF$\alpha$), and IL-2[23].

IFN$\gamma$ plays a critical role in diverse functions of the immune system. On the one hand, it promotes the activation and differentiation of various immune cells, including macrophages, DCs, and T and B cells, thereby enhancing both adaptive and innate immune responses[1]. On the other hand, IFN$\gamma$ can enhance the expression of MHC I on virus-infected or cancer cells while also increasing the expression of MHC II molecules on DCs and macrophages, facilitating proficient antigen presentation to $CD8^+$ and $CD4^+$ T cells[24,25].

In contrast to IFNγ, TNFα is initially secreted as a membrane-bound cytokine that can undergo cleavage into its soluble form by TNFα-converting enzymes (TACEs)[1]. Soluble TNFα exhibits a high binding affinity to TNF receptor 1 (TNFR1), which is involved in pro-inflammatory and apoptotic pathways and is expressed in almost every cell[26,27]. Conversely, TNFR2 signaling, associated with anti-inflammatory responses, cell proliferation, and tissue regeneration, is primarily activated by the interaction with membrane-bound TNFα, only prevalent in specific immune cell subpopulations[1,28,29].

In addition to IFNγ and TNFα, activated $CD8^+$ T cells secrete IL-2, which is one of the most important cytokines for T cell development, differentiation, survival, and function (section 1.1.4). Finally, once $CD8^+$ T cells are activated, they can release β-chemokines, specifically C-C motif chemokine ligand 3 (CCL3), CCL4, and CCL5. These chemokines selectively bind to their corresponding receptors, C-C motif chemokine receptor 3 (CCR3), CCR4, and CCR5, facilitating the recruitment of additional immune cells into inflamed tissues[30].

### 1.1.4 The role of IL-2 in $CD8^+$ T cell activation and differentiation

The glycoprotein IL-2 is known to be a pleiotropic regulator in T cells[1,31]. On the one hand, it is known as a T cell growth factor and is thus involved in T cell proliferation, differentiation, and function. On the other hand, it can trigger activation-induced cell death (AICD) in T cells[31]. The main producers of IL-2 are activated $CD4^+$ and $CD8^+$ T cells, although its presence is also noted in DCs, NK, and natural killer T (NKT) cells[32]. The activation of the TCR initiates the transcription of IL-2 messenger ribonucleic acid (mRNA), while costimulatory signals, such as CD28, contribute to mRNA stabilization, resulting in rapid IL-2 production and secretion[33,34]. Signaling of IL-2 in T cells can trigger a self-regulating feedback loop involving the activation of signal transducer and activator of transcription 5 (Stat5) and the induction of the transcriptional repressor B lymphocyte maturation protein-1 (BLIMP-1). This cascade ultimately leads to the suppression of IL-2 production[35,36].

The high-affinity IL-2 receptor (IL-2R) forms a trimer consisting of three distinct subunits: IL-2Rα (CD25), IL-2Rβ (CD122), and IL-2Rγc (common gamma chain, CD132), crucial for potent IL-2 signaling. Importantly, IL-2Rγc not only associates with IL-2 but also binds to various other cytokines, including IL-4, IL-7, IL-9, IL-15, and IL-21, classifying it as the common cytokine receptor γ-chain (γc)[37]. Initially, IL-2 engages with IL-2Rα, facilitating subsequent association with IL-2Rβ and IL-2Rγc. This interaction triggers the phosphorylation of tyrosine residues on the cytoplasmic tail of IL-2Rβ and IL-2Rγc in T cells via the activation of Janus kinases (JAKs)[37]. Subsequently, the adapter proteins such as STAT3, STAT5, and SH2 domain-containing transforming protein (Shc) become phosphorylated and activated[38,39]. Shc association with the IL-2R can trigger the activation of the mitogen-activated protein kinase (MAPK), extracellular signal-regulator kinase (ERK), and phospho-inositide 3-kinase (PI3K) pathways, essential for cell growth and survival. In contrast to that, the activation of the STAT proteins results in their dimerization and translocation into the nucleus, where they activate genes responsible for regulating $CD8^+$ T cell effector function, proliferation, and differentiation[32,40–42].

Over the past few years, numerous studies have underscored the significant role of IL-2 signaling in the development of effector $CD8^+$ T cells during chronic infection and in cancer[42,43]. IL-2 can induce alterations in intratumoral $CD8^+$ T cell gene expression profiles, leading to increased cytotoxicity, adhesion molecules, interferon response genes, pro-inflammatory proteins, and receptors for pro-inflammatory cytokines and chemokines[42].

Numerous studies have shown that the differentiation of antigen-specific effector $CD8^+$ T cells can be amplified through the combination therapy of anti-PD-1 and IL-2, observed in contexts of both cancers and chronic infections[37,43–45]. Interestingly, reports indicate that this impact is primarily associated with IL-2 rather than anti-PD-1[42,43,45].

## 1.2 Tumor immune escape

### 1.2.1 Immunoediting and tumor intrinsic escape mechanisms

In the context of developing tumor immune escape mechanisms, immune editing emerges as a critical concept, elucidating the complex interplay between the immune system and cancer cells. Immune editing consists of 3 major phases: Elimination, equilibrium, and escape.

The elimination phase is closely linked to immune surveillance, creating an anti-tumor environment with the involvement of various immune cells like NKs, DCs, macrophages, T and B cells[46]. Growing tumors release inflammatory cytokines, attracting immune cells and activating cytotoxic events that eliminate most tumor cells[47]. NK cells and macrophages produce IFNγ and interleukins, initiating proapoptotic, angiostatic, and antiproliferative processes. These events result in the release of tumor antigens captured by DCs, which migrate to draining lymph nodes to activate naive T cells. Tumor-specific $CD4^+$ and $CD8^+$ T cells then migrate to the tumor site, where they contribute to the elimination of tumor cells[47,48].

However, a small amount of cancer cells can survive the elimination process and enter the equilibrium phase with the immune system. In this phase, there is a dynamic balance between the survival of tumor cells and the immune defense system of the host[48]. Lymphocytes and IFNγ exert strong selection pressure on tumor cells, containing but not completely eradicating them. This phase may last many years in humans, allowing for Darwinian selection[46]. During this time, new tumor cell variants with diverse mutations emerge, enhancing resistance to immune attacks and resulting in a tumor population with diminished immunogenicity[46,47]. The genetic instability—particularly, chromosomal instability (CIN)—of cancer cells surviving elimination contributes to the development of tumor variants with reduced immunogenicity[49].

In the escape phase, tumor cell variants, which survived the equilibrium phase, can now grow in an immune-intact environment, escaping the host's immune defenses. This evasion likely arises from genetic and epigenetic changes that provide resistance to immune detection, enabling tumors to grow and become clinically noticeable[46]. Therefore, tumors must overcome both the adaptive and

innate components of the immune system to achieve progressive growth, employing various immunoevasive strategies, including the production of immunosuppressive cytokines like IL-10, factors such as Prostaglandin E2 ($PGE_2$), and mechanisms involving regulatory T cells ($T_{regs}$)[46,47,50,51]. Escape from immune surveillance by tumors can also stem from alterations occurring within the tumor itself, influencing recognition by immune cells or providing mechanisms for immune evasion. Dysregulation of MHC class I processing and presentation, as well as the development of IFNγ insensitivity, are additional mechanisms that allow tumors to escape from events in the elimination phase[46,48].

In summary, tumor cells have developed a variety of mechanisms, such as immunosuppressive cytokine production, dysregulation of immune recognition, and the secretion of immunosuppressive factors like $PGE_2$ to evade the host immune system and achieve progressive growth despite immunological surveillance.

### 1.2.2 Tumor-derived Prostaglandin E2 mediates tumor progression and immune suppression

$PGE_2$ is a member of the prostanoid family derived from the polyunsaturated fatty acid arachidonic acid and plays a critical role in regulating various physiological processes, including fever, kidney function, pain perception, blood vessel homeostasis, and inflammation[52]. However, over the past few decades, $PGE_2$ has emerged as a potent contributor to cancer progression[53,54]. For example, $PGE_2$ secretion within the TME contributes to tumor outgrowth by enhancing cancer cell survival, proliferation, migration, invasion, and angiogenesis[55]. Increased levels of $PGE_2$ have been identified in the TME across different human malignancies, such as breast, lung, head and neck, colorectal, and pancreatic cancer, and are linked to unfavorable prognostic outcomes[55–58]. In recent studies, the genetic knockout of the key $PGE_2$-producing enzymes, Cyclooxygenase 1 and 2 (COX-1/2), in several mouse cancer models has been found to impede cancer progression. This deficiency in $PGE_2$ production not only hinders tumor advancement but also

facilitates immune-mediated tumor control[59,60]. Over the past few years, research has not only underscored the favorable impact of $PGE_2$ signaling on tumor cells but has also elucidated the direct suppressive effects of $PGE_2$ on immune cells, which will be further examined in section 1.2.5[59–62].

### 1.2.3 Synthesis of Prostaglandin E2 in cancer cells

$PGE_2$ is produced by the oxidation of fatty acids localized within the cell membrane. Here, arachidonic acid is released by phospholipase A2 and further oxidized and reduced to prostaglandin H2 ($PGH_2$) by COX-1 (encoded by *Ptgs1*) and COX-2 (encoded by *Ptgs2*)[52]. While COX-1 is constitutively expressed in most cells and plays a role in maintaining cellular homeostasis, COX-2 is absent in most cells but can be triggered by diverse stimulants such as growth factors and cytokines[63]. Following this, $PGH_2$ undergoes further transformation into $PGE_2$ through the activity of 3 prostaglandin E synthases, with their regulation and expression being specific to tissues[64]. Within cells, the metabolic turnover of $PGE_2$ is processed through the activation of 15-hydroxyprostaglandin dehydrogenase (15-PGDH) and 15-ketoprostaglandin-13-reductase, resulting in a biologically inactive form of $PGE_2$. Notably, while 15-PGDH exhibits high expression in normal tissues, it is often absent in numerous human cancers, leading to increased concentrations (conc.) of $PGE_2$[58]. Additionally, aberrant overexpression of COX-1/COX-2 has been noted in the pathways of various human tumors, including pancreatic, lung, stomach, breast, and colorectal cancers[65,66].

### 1.2.4 Prostaglandin E2 signaling

Once $PGE_2$ is produced by tumor cells, it is secreted and exerts its influence either in an autocrine manner on the tumor cells directly or in a paracrine manner on surrounding peripheral immune cells. $PGE_2$ specifically binds to 4 isoforms of G-protein coupled receptors (GPCRs) known as EP1 (encoded by *Ptger1*) to EP4 (encoded by *Ptger4*)[63]. These receptors display varying affinities for $PGE_2$, with EP1 and EP2 (encoded by *Ptger2*) receptors exhibiting low affinity, while EP3 (encoded by *Ptger3*) and EP4 receptors demonstrate high

affinity. This variability leads to diverse receptor activation patterns, allowing $PGE_2$ to exert a broad range of effects on various cells across tissues and diseases[67]. The dynamics of $PGE_2$ and its receptor interactions are thought to rely on factors such as tissue and cell type, location, the expression of EP receptors, and variations in binding affinities[68].

For example, EP1 engagement initiates the activation of the GPCR-coupled $G\alpha q$ subunit, triggering the activation of phosphoinositide-phospholipase C. Consequently, this process elevates intracellular calcium and activates protein kinase C (PKC), inducing gene transcription via the activation of nuclear factor of activated T cells (NFAT), nuclear factor kappa-light-chain-enhancer of activated B cells (NF-$\kappa$B), and the MAPK pathways[69].

The EP2 and EP4 receptors, linked to the $G\alpha s$ subunit, activate adenylate cyclase upon receptor engagement. This activation results in elevated levels of cyclic adenosine monophosphate (cAMP), subsequently initiating the activation of protein kinase A (PKA). PKA phosphorylates and activates the transcription factor cAMP-responsive element binding protein (CREB), which regulates several cellular responses, including survival, proliferation, and differentiation[70].

With 3 different splice variants, EP3 has the capability to associate with different G-protein subunits ($G_i$, $G_s$, and $G_{13}$), enabling it to modulate cAMP levels and trigger $Ca^{2+}$ mobilization either positively or negatively. However, the predominant splice variant of EP3 is thought to couple with an inhibitory $G_i$ protein. As a result, the main effect of the $PGE_2$-EP3 axis is the inhibition of adenylate cyclase and the activation of the MAPK pathway[71,72].

In summary, $PGE_2$ signaling involves 4 GPCRs with varying affinities and activation patterns across tissues and diseases, mediating diverse downstream effects that can differ among numerous cell types.

### 1.2.5 Immunomodulation by tumor cells and tumor-derived $PGE_2$

It has been shown that tumor cells employ various strategies to induce immune suppression in the TME, which hinders immune cell function and contributes to tumor immune escape (see section 1.2.1).

Beyond alterations in the TME and the indirect impact on infiltrating cells, tumors actively release suppressive factors like $PGE_2$, which directly affects a variety of immune cells such as myeloid-derived suppressor cells (MDSCs), tumor-associated macrophages (TAMs), type 1 conventional dendritic cells (cDC1s), NK cells, and T cells[62,73].

MDSCs have been found in many cancers to play a pivotal role in creating an immunosuppressive TME[74]. They originate from hematopoietic stem cells in the bone marrow and differentiate into mature MDSCs under the influence of cancer-related mediators and cytokines[75]. MDSCs inhibit anti-tumor immune responses through various mechanisms, such as promoting the activation of $T_{regs}$, hindering T cell migration, and producing reactive oxygen species[74–76]. Notably, $PGE_2$ plays a crucial role in activating and mobilizing MDSCs. For example, while the engagement of the $PGE_2$-EP2 axis promotes an increased infiltration of immature MDSCs into the TME, $PGE_2$ signaling via EP1, EP2, and EP3 has demonstrated its role in mediating the differentiation into mature MDSCs[77]. Interestingly, it has been observed that myeloid cells in the bone marrow can take up tumor-derived exosomes containing $PGE_2$, thereby directly facilitating the formation of MDSCs[78,79]. In addition to this, $PGE_2$ signaling in MDSCs triggers COX-2 activation, leading to the autocrine synthesis of endogenous $PGE_2$[80].

Apart from MDSCs, tumor-derived $PGE_2$ can lead to the recruitment and polarization of TAMs from an inflammatory anti-tumor (M1) to a suppressive pro-tumor M2-like phenotype. This polarization further contributes significantly to the establishment of an immunosuppressive environment[81]. Once polarized, TAMs play a pivotal role in directly advancing tumor progression and angiogenesis. Notably, $PGE_2$ induces the production of vascular endothelial growth factor (VEGF) in TAMs, acting as a potent driver of angiogenesis[81]. Moreover, TAMs are potent producers of cytokines such as IL-6 and IL-8,

known to mediate epithelial-mesenchymal transition (EMT) in cancer cells, facilitating increased motility of tumor cells. Additionally, IL-6 plays a dual role by promoting anti-apoptotic processes in cancer cells[82]. Adding to their impact on the TME, TAMs secrete transforming growth factor β (TGF-β) and IL-10, contributing to immune suppression and providing additional support for the progression of tumors[82,83].

Among dendritic cell populations, cDC1s have demonstrated a substantial and beneficial impact on anti-tumor immunity. cDC1s play a crucial role in initiating $CD8^+$ T cell responses within lymph nodes by cross-presenting absorbed tumor antigens[60,61]. Additionally, they actively participate in the restimulation of $CD8^+$ T cells within the TME by providing essential costimulatory signals and cytokines, e.g., IL-12, which supports T cell survival and enhances effector functions[61,62]. However, tumor cells can develop mechanisms to overcome immune surveillance by cDC1s. For instance, tumor cells can downregulate the expression of CCL4, leading to reduced cDC1 infiltration into the TME[84]. Moreover, tumors often exhibit an increased expression of CD47, acting as a 'do not eat me' signal. CD47 binds to signal regulatory protein-α (SIRPα), resulting in the suppression of both phagocytosis and the secretion of type I interferons by cDCs[85]. Moreover, as mentioned above, TAMs are the main producers of IL-10 within the TME. IL-10 signaling on cDC1s leads to diminished IL-12 secretion, thereby also indirectly affecting $CD8^+$ T cell responses[86]. $PGE_2$ signaling in tumor-infiltrating cDC1s induces their reprogramming into a dysfunctional state. This transformation is primarily mediated by the suppression of the transcription factor interferon regulatory factor 8 (IRF8), which is initiated through cAMP signaling. Consequently, this downregulation dampens anti-cancer $CD8^+$ T cell responses by the loss of C-X-C motif chemokine ligand 9 (CXCL9) and IL-12 expression[62].

Furthermore, $PGE_2$ indirectly impairs cDC1 infiltration by influencing NK cell viability and modulating the expression of pro-inflammatory chemokines such as CCL5 and XC-chemokine ligand 1 (XCL1) in NK cells. These chemokines are well known as key mediators for the recruitment of cDC1s into the TME[87]. Moreover, $PGE_2$ signaling on NK cells results in diminished secretion of

FMS-like tyrosine kinase 3 ligand (FLT3L), a crucial factor for the development and survival of cDCs. Notably, NK cells serve as the primary producers of FLT3L[87]. Additionally, it has been reported that $PGE_2$ signaling on NK cells inhibits their cytotoxicity, migration, and production of TNF$\alpha$ and IFN$\gamma$[88]. Another factor that impairs immune surveillance by NK cells in tumors is the secretion of TGF-β by TAMs and tumor cells. TGF-β signaling on NKs leads to both an impairment in NKG2D-mediated tumor cell killing and NK cell differentiation into type 1 lymphoid cells, which do not contribute to anti-cancer immunity[89,90]. An additional factor released by tumor cells is indoleamine 2,3-dioxygenase (IDO), responsible for catabolizing extracellular tryptophan into kynurenine and other byproducts. These products exert inhibitory effects on both NK and T cells[89].

Over the past few decades, numerous studies have highlighted the impact of $PGE_2$ on T cells, predominantly focusing on $CD4^+$ T cells. Studies indicate that $PGE_2$ signaling affects both T cell differentiation and cytokine production[73]. Notably, $PGE_2$ hinders T helper 1 ($T_{h1}$)-mediated anti-tumor responses, critical for anti-cancer properties, as these $CD4^+$ T cells typically produce pro-inflammatory cytokines such as IL-2, IFN$\gamma$, and TNF$\alpha$[91]. Moreover, $PGE_2$ signaling, accompanied by increased cAMP levels, promotes a $T_{h2}$-mediated immune response, which is characterized by its limited support for anti-tumor immune responses[50,92]. This transition additionally attenuates $T_{h1}$-mediated immune responses by releasing anti-inflammatory cytokines like IL-4 and IL-10[91]. In addition, there is compelling evidence illustrating that $PGE_2$ induces the differentiation of $CD4^+$ T cells into Forkhead-Box-Protein $3^+CD25^+$ $T_{regs}$, contributing to the suppression of effector T cell functions[93].

Yet, our understanding of the impact of $PGE_2$ on $CD8^+$ T cells remains limited. Reports suggest that $PGE_2$ signaling hampers $CD8^+$ T cell proliferation and is linked to impaired $CD8^+$ T cell differentiaton[92,94–96]. Nonetheless, it is important to mention that tumor-derived $PGE_2$ is linked to a reduced abundance of tumor-infiltrating $CD8^+$ T cells in multiple mouse and human cancers and is also associated with unfavorable patient survival outcomes[52,65,97,98]. Therefore, gaining a comprehensive understanding of the interplay between $PGE_2$ and tumor-infiltrating $CD8^+$ T cells is essential and needs further investigation.

## 1.3 T cells in malignancies

### 1.3.1 T cell exhaustion

The current view of T cell differentiation is characterized by two distinct developmental pathways, which ultimately result in either memory T cells ($T_{mem}$) or 'exhausted-like' T cells ($T_{exh}$)[13,14].

In situations characterized by optimal $CD8^+$ T cell activation, such as during the resolution of acute infections or following vaccinations, $CD8^+$ T cells undergo initial differentiation into either effector cells ($T_{eff}$) or memory precursor cells ($T_{mp}$). Subsequently, as the antigen is eliminated, long-lived $T_{mem}$ cells come into existence[99,100]. The $T_{mem}$ cell population is comprised of different subsets, which can be characterized by their surface marker expression, function, differentiation potential, and localization within the body. The widely adopted categorization includes stem cell memory ($T_{scm}$), central memory ($T_{cm}$), effector memory ($T_{em}$), tissue-resident memory ($T_{rm}$), and, notably in humans, effector memory $CD45RA^+$ ($T_{emra}$) $CD8^+$ T cells[101].

In contrast, prolonged TCR engagement results in the generation of $T_{exh}$ cells, diverging from the differentiation trajectory observed in $T_{mem}$ cells. This process leads to a distinct imprinting of $CD8^+$ T cells, mediated by the transcription factor thymocyte selection-associated high mobility group box protein (TOX)[102,103]. This phenomenon has been observed in numerous persistent infections, such as those caused by the hepatitis C virus or HIV, as well as in various types of cancers[104]. $T_{exh}$ cells are commonly characterized by the coexpression of inhibitory receptors such as PD-1, CD39, and LAG-3 and reduced effector cytokine production, including IFN$\gamma$, TNF$\alpha$, and IL-2[104]. These cells exhibit a unique transcriptional and epigenetic profile distinct from naive, effector, and memory T cells[105]. Contrary to the misconception that they are non-functional, 'exhausted-like' T cells exhibit adjusted effector functions, enabling them to withstand prolonged stimulation in persistent infections and tumors. As a result, they play a pivotal role in processes such as maintaining moderate viral control during chronic infections or boosting anti-tumor responses in patients undergoing treatment with immune checkpoint blockade (ICB)[106,107].

Recent studies have identified at least three distinct subtypes within the 'exhausted-like' CD8+ T cell population. These subtypes include 'exhausted-like' progenitor T cells ($T_{exh\text{-}prog}$), here denoted as stem-like TCF1+CD8+ T cells, intermediate 'exhausted-like' T cells ($T_{exh\text{-}int}$) showing effector functions, and terminal 'exhausted-like' T cells ($T_{exh\text{-}term}$) (**Figure 1**)[108–112].

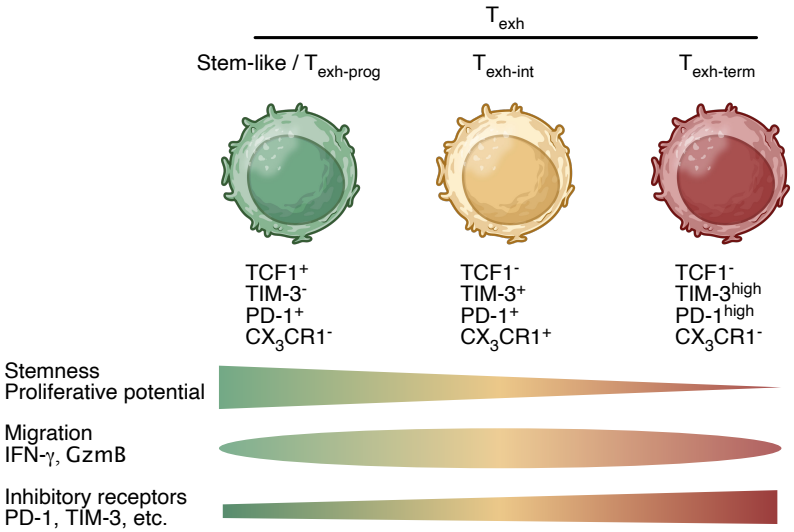


**Figure 1: 3 distinct CD8+ T cell populations are observed in chronic infection and cancer.**
Adapted from Giles et al., 2023. Created with BioRender.com.

Stem-like CD8+ T cells express the transcription factor T cell factor 1 (TCF1) and are present during chronic infections and cancers as well as within secondary lymphoid organs. Stem-like TCF1+CD8+ T cells display a unique combination of exhausted and stem-like features and they are often located near antigen-presenting cells, including cDC1s[62,113]. The interaction between cDC1s and stem-like TCF1+CD8+ T cells promotes enhanced T cell activation and differentiation, which is crucial for the expansion into the other $T_{exh}$ subtypes[14,61,62]. These cells will be further discussed in section 1.3.2.

$T_{exh\text{-}int}$ cells demonstrate functional diversity, expressing both exhaustion-related and effector-associated molecules. Although these cells exhibit an epigenetic exhaustion signature, they have been recognized as an effector-like population due to their production of effector molecules such as IFNγ and GzmB, as well as their increased oxidative phosphorylation signature[14,114–116].

$T_{exh\text{-}term}$ cells exhibit the least proliferative capacity yet display a strong association with an exhausted signature, primarily attributed to their elevated expression of inhibitory receptors. Nevertheless, these cells might play a role in

supporting local inflammation and the recruitment of other leukocytes, given their expression of CCL3, CCL4, and CCL5[115].

Taken together, these three $T_{exh}$ subsets share an exhausted and epigenetic signature in which the transcription factor TOX is one of the main drivers[113].

Extensive research is underway to unravel the developmental trajectory of these cells. To date, data indicate two distinct paths in their T cell development. The first is a linear progression, starting with stem-like $TCF1^+CD8^+$ T cells, transitioning through $T_{exh\text{-}int}$, and ending in $T_{exh\text{-}term}$ cells. The second path follows a branched pattern, initiating from stem-like $TCF1^+CD8^+$ T cells, diverging into $T_{exh\text{-}int}$ and stem-like $TCF1^+CD8^+$ T cells, and concluding in $T_{exh\text{-}term}$ cells[116,117].

Despite challenges such as phenotypic diversity and discrepancies in nomenclature across studies, understanding the origins and potential of these progenitor or stem-like $TCF1^+CD8^+$ T cells, which can evolve into anti-tumor effector cells, is crucial for advancing our understanding of anti-tumor immunity.

### 1.3.2 Stem-like $TCF1^+CD8^+$ T cells in cancers and chronic infections

In recent years, stem-like cells have emerged as a distinct subset of virus-specific $CD8^+$ T cells. These cells can be distinguished by an exhausted and stemness-like phenotype, characterized by the expression of PD-1 and TCF1, respectively[118–120]. Initially observed during chronic infections, stem-like $TCF1^+CD8^+$ T cells have also been identified in human and murine tumors. They play a crucial role in coordinating antigen-specific $CD8^+$ T cell responses by giving rise to effector $CD8^+$ T cells[107,121–124]. More specifically, these cells exhibit self-renewal potential, ensuring their persistence while also differentiating into a $CX_3CR1^+$ transitory population and eventually terminally differentiated $CD8^+$ T cells[118–120,125]. This process is thought to be orchestrated by the basic leucine zipper transcription factor (BATF) and, to a certain extent, by the activity of the T-box transcription factor (TBX21) within the stem-like $TCF1^+CD8^+$ T cell population[113,126].

Studies have identified a common core signature within the stem-like $TCF1^+CD8^+$ T cell compartment, shared among chronically infected

mice as well as in mice harboring tumors. This genetic profile encompasses crucial components such as inhibitory receptors, costimulatory molecules, self-renewal factors, chemokines, chemokine receptors, and transcription factors. Examples of these include *Tcf7*, *Slamf6*, *Pdcd1*, *Ccl5*, *Kit*, *Tox*, *Il7r*, *Havcr2*, *Lef1*, *Sell*, *Icos*, *Id2*, *mTOR*, among others[113,118,127]. Moreover, stem-like TCF1$^+$CD8$^+$ T cells from chronically infected mice show a preference for residing in environments with a limited number of virus-infected cells, such as LNs and the white pulp of spleens (in contrast to the red zones)[127,128]. Similarly, stem-like TCF1$^+$CD8$^+$ T cells within tumors tend to localize in niches distinct from the tumor parenchyma, as evidenced by their prevalence in locations away from the tumor bulk in Non-small cell lung cancers (NSCLCs) and head and neck squamous cell carcinomas[123,127]. Furthermore, recent studies highlighted the role of TOX, which plays a crucial role in maintaining the TCF1$^+$CD8$^+$ phenotype, directing CD8$^+$ T cell differentiation, and contributing to T cell exhaustion[129,130]. Linked with epigenetic remodeling, TOX ensures stable fixation of a dysfunctional phenotype[131,132]. It actively regulates the maintenance of the stem-like TCF1$^+$CD8$^+$ T cell properties and promotes PD-1 expression[129,130]. Consequently, TOX is a critical regulator, ensuring both the persistence of stem-like TCF1$^+$CD8$^+$ T cells and preventing T cell overstimulation by inducing an 'exhausted-like' phenotype in differentiated CD8$^+$ T cells[129].

Interestingly, besides shared core signatures, studies have revealed distinctive variations in gene profiles between stem-like TCF1$^+$CD8$^+$ T cells from chronically infected mice and those infiltrating tumors. For example, stem-like TCF1$^+$CD8$^+$ T cells from chronically infected mice exhibited a marked upregulation in pathways linked to glucose metabolism and IFN$\alpha\beta$ signaling[127]. In contrast, stem-like TCF1$^+$CD8$^+$ T cells found within the TME demonstrated elevated gene expression associated with pathways involving the epidermal growth factor receptor (EGFR), G-protein-coupled receptor signaling, and pathways linked to hypoxia[113,127].

As a result, research strongly emphasizes the vital role played by the distinct microenvironments in chronic infections and tumors in shaping the phenotypes of $CD8^+$ T cells[127]. Understanding these environmental factors is crucial for developing immunotherapeutic strategies that effectively harness the potential of $CD8^+$ T cells to combat chronic infections and tumors. Moreover, it is important to note that our current knowledge about stem-like $TCF1^+CD8^+$ T cells is limited, highlighting the need for further research to comprehensively understand their biology and to develop innovative targeted therapeutic approaches.

### 1.3.3 T cell-directed cancer immunotherapy

Several studies have established that $TCF1^+CD8^+$ T cells can be a prognostic marker for positive clinical outcomes. These cells demonstrate initial responsiveness to ICB in the context of tumors and chronic infections, thereby facilitating their differentiation and expansion into terminally differentiated $CD8^+$ T cells[45,107,122,124,127]. Importantly, since the 'exhausted-like' phenotype of stem-like $TCF1^+CD8^+$ T cells is imprinted and remains unaltered even with ICB, this phenotype is transferred to their progeny[113,131,132]. Studies indicated that stem-like $TCF1^+CD8^+$ T cells commit early to the path of exhaustion, marked by distinct transcriptional and epigenetic differences[113]. However, the full establishment of an exhausted phenotype takes time to stabilize, possibly explaining the continuous progression of cancer and chronic infections despite robust initial responses from stem-like $TCF1^+CD8^+$ T cells to ICB[103,113,129,130]. In line with this, studies revealed that at later time points, the stem-like $TCF1^+CD8^+$ T cells acquire a quiescent phenotype in both chronic infections and in tumors[113,121,127]. Therefore, understanding the biology of stem-like $TCF1^+CD8^+$ T cells is crucial for advancing targeted therapies, particularly in addressing challenges related to increased T cell responses post-treatment. The need to potentiate the capacity of stem-like $TCF1^+CD8^+$ T cells to generate effector $CD8^+$ T cells without compromising their long-term persistence remains a significant challenge,

highlighting the necessity for research focused on unraveling the biology of stem-like TCF1$^+$CD8$^+$ T cells in the context of targeted therapy.

One potential strategy to address this challenge may be the combination of ICB with IL-2-targeted treatment. IL-2 has been employed since 1992 as the first and pioneering immunotherapeutic treatment for metastatic renal cell carcinoma, followed by its approval for metastatic melanoma in 1998[133,134]. However, IL-2 exhibits a dual role, activating both cytotoxic CD8$^+$ T cells and $T_{regs}$, thus contributing to the establishment of an immunosuppressive environment[135]. Consequently, IL-2 is recognized as a crucial regulator in maintaining the balance between immune activation and suppression. Additionally, IL-2 treatment often leads to side effects such as vascular leak syndrome induced by off-target stimulation of endothelial cells in the lungs, brain, and liver[136–138]. Furthermore, the short half-life of IL-2 requires multiple administrations, while emerging evidence suggests that IL-2 signaling may significantly impact the development and progression of cancer[139–142]. These limitations impede its efficacy in anti-cancer therapy, prompting the development of new IL-2 agents with enhanced selectivity for effector cells, reduced toxicity, and a prolonged half-life.

One promising advancement lies in the development of novel classes of IL-2 variants engineered to disable or limit IL-2R$\alpha$ binding, primarily stimulating CD8$^+$ and NK cells rather than $T_{regs}$[135,143–146]. As previously mentioned, the proliferation and differentiation of stem-like TCF1$^+$CD8$^+$ T cells into effector CD8$^+$ T cells are pivotal for the success of immunotherapies based on ICB[45,107,122,124,127]. Building on these findings, a novel therapeutic approach has demonstrated effectiveness in selectively enhancing the differentiation of stem-like TCF1$^+$CD8$^+$ T cells into effector CD8$^+$ T cells by circumventing the need for IL-2R$\alpha$ binding[43,135]. This approach involves covalently linking an anti-PD-1 antibody to an IL-2 variant designed to selectively bind to IL-2R$\beta$ and IL-2R$\gamma$c. Compared to non-targeted IL-2 combination therapies, this strategy has proven effective in both chronic infection and cancer models[43,45,147,148]. However, it has been suggested that the inhibition of PD-1 signaling via PD-1-IL-2 variant therapeutics may only be partial, as the addition of anti-PD-L1

blocking antibodies further enhances the effect in cancer and chronic infections[135,148,149]. Therefore, it remains to be determined whether selective engagement of the IL-2R-axis needs to be mediated by PD-1 or if other surface markers would also be effective for targeted $CD8^+$ T cell therapy.

In conclusion, IL-2 has demonstrated its therapeutic potential in promoting stimulatory effects on stem-like $TCF1^+CD8^+$ T cells, particularly when combined with ICB. Nonetheless, additional preclinical and clinical investigations are necessary to fully elucidate its efficacy and safety profile in future studies.

Besides these novel approaches, chimeric antigen receptor (CAR) T cell therapy might be a promising T cell targeted therapy to treat solid cancers. CAR T cell therapy begins by genetically modifying a patient's T cells to introduce an engineered CAR that can specifically recognize an antigen on the surface of cancer cells, independent of MHC-I. Additionally, CARs contain an intracellular domain capable of triggering $CD8^+$ T cell activation[150,151]. Although CAR T cell therapy has demonstrated significant success primarily in treating hematological malignancies such as multiple myeloma, B cell leukemias, and certain lymphomas, ongoing clinical trials are investigating its potential efficacy in treating solid tumors, including lung, liver, gastric, and prostate cancer[151–154]. Nevertheless, it is worth noting that CAR T cell therapy faces several limitations when applied to the treatment of solid cancers. For instance, studies have demonstrated that CAR T cells frequently show limited infiltration into the TME. Therefore, strategies to overcome this have been developed involving the simultaneous expression of chemokine receptors or surface molecules, which can facilitate the entry into the tumor. Moreover, strategies to deliver CAR T cells directly into the TME have also been considered[151,155,156]. Another limitation arises from the tumor cells' ability to lose tumor antigens over time. To address this challenge, strategies such as transferring two or more CAR T cell populations into the patient or generating bi-specific CAR T cells to target multiple antigens simultaneously have been investigated[151,157,158]. Furthermore, CAR T cell therapy is associated with cytokine release syndrome, a potentially life-threatening inflammatory condition caused by the immune system's overactivation following CAR T cell treatment. This is primarily mediated by the

release of cytokines such as IFN-γ, IL-1, IL-6, and IL-10. Consequently, strategies have been developed to further inhibit IL-1R or IL-6R signaling in patients[159,160]. Moreover, CAR T cells often encounter an immunosuppressive microenvironment characterized by hypoxic regions and the presence of immunosuppressive cells such as $T_{regs}$, MDSCs, and TAMs[161,162]. The existence of such an immunosuppressive milieu can compromise the effectiveness of CAR T cells, resulting in reduced tumor infiltration, impaired functionality, and restricted longevity within the TME. To address these limitations, CAR T cells have been engineered to secrete immunostimulatory cytokines such as IL-12, IL-18, or IL-15. This alteration improves the survival of CAR T cells and facilitates the recruitment of endogenous immune cells, such as T cells and NK cells, thus fostering an inflammatory microenvironment[163,164].

In conclusion, despite encountering numerous challenges, ongoing advancements in CAR T cell therapy offer promising prospects for advancing effective anti-cancer treatments for solid tumors.

Another promising strategy for targeted T cell therapeutics may be the use of antibody-drug conjugates (ADCs). These innovative compounds comprise monoclonal antibodies covalently linked to cytotoxic drugs via a chemical or biochemical linker. ADCs demonstrate exceptional precision in cell targeting, delivering potent cytotoxic payloads to effectively eliminate cancer cells. To date, the development of ADCs has mostly focused on targeting tumors, with 14 ADCs having achieved global market approval and over 100 ADC components undergoing clinical trials (as of 2022)[165]. Mechanistically, ADCs bind to targets associated with solid tumors such as HER2, TROP2, or EGFR and undergo subsequent internalization through endocytosis. This process mediates the release of the cytotoxic payload into the cancer cell. Most drugs have been engineered to focus on disrupting the synthesis of microtubules, playing an indispensable role in the process of mitosis[165]. Notably, only 2% of ADCs successfully reach their target at the tumor site following i.v. administration. As a result, the payloads are crafted to be highly potent in carrying out their cytotoxic functions. However, this potency is accompanied by significant side effects, including neutropenia, thrombocytopenia, leukopenia, and anemia.

Additionally, hepatotoxicity, nephrotoxicity, and gastrointestinal reactions may occur, likely due to the premature release of cytotoxic payloads into the bloodstream[166]. Another limitation of ADCs is that these drugs have a much bigger molecular weight than conventional cytotoxic drugs, limiting the infiltration into the TME[165].

These limitations make them less attractive as candidates for anti-cancer treatment. However, using this strategy to target T cells specifically may represent an innovative approach. For instance, ADCs designed to target $T_{regs}$ within the TME by binding to CD25 and delivering their cytotoxic payload have shown efficacy in three mouse cancer cell lines, thereby enhancing the $CD8^+$ T cell-mediated anti-cancer immune response[167]. Additionally, ADCs can be employed to target B cell malignancies such as leukemias and non-Hodgkin lymphomas[168]. Nevertheless, current ADC therapeutics primarily deliver cytotoxic payloads to their target cells, often resulting in the aforementioned side effects due to their premature release of the payload[169]. To address this issue, it could be suggested to design ADCs with molecules that specifically inhibit pathways instead of fulfilling cytotoxic functions. This approach may reduce the severe side effects associated with ADCs and potentially revolutionize targeted $CD8^+$ T cell treatment strategies. However, these approaches are currently under investigation, and further research is needed to fully assess their efficacy and safety profiles in clinical settings[169].

## 2 Aim of the thesis

Many murine and human cancers show an aberrant COX1/2 activity in their pathway, leading to the secretion of the immunosuppressive bioactive lipid $PGE_2$. Tumor-derived $PGE_2$ has been demonstrated to limit effective anti-cancer $CD8^+$ T cell responses. However, the direct effects of $PGE_2$ signaling on tumor-infiltrating $CD8^+$ T cells have yet to be fully elucidated.

Recent studies underscore the importance of stem-like $TCF1^+CD8^+$ T cells for effective anti-tumor immunity. These stem-like cells possess the unique ability to give rise to effector $CD8^+$ T cells, thereby fueling anti-cancer T cell responses. However, despite acknowledging their pivotal role, our understanding of the differentiation mechanisms governing stem-like $TCF1^+CD8^+$ T cell differentiation and the factors regulating stem-like $TCF1^+CD8^+$ T cell responses in cancer remain poorly understood. Furthermore, it remained unclear whether $PGE_2$ produced by cancer cells influences the biology of stem-like $TCF1^+CD8^+$ T cells and whether protecting these cells from $PGE_2$ signaling can lead to potent $CD8^+$ T cell-mediated anti-cancer immunity.

Therefore, this study aimed to pose the following central questions:

- Does direct $PGE_2$ signaling on $CD8^+$ T cells affect anti-cancer immunity?
- Does $PGE_2$ affect stem-like $TCF1^+CD8^+$ T cell function in secondary lymphoid organs and/or locally within the TME?
- How does $PGE_2$ affect $CD8^+$ T cell responses originating from stem-like $TCF1^+$ $CD8^+$ T cells?
- What are the molecular T cell-intrinsic mechanisms underlying $PGE_2$-mediated impairment of anti-cancer T cell responses in tumors?
- Can the blockade of $PGE_2$ signaling on tumor-specific stem-like $TCF1^+CD8^+$ T cells rescue T cell-mediated tumor control?

# 3 Materials and methods

## 3.1 Materials

### 3.1.1 Chemicals and reagents

**Table 1: List of used chemicals, agents, and solutions.**

| Chemicals, agents, and solutions | Manufacturer | Catalog number |
|---|---|---|
| 0.05% Trypsin/EDTA | Thermo Fisher Scientific | 25300054 |
| 2-Mercaptoethanol | Thermo Fisher Scientific | 31350010 |
| Alt-R Cas9 electroporation enhancer | IDT | 1075915 |
| Alt-R CRISPR-Cas9 tracrRNA | IDT | 1072532 |
| Alt-R S.p. Cas9 nuclease | IDT | 1081058 |
| Antigenfix | Diapath | P0016 |
| Collagenase IV | eBioscience | 65-0850-84 |
| DMEM | Thermo Fisher Scientific | 41965039 |
| DMEM/F12 | Thermo Fisher Scientific | 31331028 |
| DNase I | Roche | 11284932001 |
| EDTA | Carl Roth | 8043.1 |
| Ethanol | Thermo Fisher Scientific | 10644795 |
| Fetal calf serum | PAA | A15-649 |
| FTY720 | Merck | SML0700-25MG |
| Indomethacin | Merck | 405268 |
| Isoflurane | CP-Pharma | 1214 |
| L-glutamine | Thermo Fisher Scientific | 25030081 |

| | | |
|---|---|---|
| MEM non-essential amino acids | Thermo Fisher Scientific | 11140035 |
| Mouse αCD3/CD28 microbeads | Thermo Fisher Scientific | 11456D |
| Mowiol | Merck | 81382 |
| Normal mouse serum | Merck | NS03L |
| Pancoll | PAN Biotech | P04-60500 |
| Penicillin-streptomycin | Thermo Fisher Scientific | 15070063 |
| Prostaglandin E2 | Sigma-Aldrich | P5640 |
| Recombinant human IL-2 | Miltenyi | 130-097-743 |
| Recombinant murine IL-12 | Biolegend | 577002 |
| Recombinant murine IL-15/15Rα | Thermo Fisher Scientific | 14-8152-80 |
| Recombinant murine IL-7 | Miltenyi | 130-098-222 |
| RPMI 1640 | Thermo Fisher Scientific | 11875093 |
| Sodium pyruvate | Thermo Fisher Scientific | 11360039 |
| Trypan blue solution | Sigma-Aldrich | T8154 |
| Viability dye APC-eF780, fixable (1:1000) | Thermo Fisher Scientific | 65-0865-14 |
| Viability dye eF450, fixable (1:500) | Thermo Fisher Scientific | 65-0863-18 |
| Viability dye sytox-blue (1:2000) | Thermo Fisher Scientific | S34857 |

### 3.1.2 Laboratory devices

**Table 2: List of used devices.**

| Device | Model | Manufacturer |
|---|---|---|
| 4D-nucleofactor core unit | N/A (not available) | Lonza |
| Bio-safety cabinet class 2 | Herasafe | Thermo Fisher Scientific |
| Cell culture incubator | Heracell 150i | Thermo Fisher Scientific |
| Cell sorter | FACSAria™ III, FACSAria™ Fusion | BD Bioscience |
| Centrifuge | Fresco 17, Megafuge 8R, Multifuge X3R | Thermo Fisher Scientific |
| Digital caliper | N/A | Cole-Parmer |
| GentleMACS dissociator | Octo Dissociator with Heaters | Miltenyi Biotec |
| Light microscope | Axioscope 10 (AX 10) | Zeiss |
| LightCycler 480 | N/A | Roche |
| LSRFortessa cell analyzer | N/A | BD Bioscience |
| MagniSort™ magnet | N/A | Thermo Fisher Scientific |
| Neubauer counting chamber | N/A | Paul Marienfeld & Co.KG |
| Real-time cell analyzer | xCELLigence RTCA MP-Multiple Plates | ACEA Bioscience |
| Spectral cell analyzer | SA3800, SP6800 | SONY Biotechnology |
| Spectral cell sorter | SH800Z | SONY Biotechnology |
| Spectrophotometer | P380 | Implen |
| Water bath | N/A | GFL |

### 3.1.3 Cell lines

All tumor cell lines used in this doctoral thesis were derived from mice.

**Table 3: List of used cell lines.**

| Cell line | Description/characteristics | Source |
|---|---|---|
| $BRAF^{V600E}$ (Control) | Murine melanoma cell line, oncogenic $BRAF^{V600E}$ mutation, COX-1/2 sufficient, $PGE_2$ production | Provided by Caetano Reis e Sousa |
| $BRAF^{V600E}$-OVA | Murine melanoma cell line, oncogenic $BRAF^{V600E}$ mutation, COX-1/2 sufficient, $PGE_2$ production, ovalbumin (OVA, as a model antigen) expression | Generated in our laboratory |
| D4M.3A-pOVA | Dartmouth murine mutant malignant melanoma.3A cell line, $PGE_2$ production, OVA expression | Provided by Mauro Di Pilato |
| MC38 | Murine colon adenocarcinoma cell line, $PGE_2$ production | Provided by Achim Krüger |
| MC38-OVA | Murine colon adenocarcinoma cell line, $PGE_2$ production, OVA expression | Provided by Veit Buchholz |
| Panc02 | Pancreatic adenocarcinoma cancer cell line, $PGE_2$ production | Provided by Veit Buchholz |
| *Ptgs1/Ptgs2*$^{-/-}$ $BRAF^{V600E}$ | Murine melanoma cell line, oncogenic $BRAF^{V600E}$ mutation, COX-1/2 deficient, no $PGE_2$ production | Provided by Caetano Reis e Sousa |
| *Ptgs1/Ptgs2*$^{-/-}$ $BRAF^{V600E}$-OVA | Murine melanoma cell line, oncogenic $BRAF^{V600E}$ mutation, COX-1/2 deficient, no $PGE_2$ production, OVA expression | Generated in our laboratory |

### 3.1.4 Buffers and media

**Table 4: List of used buffers and media.**

| Buffers and media | Composition |
|---|---|
| Ammonium chloride potassium (ACK) lysis buffer | 150 mM $NH_4Cl$ + 10 mM $KHCO_3$ + 0.1 mM EDTA |
| Digestion medium | RPMI 1640 + collagenase IV (200 U/ml) + DNaseI (100 $\mu$g/ml) |
| FACS buffer | 1x PBS + 1% FCS (v/v) + 2 mM EDTA + at pH 7.0 |
| Homogenization buffer | 0.1 M PBS + 1 mM EDTA + 10 $\mu$M indomethacin + at pH 7.4 |
| T-cell-medium | RPMI 1640 + 10% FCS (v/v) + 50 µM β-mercaptoethanol + 100 U/ml penicillin + 100 mg/ml streptomycin + 2 mM L-glutamine + 1x MEM non-essential amino acids + 1 mM sodium pyruvate |

### 3.1.5 Experimental mouse models

All mice in this doctoral thesis were purchased from the Jackson Laboratory and on a background of C57BL/6J (wildtype, WT). For all animal experiments, mice aged 6-12 weeks were sex-matched, randomly assigned to control or treatment groups, and euthanized by cervical dislocation under anesthesia.

All mice were maintained and bred at the Klinikum rechts der Isar, Technical University of Munich (TUM) under specific-pathogen-free conditions and following the Federation of Laboratory Animal Science Association guidelines. All animal experiments conducted in this study were authorized by local authorities and complied with national policies.

**Table 5: List of used mouse lines.**

| Mouse | Strain | RRID number |
|---|---|---|
| C57BL/6J | C57BL/6J | JAX:000664 |
| *CD4$^{Cre}$* | B6.Cg-Tg(Cd4-cre)1Cwi/BfluJ | JAX:022071 |
| *CD4$^{Cre}$Ptger2$^{-/-}$ Ptger4$^{fl/fl}$* | B6.Cg-Tg(Cd4-cre)1Cwi/BfluJ x B6.129-Ptger2tm1Brey/J x B6.129S6(D2)-Ptger4tm1.1Matb/BreyJ | N/A |
| *CD4$^{Cre}$Ptger2$^{-/-}$ Ptger4$^{fl/fl}$* OT-I | B6.Cg-Tg(Cd4-cre)1Cwi/BfluJ x B6.129-Ptger2tm1Brey/J x B6.129S6(D2)-Ptger4tm1.1Matb/BreyJ x C57BL/6-Tg(TcraTcrb)1100Mjb/J x B6.SJL-Ptprca Pepcb/BoyJ | N/A |
| *GzmB$^{Cre}$* | B6;FVB-Tg(GZMB-cre)1Jcb/J | JAX:003734 |
| *Rag1$^{-/-}$* | B6.129S7-Rag1tm1Mom/J | JAX:002216 |
| *GzmB$^{Cre}$Ptger2$^{-/-}$ Ptger4$^{fl/fl}$* | B6;FVB-Tg(GZMB-cre)1Jcb/J x B6.129-Ptger2tm1Brey/J x B6.129S6(D2)-Ptger4tm1.1Matb/BreyJ | N/A |
| OT-I | C57BL/6-Tg(TcraTcrb)1100Mjb/J | JAX:003831 |
| *Ptger2$^{-/-}$* | B6.129-Ptger2tm1Brey/J | JAX:004376 |
| *Ptger2$^{-/-}$Ptger4$^{fl/fl}$* | B6.129-Ptger2tm1Brey/J x B6.129S6(D2)-Ptger4tm1.1Matb/BreyJ | N/A |
| *Ptger2$^{-/-}$Ptger4$^{fl/fl}$* OT-I | B6.129-Ptger2tm1Brey/J x B6.129S6(D2)-Ptger4tm1.1Matb/BreyJ x C57BL/6-Tg(TcraTcrb)1100Mjb/J x B6.SJL-Ptprca Pepcb/BoyJ | JAX:028102 |
| *Ptger4$^{fl/fl}$* | B6.129S6(D2)-Ptger4tm1.1Matb/BreyJ | JAX:028102 |
| CD45.1 | B6.SJL-Ptprca Pepcb/BoyJ | JAX:002014 |
| OT-I x CD45.1 | C57BL/6-Tg(TcraTcrb)1100Mjb/J x B6.SJL-Ptprca Pepcb/BoyJ | N/A |

### 3.1.6 Commercial kits

**Table 6: List of used commercial kits.**

| Commercial kit | Manufacturer | Catalog number |
|---|---|---|
| Arcturus PicoPure RNA isolation kit | Thermo Fisher Scientific | KIT0204 |
| EdU assay / EdU staining proliferation kit (iFluor 488) | Abcam | Ab219801 |
| Intracellular fixation & permeabilization buffer set | Thermo Fisher Scientific | 88-8824-00 |
| Monarch™ total RNA miniprep kit | New England Biolabs | T2010S |
| P3 primary cell 4D-nucleofector X kit S | Lonza | V4XP-3032 |
| Prostaglandin E2 ELISA kit | Cayman Chemicals | 514010 |
| SensiFAST cDNA synthesis kit | Bioline | BIO-65053 |
| Takyon no rox SYBR master mix dTTP blue kit | Eurogentec | UF-NSMT-B0701 |
| True-nuclear™ transcription factor buffer set | Biolegend | 424401 |

### 3.1.7 Software and tools

**Table 7: List of used software.**

| Software | Version | Manufacturer |
|---|---|---|
| Affinity designer | v1.10.6 | Serif |
| BD FACSDiva™ software | v8.0.1 and v9.0.1 | BD Bioscience |
| Bioanalyzer 2100 | N/A | Agilent |
| FlowJo™ | v10.8.1 and v10.8.2 | BD Bioscience |
| Graphpad prism | v9.5.0 and v9.5.1 | GraphPad |
| Microsoft 365 | v16.69.1 | Microsoft |
| R-studio | v4.0.4 | R Core Team, 2020 |

| | | |
|---|---|---|
| SA3800 spectral analyzer software | v2.0.5.54250 | SONY Biotechnology |
| SH800 cell sorter software | v2.1.6 | SONY Biotechnology |
| SP6800 spectral analyzer software | v2.0.2.14140 | SONY Biotechnology |
| xCELLigence RTCA software | v1.3 | Agilent |

**Table 8: Software, tools, and data sets for sequencing.**

| Software, tool, data set | Description |
|---|---|
| GRCm38/mm10 | Mouse reference genome, NCBI, https://www.ncbi.nlm.nih.gov/assembly/GCF_000001635.27 |
| pre-built mouse reference v2020-A | Pre-built reference genome for Cellranger, https://support.10xgenomics.com/single-cell-gene-expression/software/release-notes/build |
| R packages | DESeq2, ggplot2, ggrepel, Seurat v4.0.1 and Seurat v4.1.1, sctransform v0.3.2, slingshot v2.4.0, scRepertoire v1.6.0, decoupleR v2.2.2, tidygraph v1.2.1, igraph v1.3.2 |
| KAECH_NAIVE_VS_DAY8_EFF_CD8_TCELL_DN | T cell gene signature, Kaech et al., 2002 |
| $CD8^+$ T cell proliferation signature | MSigDB, GO:2000566 |
| FeatureCounts v1.5.0-p3 | Counting of mapped reads, https://subread.sourceforge.net/featureCounts |
| dorothea v1.8.0 | Transcription factor interactions, https://saezlab.github.io/dorothea/ |
| Cellranger multi v6.1.1 | For the analysis of 3´cell multiplexing data, https://support.10xgenomics.com/single-cell-gene-expression/software/pipelines/latest/using/multi |
| GSEA v4.3.2 | Gene set enrichment analysis, https://www.gsea-msigdb.org/gsea/index.jsp |

| | |
|---|---|
| mh.all.v2023.1.Mm | Hallmark gene set from MSigDB, https://data.broadinstitute.org/gsea-msigdb/msigdb/release/2023.1.Mm/ |
| Hisat2 v2.0.5 | Mapping tool, http://daehwankimlab.github.io/hisat2/ |
| pre-built ensembl GRCm38 mouse V(D)J reference v5.0.0 | Pre-built reference genome for V(D)J genes for Cellranger, https://support.10xgenomics.com/single-cell-vdj/software/pipelines/latest/advanced/built-in-refs |

### 3.1.8 Antibodies

If not stated otherwise, all antibodies were anti-mouse antibodies.

**Table 9: List of used antibodies.**

| Antibody | Fluorophore/ conjugate | Dilution /conc. | Clone | Manufacturer | Catalog number |
|---|---|---|---|---|---|
| Anti-H-2K$^{b}$ bound to SIINFEKL | PE | 1:100 | 25-D1.16 | Biolegend | 141603 |
| Anti-mouse CD4 | Depleting | 100 µg/ mouse | GK1.5 | BioXCell | BP0003-1 |
| Anti-mouse CD8β | Depleting | 100 µg/ mouse | 53-5.8 | BioXCell | BE0223 |
| Anti-mouse IL-2Rβ/ CD122 | Blocking | 300 µg/ mouse | TM-Beta 1 | BioXCell | BE0298 |
| Anti-mouse IL-2Rγc/ CD132 | Blocking | 300 µg/ mouse | 3E12 | BioXCell | BE0271 |
| CD103 | FITC | 1:100 | M290 | BD Pharmingen | 557494 |
| CD11b | BV605 | 1:200 | M1/70 | Biolegend | 101237 |
| CD11c | PE-Cy7 | 1:200 | N418 | Biolegend | 117317 |
| CD132 | APC | 1:100 | TUGm2 | Biolegend | 132307 |

| | | | | | |
|---|---|---|---|---|---|
| CD186 (CXCR6) | AF647 | 1:200 | SA051 D1 | Biolegend | 151114 |
| CD186 (CXCR6) | PE-Dazzle594 | 1:200 | SA051 D1 | Biolegend | 151116 |
| CD3 | APC | 1:100 | 17A2 | Invitrogen | 17-00 32-82 |
| CD366 (TIM-3) | BV421 | 1:200 | RMT3-23 | Biolegend | 119723 |
| CD4 | PE | 1:200 | GK1.5 | Biolegend | 100407 |
| CD4 | AF647 | 1:200 | GK1.5 | Biolegend | 100426 |
| CD4 | PerCP-Cy5.5 | 1:200 | GK1.5 | Biolegend | 100433 |
| CD44 | BV570 | 1:100 | IM7 | Biolegend | 103037 |
| CD44 | BV711 | 1:100 | IM7 | Biolegend | 103057 |
| CD44 | PerCP-Cy5.5 | 1:100 | IM7 | Biolegend | 103031 |
| CD45.1 | AF647 | 1:100 | A20 | Biolegend | 110720 |
| CD45.1 | PE | 1:100 | A20 | Biolegend | 110707 |
| CD45.2 | BV510 | 1:100 | 104 | Biolegend | 109837 |
| CD45.2 | FITC | 1:100 | 104 | Biolegend | 109805 |
| CD45.2 | PerCP-Cy5.5 | 1:100 | 104 | Biolegend | 109827 |
| CD62L | FITC | 1:100 | MEL-14 | Biolegend | 104405 |
| CD62L | PE-Dazzle594 | 1:100 | MEL-14 | Biolegend | 104447 |
| CD8$\alpha$ | BV421 | 1:200 | 53-6.7 | Biolegend | 100737 |
| CD8$\alpha$ | PE-Dazzle594 | 1:200 | 53-6.7 | Biolegend | 100761 |
| CD8$\alpha$ | PE-Cy7 | 1:200 | 53-6.7 | Biolegend | 100721 |
| $CX_3CR1$ | PE | 1:100 | SA011 F11 | Biolegend | 149005 |

| | | | | | |
|---|---|---|---|---|---|
| Donkey-anti-goat | AF680 | 1:200 | Poly-clonal | Jackson ImmunoResearch | 705-625-147 |
| Donkey-anti-rabbit | AF647 | 1:200 | Poly 4064 | Biolegend | 406414 |
| Donkey-anti-rabbit | AF594 | 1:200 | Poly 4064 | Biolegend | 406418 |
| Donkey-anti-rabbit | DL488 | 1:200 | Poly 4064 | Biolegend | 406416 |
| Goat-anti-rabbit CD103 | Primary antibody | 1:100 | Poly-clonal | R&D Systems | AF1990 |
| GzmB | APC | 1:200 | GB12 | Invitrogen | MHGB05 |
| IFNγ | BV421 | 1:100 | XMG1.2 | Biolegend | 505829 |
| Ki67 | FITC | 1:100 | SolA-15 | Invitrogen | 11-5698-82 |
| Ki67 | AF700 | 1:100 | SolA-15 | Invitrogen | 56-5698-82 |
| MHCII (anti-I-A/I-E) | AF700 | 1:500 | M5/114.15.2 | Biolegend | 107621 |
| Mouse-IgG1-κ isotype-control | APC | 1:200 | P3.6.2.8.1 | Invitrogen | 17-4714-42 |
| Mouse-IgG1-κ isotype-control | AF488 | 0.03 µg per test | MOPC-21 | Biolegend | 400132 |
| PD-1 (CD279) | BV605 | 1:100 | 29F.1A12 | Biolegend | 135219 |
| pSTAT5 | AF488 | 0.03 µg per test | 47/Stat5 (pY694) | BD Pharmingen | 612598 |

| | | | | | |
|---|---|---|---|---|---|
| Rabbit-anti-mouse TCF1/TCF7 | Primary antibody | 1:100 | C.725.7 | Invitrogen | MA5-14965 |
| Rat-IgG2α-κ isotype-control | eF660 | 1:100 | eBR2a | Invitrogen | 50-65 02-82 |
| TCF1/TCF7 | PE | 1:40 | S33-966 | BD Pharmingen | 564217 |
| TCRβ | PerCP-Cy5.5 | 1:100 | H57-597 | Biolegend | 109227 |
| TNFα | PE-Cy7 | 1:100 | MP6-XT22 | Invitrogen | 25-73 21-82 |
| TotalSeq-C 0301 | Oligo-seq: ACCCACCA GTAAGAC | 1:250 | M1/42;30-F11 | Biolegend | 155861 |
| TotalSeq-C 0302 | Oligo-seq: GGTCGAGA GCATTCA | 1:250 | M1/42;30-F11 | Biolegend | 155863 |
| TotalSeq-C 0303 | Oligo-seq: CTTGCCGC ATGTCAT | 1:250 | M1/42;30-F11 | Biolegend | 155865 |
| TotalSeq-C 0304 | Oligo-seq: AAAGCATTC TTCACG | 1:250 | M1/42;30-F11 | Biolegend | 155867 |
| TOX | eF660 | 1:100 | TXRX10 | Invitrogen | 50-65 02-82 |

### 3.1.9 Additional material

**Table 10: List of additional materials.**

| Material | Manufacturer | Catalog number |
|---|---|---|
| 150 mm cell culture dish | Merck | CLS430599 |
| 26Gx1” needles | Braun | 4665457 |
| 30 *µ*m cell strainer | Miltenyi Biotec | 130-110-915 |
| 48-well suspension cell plate | Greiner Bio-one | 677102 |
| 70 *µ*m cell strainer | Miltenyi Biotec | 130-110-916 |
| 96-well v bottom plate | Thermo Fisher Scientific | 277143 |
| CountBright absolute counting beads | Thermo Fisher Scientific | C36950 |
| GentleMACS M tubes | Miltenyi Biotec | 130-093-236 |
| Heparin tubes | Sarstedt | 20.1291 |
| Lancet | VWR | SARS85.1017 |

### 3.1.10 Quantitative real-time PCR primers

**Table 11: List of primers for real-time PCR.**

| Primer sequence (3´to 5´), target | Source | Manufacturer |
|---|---|---|
| CGCTTGTCCACGTAGTGGCT, *Ptger4* (reverse) | Bayerl et al., 2023, Immunity | Eurofins |
| GCCTAAGATGAGCGCAAGTTG, *Hprt* (forward) | Bayerl et al., 2023, Immunity | Eurofins |
| TACTAGGCAGATGGCCACAGG, *Hprt* (reverse) | Bayerl et al., 2023, Immunity | Eurofins |
| TTTCTTCGGTCTGTCGGGTC, *Ptger4* (forward) | Bayerl et al., 2023, Immunity | Eurofins |

### 3.1.11 CRISPR-Cas9-gRNA sequences

**Table 12: List of guide-RNA sequences**

| gRNA sequence (3´to 5´), target | Source | Manufacturer |
|---|---|---|
| GCCTGCCCTAAACCCCGGAA, no target (as crRNA, mock) | N/A | IDT |
| TATGTCAAGGAGGTCCACGG and CTGGGAACGACCCGAGGATC, *Cd122* | N/A | IDT |

### 3.1.12 Sequencing data

The data from RNA, single cell RNA (scRNA), and scTCR sequencing has been deposited in the gene expression omnibus (GEO) database under the SuperSeries number GSE231340 (SubSeries numbers: GSE231301 and GSE231302) and are publicly available.

## 3.2 Methods

### 3.2.1 Crossbreeding of mice

All mice used in this work were of C57BL/6J origin and if not stated otherwise, on a CD45.2/CD45.2 background. OT-I (CD45.1) mice were generated through the crossbreeding of OT-I mice with CD45.1 mice. To obtain *Ptger2*$^{-/-}$*Ptger4*$^{fl/fl}$ mice, *Ptger2*$^{-/-}$ and *Ptger4*$^{fl/fl}$ mice were crossed. These mice were subsequently bred with either *CD4*$^{Cre}$, *GzmB*$^{Cre}$, and OT-I mice to generate *CD4*$^{Cre}$*Ptger2*$^{-/-}$*Ptger4*$^{fl/fl}$, *GzmB*$^{Cre}$*Ptger2*$^{-/-}$*Ptger4*$^{fl/fl}$, and *Ptger2*$^{-/-}$*Ptger4*$^{fl/fl}$ OT-I (CD45.1/CD45.1), respectively. For the generation of *CD4*$^{Cre}$*Ptger2*$^{-/-}$*Ptger4*$^{fl/fl}$ OT-I (CD45.1/CD45.2) mice, *CD4*$^{Cre}$*Ptger2*$^{-/-}$*Ptger4*$^{fl/fl}$ were crossed with OT-I (CD45.1) mice. Notably, no mouse strain used in this study exhibited any pathologies or abnormalities throughout the breeding and housing process.

### 3.2.2 Cell lines and tissue culture

BRAF$^{V600E}$ (control) and *Ptgs1/Ptgs2*$^{-/-}$ BRAF$^{V600E}$ melanoma cells were created using the CRISPR/Cas9 system based on established techniques and were generously given by Caetano Reis e Sousa[59,62]. Lentiviral transduction was employed to generate BRAF$^{V600E}$-OVA and *Ptgs1/Ptgs2*$^{-/-}$ BRAF$^{V600E}$-OVA cells, as previously outlined in detail by Bayerl et al.[62]. In brief, the OVA cDNA was incorporated into a pHIV-7 transfer vector containing the phosphoglycerate kinase (PGK) promoter and an internal ribosome entry site (IRES)-puromycin-N-acetyltransferase (PAC) sequence, which led to the expression of both OVA cDNA and PAC. PAC mediates puromycin resistance through the acetylation of puromycin[170]. The third-generation lentiviral vectors were produced, which were self-inactivating and pseudotyped with the vesicular stomatitis virus-glycoprotein (VSV-G) to enable clathrin-mediated uptake through the recipient cells, following previously described procedures[171]. Packaging cells were transfected for 2 days, releasing viral particles into the supernatants. This supernatant was filtered and used to transduce tumor cell lines. To neutralize the charge repulsion between virions and the recipient cell surface, polybrene (8 µg/ml) was added to the culture, enhancing the lentiviral

infection rate. After 5 hours of incubation, the medium was replaced with fresh medium, and the transfected cells were passaged three times before antibiotic-mediated selection using puromycin.

Panc02 and MC38-OVA cells were generously provided by Veit Buchholz (Institute for Medical Microbiology, Immunology, and Hygiene, TUM), and the MC38 cell line was provided by Achim Krüger (Institute of Experimental Oncology, TUM).

$BRAF^{V600E}$, *Ptgs1/Ptgs2*$^{-/-}$ $BRAF^{V600E}$, $BRAF^{V600E}$-OVA, and *Ptgs1/Ptgs2*$^{-/-}$ $BRAF^{V600E}$-OVA cells were cultured in Roswell Park Memorial Institute (RPMI) 1640 medium, which was supplemented with 10% fetal calf serum (FCS), 50 µM β-mercaptoethanol, 50 Units (U)/ml penicillin, 50 mg/ml streptomycin, and 2 mM L-glutamine (complete-RPMI). D4M.3A-pOVA cells were generously given to us by Mauro Di Pilato and cultured in Dulbecco´s Modified Eagle´s Medium (DMEM)/F12[172]. MC38, MC38-OVA, and Panc02 cells were cultured in DMEM medium. Both the DMEM/F12 and DMEM were supplemented with 10% FCS, 50 µM β-mercaptoethanol, 50 U/ml penicillin, 50 mg/ml streptomycin, 2 mM L-glutamine, 1x MEM non-essential amino acids solution, and 1 mM sodium pyruvate.

0.05% trypsin/ethylenediaminetetraacetic acid (EDTA) was used to detach and split the cells. All cell lines were cultured in 150 mm tissue culture dishes at 37 °C and 5% $CO_2$.

### 3.2.3 Tumor cell inoculation and measurement of tumor size

Tumor cell lines with 80 to 90% confluency were trypsinized, washed three times with sterile phosphate-buffered saline (PBS), counted using a Neubauer counting chamber, and diluted in sterile PBS. Unless specified otherwise, recipient mice received subcutaneous (s.c.) injections on their shaved flanks with $2x10^6$ cells suspended in 100 µl of sterile PBS. To inoculate the tumor cells, 1 ml syringes with 26Gx1” needles were used.

The tumor diameters indicated in the figures correspond to the arithmetic means of each tumor's longest diameter and its perpendicular counterpart, measured using a digital caliper.

### 3.2.4 *In vivo* depletion of CD4$^+$ and CD8$^+$ T cells

Starting from day 1 after tumor cell transplantation, mice received intraperitoneal (i.p.) injections of 100 µl of anti-mouse CD4 (100 µg/mouse) or anti-mouse CD8β (100 µg/mouse) antibodies every 5 days to deplete CD4$^+$ or CD8$^+$ T cells, respectively.

### 3.2.5 *In vivo* FTY720 administration

Mice were injected i.p. with 100 µl FTY720 (20 µg/mouse, diluted in sterile isotonic NaCl) on day 1 or day 6 after tumor cell inoculation. As a control, 100 µl sterile isotonic NaCl was administered.

### 3.2.6 *In vivo* blockade of IL-2 receptor signaling

Mice were injected i.p. with 150 µL anti-mouse CD122/IL-2Rβ (300 µg/mouse, diluted in sterile isotonic NaCl) and anti-mouse CD132/IL-2Rγc (300 µg/mouse, diluted in sterile isotonic NaCl) antibodies on day 6 and day 7 after tumor cell transplantation. As a control, 150 µL sterile isotonic NaCl was injected.

### 3.2.7 Tissue processing for flow cytometry and cell sorting

At indicated time points after tumor cell inoculation, tumors, lymph nodes, and spleens were excised, and their weights were determined using a microscale. For further analyses involving flow cytometry or cell sorting, tumors were mechanically cut with scissors for a minimum of 3 minutes and subsequently disaggregated by incubating them in 1 ml of digestion medium containing collagenase IV (200 U/ml) and DNaseI (100 µg/ml) at 37 °C for 40 minutes. After incubation, digestion was stopped by adding 1 ml of cold FACS buffer (1x PBS, 1% FCS, and 2 mM EDTA). The digested tumors were filtered through both a 70 µm and a 30 µm cell strainer, generating single-cell suspensions. Lymph nodes were filtered using a 30 µm cell strainer, and for the

isolation of migratory cDC1 cells, the lymph nodes underwent the same processing steps as outlined for tumor tissues.

Spleens were passed through a 70 $\mu$m cell strainer and incubated in ammonium-chloride-potassium (ACK) lysis buffer for 3 minutes at room temperature (RT) to lyse red blood cells. After the incubation phase, red blood cell lysis was stopped by adding FACS buffer, and the cells were filtered through a 30 $\mu$m cell strainer.

For the adoptive T cell transfers, blood from mice was drawn by puncturing the submandibular (facial) vein using a lancet. Blood samples were obtained using heparin-coated tubes, followed by the lysis of red blood cells in ACK lysis buffer for 10 minutes at RT. Red blood cell lysis was stopped by adding FACS buffer.

### 3.2.8 Flow cytometry and cell sorting

For surface staining and the assessment of cell viability, cells were stained in FACS buffer containing fluorophore-conjugated antibodies specifically targeting surface molecules, along with a fixable viability dye capable of crossing dead cell membranes. Stains were protected from light and carried out at 4 °C for 15 minutes. When staining the SIINFEKL:MHC class I complex on cDC1 to determine the OVA cross-presentation, cells were stained for a total of 40 minutes. Cells were washed three times in FACS buffer (600 x gravitational force equivalent (*g*), 4 °C, 3 minutes) before conducting flow cytometry, cell sorting, or intracellular staining.

Intracellular assessment of STAT5 phosphorylation was done by fixing and permeabilizing the cells using BD cytofix and BD phosflow perm buffer III, abiding by the manufacturer´s recommended protocols (BD protocol II and III for mild or harsh alcohol method). Cells were stained for pSTAT5 in FACS buffer for 1 hour at RT and washed thrice in FACS buffer (1000 x *g*, 4 °C, 5 minutes) before flow cytometric analysis.

Intracellular staining of Ki-67, TCF1, GzmB, and TOX was carried out after fixation and permeabilization of cells using the true-nuclear transcription factor buffer set following the manufacturer´s protocol. Intracellular stains were

conducted overnight in permeabilization buffer at 4 °C. Cells were washed thrice in FACS buffer (700 x *g*, 4 °C, 5 minutes) before flow cytometric analysis.
To determine the incorporation of 5-ethynyl-2´-deoxyuridine (EdU) into newly synthesized DNA, the EdU proliferation kit (iFluor 488) was used following the manufacturer´s methods. EdU was added to CD8 T cell cultures at a final concentration of 15 $\mu$M 3 hours before conducting cell surface and intracellular staining.
Before analysis using flow cytometry, countbright absolute counting beads were added to samples for assessing cell quantities. All flow cytometric analyses were carried out on an SP6800 spectral analyzer, an SA3800 spectral analyzer, or an LSRFortessa cell analyzer.
Intratumoral $CD8^+$ T cells ($LD^-CD45.2^+CD3^+CD8^+$), tumor-infiltrating stem-like *CD4$^{Cre}$Ptger2$^{-/-}$Ptger4$^{fl/fl}$* OT-I T cells ($LD^-$ $CD45.1^+CD8^+CD44^+$TIM-$3^-$(C-X-C motif chemokine receptor 6) $CXCR6^-$), and tumor-infiltrating differentiated effector *CD4$^{Cre}$Ptger2$^{-/-}$Ptger4$^{fl/fl}$* OT-I T cells (live $CD45.1^+CD8^+CD44^+$TIM-$3^+CXCR6^+$) were sorted using the FACS aria III cell sorter.
To perform adoptive T cell transfers, blood-derived naive OT-I T cells ($CD45.1^+CD8^+CD62L^+CD44^-$) were sorted using an SH800S cell sorter.

### 3.2.9 *Ex vivo* restimulation of tumor-infiltrating TIM-$3^+$ $CD8^+$ T cells

$BRAF^{V600E}$ and *Ptgs1/Ptgs2$^{-/-}$* $BRAF^{V600E}$ tumors from WT, *Ptger2$^{-/-}$Ptger4$^{fl/fl}$*, and *CD4$^{Cre}$Ptger2$^{-/-}$Ptger4$^{fl/fl}$* mice were isolated on day 11 after tumor cell transplantation. Tumor-infiltrating $CD8^+$ T cells were sorted ($LD^-CD45^+CD3^+CD8^+$). Subsequently, $CD8^+$ T cells were incubated for 1 hour with $\alpha$CD3/CD28 microbeads and brefeldin A (5 $\mu$g/ml) was added for an additional 3 hours of incubation. After stimulation, cells were surface stained, fixed, and intracellularly stained for TNF$\alpha$, and IFN$\gamma$.

### 3.2.10 Adoptive T cell transfer

For the adoptive T cell transfers of naive T cells, blood from OT-I (CD45.1/CD45.1) or *CD4$^{Cre}$Ptger2$^{-/-}$Ptger4$^{fl/fl}$* OT-I (CD45.1/CD45.2) mice was drawn and prepared as outlined in 3.2.7. Naive CD8$^+$ T cells were surface stained and sorted. 1x10$^3$ naive CD8$^+$ T cells were injected intravenously (i.v.) in 100 µl sterile NaCl into sex-matched recipient WT (CD45.2/CD45.2) mice using an insulin syringe. 6 hours later, the WT mice were s.c. inoculated with OVA-expressing tumor cells.

For the adoptive T cell transfer of CRISPR-Cas9-edited *in vitro* generated *CD4$^{Cre}$Ptger2$^{-/-}$Ptger4$^{fl/fl}$* OT-I T cells, 1x10$^3$ OT-I cells were injected i.v. into recipient mice 2 days after tumor cell inoculation.

### 3.2.11 Experimental setup to determine the effect of tumor-derived $PGE_2$ on CD8$^+$ T cell priming in draining lymph nodes

To examine whether tumor-derived $PGE_2$ affects CD8$^+$ T cell priming in tumor-draining lymph nodes (tdLNs), 1x10$^3$ naive OVA-specific CD45.1$^+$ OT-I T cells were isolated from OT-I mice, sorted, and adoptively transferred into WT recipient mice. WT mice then received 2x10$^6$ *Ptgs1/Ptgs2$^{-/-}$*-OVA or control BRAF$^{V600E}$-OVA cells into their flanks. As a control, WT mice received non-OVA-expressing *Ptgs1/Ptgs2$^{-/-}$* BRAF$^{V600E}$ tumor cells. After 6 days, tdLNs were isolated and stained for cDC1s cross-presenting OVA and antigen-specific OT-I T cells (**Figure 2**). Migratory cDC1s were identified as follows: LD$^-$CD45$^+$CD11c$^+$MHCII$^{hi}$CD103$^+$CD8α$^-$CD11b$^-$. The experiment involving the OVA-cross-presentation by cDC1s was performed in collaboration with Felix Bayerl (Institute of Molecular Immunology, School of Medicine, Technical University of Munich (TUM), Munich).

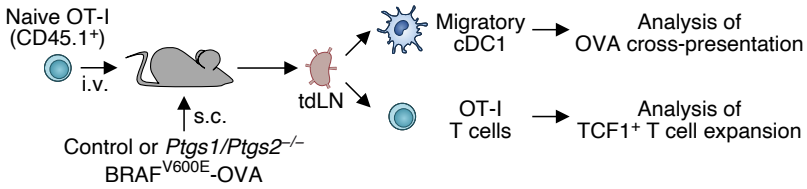


**Figure 2: Experimental setup to determine the effects of $PGE_2$ on CD8$^+$ T cell priming in tdLNs.**

### 3.2.12 Experimental setup to examine the proliferative capacity of retransferred intratumoral TCF1⁺ OT-I T cells

To determine whether the proliferation of intratumoral CD8⁺ T cells has their origin in the stem-like TCF1⁺ or the terminally differentiated TIM-3⁺CXCR6⁺ CD8⁺ T cell population, both populations were sorted from mice and retransferred. Therefore, 1x10$^3$ naive CD45.1⁺ *CD4$^{Cre}$Ptger2$^{-/-}$Ptger4$^{fl/fl}$* OT-I T cells were adoptively transferred into WT mice and challenged with 2x10$^6$ OVA-expressing MC38 tumor cells. 8 days later, tumors were harvested and 7x10$^3$ stem like (TIM-3$^-$CXCR6$^-$) or differentiated effector (TIM-3⁺CXCR6⁺) CD8⁺ T cells were sorted and separately retransferred into recipient *Rag1$^{-/-}$* mice, which had been challenged with 2x10$^5$ OVA-expressing MC38 tumor cells 2 days before the transfer. Tumors were then analyzed 8 days post-retransfer (**Figure 3**).

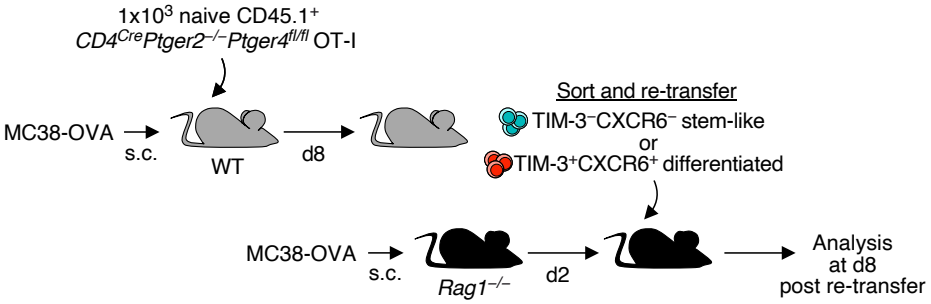


**Figure 3: Experimental setup to determine the expansion of retransferred intratumoral TCF1⁺ OT-I T cells.**

### 3.2.13 Generation of repetitively activated antigen-experienced TCF1⁺ and TCF1⁻ CD8⁺T cells

To generate repetitively activated antigen-experienced CD8⁺ T cells, spleens were separated and processed as described above, and subsequently, the naive CD8α⁺ T cell isolation kit was used to isolate naive CD8⁺ T cells following the manufacturer´s instructions. TCF1⁺CD8⁺ T cells were differentiated using the method previously outlined by Di Pilato et al., incorporating slight adaptations[173]. 1x10$^6$ naive CD8⁺ T cells were cultured in a 48-well suspension cell plate in T-cell-medium (RPMI 1640 medium, supplemented with 10% FCS, 50 µM β-mercaptoethanol, 100 U/ml penicillin, 100 mg/ml streptomycin, 2 mM L-glutamine, 1x MEM non-essential amino acids, and 1 mM sodium

pyruvate). To initiate TCF1$^+$CD8$^+$ T cell differentiation, low-dose IL-2 (85 U/ml) and mouse αCD3/CD28 microbeads were added to the culture. After 2 days, CD8$^+$ T cells were split in a 1:2 ratio and seeded while maintaining the same differentiation conditions. Following an additional 2-day differentiation period, TCF1$^+$CD8$^+$ T cells were purified for viability using density gradient centrifugation with pancoll (1,440 x *g*, 20 minutes, RT). To differentiate TCF1$^-$CD8$^+$ T cells, the same procedure was performed using high-dose IL-2 (350 U/ml) and IL-12 (10 ng/ml) instead.

### 3.2.14 TCF1$^+$CD8$^+$ T cell effector differentiation and expansion

Differentiation of antigen-experienced TCF1$^+$CD8$^+$ T cells into effector CD8$^+$ T cells was adapted from Di Pilato et al.,[173]. Both tumor-infiltrating TIM-3$^-$CD8$^+$ T cells sorted 11 days post-tumor cell inoculation from tumor-bearing mice and TCF1$^+$CD8$^+$ T cells were cultured in T-cell-medium with mouse αCD3/CD28 microbeads and high-dose IL-2. As specified in the figures, cultures were supplemented with $PGE_2$ (100 ng/ml, dissolved in 70% EtOH), IL-7 (10 ng/ml), IL-12 (10 ng/ml), or IL-15/15Rα (1 ng/ml). 70% EtOH served as a control for $PGE_2$. To evaluate T cell expansion, T cells (LD$^-$CD45.2$^+$CD3$^+$CD8$^+$) were quantified using flow cytometry 72 hours after the differentiation and proliferation had been initiated.

### 3.2.15 Restimulation of repetitively activated TCF1$^-$CD8$^+$ T cells

To determine the specific cytotoxicity, TCF1$^-$CD8$^+$ cells from both OT-I and WT mice were generated, pre-incubated for 20 hours with or without $PGE_2$, and then co-cultured with *Ptgs1/Ptgs2*$^{-/-}$BRAF$^{V600E}$-OVA cells at an effector to target ratio of 1:1. The impedance was measured every 15 minutes, using the xCELLigence-RTCA system.

### 3.2.16 IL-2Rβ knockout by CRISPR-Cas9-gRNA complex electroporation

Spleens of *CD4$^{Cre}$Ptger2$^{-/-}$Ptger4$^{fl/fl}$* OT-I were separated and processed, and subsequently, the naive CD8α$^+$ T cell isolation kit was used to isolate naive CD8$^+$ T cells following the manufacturer's instructions. Naive T cells were cultured in T-cell-medium supplemented with IL-2 (10 U/ml), IL-7 (5 ng/ml), and mouse αCD3/CD28 microbeads. After 24 hours, microbeads were removed by magnetic separation, and T cells were electroporated in P3 electroporation buffer supplemented with Cas9 protein, Cas9 electroporation enhancer, and *Cd122*-targeting or non-targeting (as mock) guide RNA as previously described[174]. After electroporation, cells were rested in T-cell-medium supplemented with IL-7 (5 ng/ml) for 2 days at 37 °C. Knockout specificity was confirmed by CD122 surface staining prior to i.v. injections. This step was performed in collaboration with Janina Dörr (Division of Clinical Pharmacology, Department of Medicine IV, Ludwig Maximilian University (LMU), Munich).

### 3.2.17 Analysis of IL-2 signaling and the expression of IL-2Rγc

5x10$^5$ repetitively stimulated antigen-experienced TCF1$^+$CD8$^+$ T cells were resuspended in 1 ml of T-cell-medium containing low-dose IL-2 and cultured in a 48-well suspension cell plate for 20 hours. After resting the cells, the medium was changed, and cells were seeded with mouse αCD3/CD28 microbeads and low-dose IL-2. CD8$^+$ T cells were incubated with or without $PGE_2$ (100 ng/ml) for 24 hours before analysis.

To evaluate the IL-2R expression, cells were harvested, stained for IL-2Rγc, and analyzed via flow cytometry.

To assess IL-2 signaling, magnetic separation was employed to remove mouse αCD3/CD28 microbeads, and subsequently, the cells were surface stained. To dephosphorylate pSTAT5, the TCF1$^+$CD8$^+$ T cells were incubated in T-cell-medium at 37 °C for 30 minutes. After dephosphorylation, the cells were stimulated with different concentrations of IL-2 (10-100 U/ml) in the absence or presence of $PGE_2$ (100 ng/ml) for 30 minutes before IL-2 signaling and phosphorylation of STAT5 was terminated by directly adding cytofix buffer. Cells were permeabilized, stained intracellularly, and analyzed by flow cytometry.

### 3.2.18 Determination of $PGE_2$ concentration in tissues

Tumors and organs were collected from mice 11 days after tumor cell inoculation. The weights of the samples were recorded, and the tissues were immediately frozen in liquid nitrogen and stored at -80 °C. A gentleMACS dissociator and gentleMACS M tubes were used to homogenize the samples, using a homogenization buffer consisting of 0.1 M PBS, 10 µM of the COX1/2 inhibitor indomethacin, 1 mM EDTA, which was adjusted to a pH of 7.4. The homogenization process was followed by a freeze-thaw cycle at -20 °C. $PGE_2$ concentrations were quantified using an ELISA assay in accordance with the manufacturer´s protocol. $PGE_2$ concentrations were normalized to tissue weight.

### 3.2.19 RNA isolation and quantitative real-time PCR

RNA extraction from T cell cultures was performed using the arcturus PicoPure RNA isolation kit in accordance with manufacturer methods. cDNA was generated using the SensiFAST cDNA synthesis kit, according to the manufacturer´s protocol. Quantitative real-time PCR was conducted on a LightCycler 480 using the TAKYON No ROX SYBR master mix dTTP blue kit, following the manufacturer´s protocol. For calculating the relative fold gene expression of *Ptger4*, the ΔCt method ($2^{-\Delta\Delta Ct}$) was used with *Hypoxanthine-phosphoribosyl-transferase 1* (*Hprt*) as a reference gene.

### 3.2.20 RNA sequencing

$TCF1^+CD8^+$ T cells were generated and incubated in T-cell-medium with or without $PGE_2$ (100 ng/ml) at 37 °C for 1 hour. After the initial incubation, $CD8^+$ T cells were stimulated with low-dose IL-2 or low-dose IL-2 and mouse αCD3/CD28 microbeads for an additional 4 hours. Total RNA was isolated using the total RNA miniprep kit, following the manufacturer´s protocol. The isolated RNA was sent to Novogene for library preparation and sequencing.

For a comprehensive description of the analysis of the acquired RNA sequencing data, please refer to the related work by Lacher et al., 2024. In brief, library preparation was performed using the NEB Next® Ultra™ RNA

library prep kit. Sequencing was carried out on a NovaSeq6000 PE150 platform in paired-end mode using the corresponding Illumina sequencing kits. After aligning the obtained reads to the mouse reference genome (GRCm38/mm10), the gene expression levels and the fragments per kilobase of transcript sequence per million mapped reads (FPKMs) were determined. Genes identified by the DESeq2 R package 1.20.0 with adjusted *P*-values (*P*)≤ 0.05 were considered differentially expressed genes (DEGs). Principal component analysis (PCA) and volcano plots were visualized using the R packages ggplot2, prcomp, and ggrepel. Based on the log2 fold change values of the DEGs obtained from the comparison of the groups 'αCD3/CD28 + IL-2' and '$PGE_2$-treated + αCD3/CD28 + IL-2', the DEGs were arranged accordingly and subjected to gene set enrichment analysis (GSEA) to examine hallmark genes (mh.all.v2023.1.Mm). Normalized enrichment scores (NES) and significance by adjusted *P*-values were determined. Analysis of the RNA sequencing data was performed in collaboration with Felix Bayerl (Institute of Molecular Immunology, School of Medicine, Technical University of Munich (TUM), Munich).

### 3.2.21 Single-cell RNA and single-cell TCR sequencing

$BRAF^{V600E}$ tumor cells were inoculated into WT, *Ptger2*$^{-/-}$*Ptger4*$^{fl/fl}$, *CD4*$^{Cre}$*Ptger2*$^{-/-}$*Ptger4*$^{fl/fl}$, and *GzmB*$^{Cre}$*Ptger2*$^{-/-}$*Ptger4*$^{fl/fl}$ mice and 11 days later, tumors were excised and processed as outlined previously. In addition to the surface staining, all $CD45^+$ cells were labeled with TotalSeq-C anti-mouse hashtag antibodies which contained a unique oligonucleotide sequence (WT: Hashtag1, *Ptger2*$^{-/-}$*Ptger4*$^{fl/fl}$: Hashtag2, *CD4*$^{Cre}$*Ptger2*$^{-/-}$*Ptger4*$^{fl/fl}$: Hashtag3, and *GzmB*$^{Cre}$*Ptger2*$^{-/-}$*Ptger4*$^{fl/fl}$: Hashtag4). After cell hashing, 6,000 tumor-infiltrating $CD8^+$ T cells from one mouse of each experimental group were sorted and pooled, resulting in 4 biological replicates.

Each replicate was loaded on a chromium next GEM chip to generate gel bead-in-emulsion (GEM) partitions, effectively encapsulating each tiny micro-reaction within the chromium system. Within these GEMs, mRNA underwent transcription into cDNA through reverse transcription while being labeled with an additional 10x barcode. RNA sequencing libraries were

generated using the chromium next GEM single cell 5' reagent kits v2 user guide and the feature barcode technology for cell surface protein (Rev D). After evaluating the quality of the RNA sequencing libraries with the high-sensitivity DNA kit, a bioanalyzer 2100, and the qubit dsDNA HS assay kit, the libraries were combined into a pooled sample and subsequently submitted to Novogene for sequencing. The pooling of the samples aimed to minimize batch effects during sequencing. Paired-end sequencing was carried out on a NovaSeq6000 platform using an S4 v1.5 (300 cycles) sequencing kit. For gene expression, a minimum depth of $2x10^4$ reads per cell was sequenced, while for T cell receptor libraries, the sequencing depth targeted a minimum of $5x10^3$ reads per cell.

The first round of scRNA-seq analyses encompassed all samples within the *Ptger2*$^{-/-}$*Ptger4*$^{fl/fl}$, *CD4*$^{Cre}$*Ptger2*$^{-/-}$*Ptger4*$^{fl/fl}$, and *GzmB*$^{Cre}$*Ptger2*$^{-/-}$*Ptger4*$^{fl/fl}$ groups. Subsequently, data from the WT group was added in a later phase to validate the read coverage for *Ptger2* and *Ptger4* (refer to the details below).

For a more detailed and comprehensive analysis description of the obtained scRNA-seq and scTCR-seq data, I recommend referring to Lacher et al., 2024. In brief, gene expression libraries were aligned to the mouse reference genome mm10/GRCm38. To improve the data set's quality, cells that showed less than 1,000 detected genes, more than 10% of mitochondrial genes, and unique molecular identifier (UMI) counts more than 3 standard deviations above the mean were removed. UMIs are unique barcodes attached to each RNA molecule. They enable accurate quantification of transcript abundance and detection of PCR duplicates. UMIs provide a means to differentiate individual RNA molecules and allow for more precise measurements of gene expression levels. To enhance the reliability of the analysis, genes detected in less than 3 cells were excluded. Subsequently, the read counts of the remaining genes were normalized, ensuring a standardized basis for comparisons. The identification of anchors between cells originating from different replicates enabled data integration. Subsequently, PCA was performed on the integrated data to capture the major sources of variation. A k-nearest neighbors (KNN) graph was constructed to visualize the relationships between cells, and a uniform manifold approximation and projection (UMAP) was computed. Louvain

clusters (cl.) were identified using the shared nearest neighbor (SNN) modularity optimization algorithm. This approach leverages the SNN method to calculate the similarity between cells based on their shared neighbors and then optimizes the modularity metric to assign cells into clusters. Contaminating myeloid and cycling cells were detected by evaluating the average marker gene expression within the clusters, followed by their removal from the data set. After the initial data preprocessing and removal of contaminating cells, read counts were normalized independently, and anchors between cells from different experimental groups and their replicates were identified. Subsequently, PCA was computed on the integrated data, followed by the calculation of a KNN graph and a UMAP projection. Additionally, Louvain clusters were determined using the SNN modularity optimization algorithm.

DEGs were determined, and gene set expression scores were computed at a single-cell level, considering only the detected genes.

Gene profiles were acquired from Kaech et al., 2002 (M3013: KAECH_NAIVE_VS_DAY8_EFF_CD8_TCELL_DN) and MSigDB (GO:2000566) to visualize the signatures associated with $CD8^+$ T cell effector function and proliferation, respectively[175]. Based on the UMAP computed on the integrated data, transcriptional trajectories among clusters were determined, and pseudotime analysis was calculated. Transcription factor (TF) activity was determined using the weighted mean method, considering TF-target interactions with confidence levels ranging from A to C. The TF activity scores were normalized to the *Ptger2*$^{-/-}$*Ptger4*$^{fl/fl}$ experimental group. A network visualization was created using the top 100 variable TFs from each group, focusing on TFs with a minimum of 2 common targets.

Clonotypes for TCR analysis were determined by considering both the V(D)J genes and the nucleotide sequences of the CDR3 regions of the TCR.

To integrate scRNA-seq data from the WT group, initial pre-processing was conducted on the samples, following the previously outlined procedure. These pre-processed samples were aligned with a reference data set, which was formed by integrating data from the *Ptger2*$^{-/-}$*Ptger4*$^{fl/fl}$, *CD4*$^{Cre}$*Ptger2*$^{-/-}$*Ptger4*$^{fl/fl}$, and *GzmB*$^{Cre}$*Ptger2*$^{-/-}$*Ptger4*$^{fl/fl}$ groups using the R package Seurat v4.1.1[176].

The integration process involved identifying anchors between cells from the reference and the WT groups, as well as all replicates. This was achieved through reciprocal PCA on the top 1000 highly variable genes, selecting anchors based on the first 20 dimensions and a single neighbor. Following this, annotations were transferred using the *TransferData* function, and data integration was performed using *IntegrateEmbeddings*. Subsequently, cells from the additional WT group were then projected onto the coordinates of the reference UMAP using *ProjectUMAP* with 30 nearest neighbors.

For estimating read coverage, deepTools (v3.5.4) was employed, utilizing *bamCoverage* with a bin size of 10 bp and normalization by bins per million mapped reads[177]. Specifically, to analyze coverage on *Tcf7*$^{+}$ and *Tcf7*$^{-}$ clusters, BAM files were divided by cell barcodes from clusters 1-2 or clusters 3-8 using samtools v1.13 before estimating coverage[178]. The resulting read coverage on gene tracks was visualized using the R package trackViewer v1.32.1[179]. Analysis of the scRNA-seq and scTCR-seq Analysis of the RNA sequencing data was performed in collaboration with Gustavo P. de Almeida (Division of Animal Physiology and Immunology, School of Life Sciences Weihenstephan, TUM, Freising).

### 3.2.22 Statistical analyses

Statistical analyses were performed using GraphPad prism. The dissimilarities between 2 experimental groups were assessed using an unpaired two-tailed student´s t-test. Statistical significance was determined using ANOVA for comparisons involving more than two experimental groups and tumor growth profiles. The data are presented as mean ± standard deviation (SD) or mean ± standard error of the mean (SEM) as specified in the figure legends.

# 4 Results

## 4.1 The $PGE_2$-EP2/EP4 axis impairs anti-cancer $CD8^+$ T cell responses

Numerous human and mouse tumors exhibit abnormal COX-1 (encoded by *Ptgs1*) and COX-2 (encoded by *Ptgs2*) activity, resulting in increased production of the bioactive lipid $PGE_2$. Beyond its physiological functions, $PGE_2$ has been linked to the advancement of tumors and unfavorable outcomes for patients, indicating its involvement in tumor progression and diminished survival rates[65,98,180]. The ablation of COX-1 and COX-2 in several mouse cancer models has been shown to impede cancer advancement, primarily facilitated through immune-mediated control. These findings emphasize the pivotal role of $PGE_2$ and its immunomodulatory functions within the context of tumors[59,60]. $PGE_2$ signaling is mediated by binding to 4 G-protein coupled receptors known as EP1-EP4 (encoded by *Ptger1*-*Ptger4*). Notably, signaling through EP2 and EP4 has been identified to mediate direct immune suppressive functions[62,181]. Within the last few years, several studies have identified $PGE_2$ as a critical regulator influencing the biology and function of $CD8^+$ T cells[182–184]. However, the mechanisms through which $PGE_2$ may contribute to tumor immune evasion and the specific influence of tumor-derived $PGE_2$ on the regulation of infiltrating stem-like $TCF1^+CD8^+$ T cells remain unclear and warrant further investigation.

To this end, a novel mouse line has been developed to selectively inhibit the $PGE_2$-EP2/EP4 axis in $CD8^+$ T cells. The *Cre-loxP*-system was used to generate $CD4^{Cre}Ptger2^{-/-}Ptger4^{fl/fl}$ mice. In this mouse model, the active Cre-recombinase triggers the ablation of *Ptger4* expression in both $CD4^+$ and $CD8^+$ T cells, as they were double positive for both coreceptors during their maturation in the thymus. To specifically address the impact of $PGE_2$ on more differentiated $CD8^+$ T cells, $GzmB^{Cre}Ptger2^{-/-}Ptger4^{fl/fl}$ mice were generated. In these mice, GzmB-expressing cells, including effector $CD8^+$ T cells, lack *Ptger4* expression. As genetic controls, global EP2 deficient mice ($Ptger2^{-/-}Ptger4^{fl/fl}$) were used.

To determine whether the transgenic mouse models show an altered CD4+ or CD8+ T cell composition, inguinal lymph nodes and the spleens of healthy wildtype (WT), *Ptger2*$^{-/-}$*Ptger4*$^{fl/fl}$, *CD4*$^{Cre}$*Ptger2*$^{-/-}$*Ptger4*$^{fl/fl}$, and *GzmB*$^{Cre}$Ptger2$^{-/-}$*Ptger4*$^{fl/fl}$ were harvested and analyzed. Neither CD4+ nor CD8+ T cell numbers in inguinal lymph nodes or the spleens were significantly altered among the transgenic mice compared to WT (**Figure 4**).

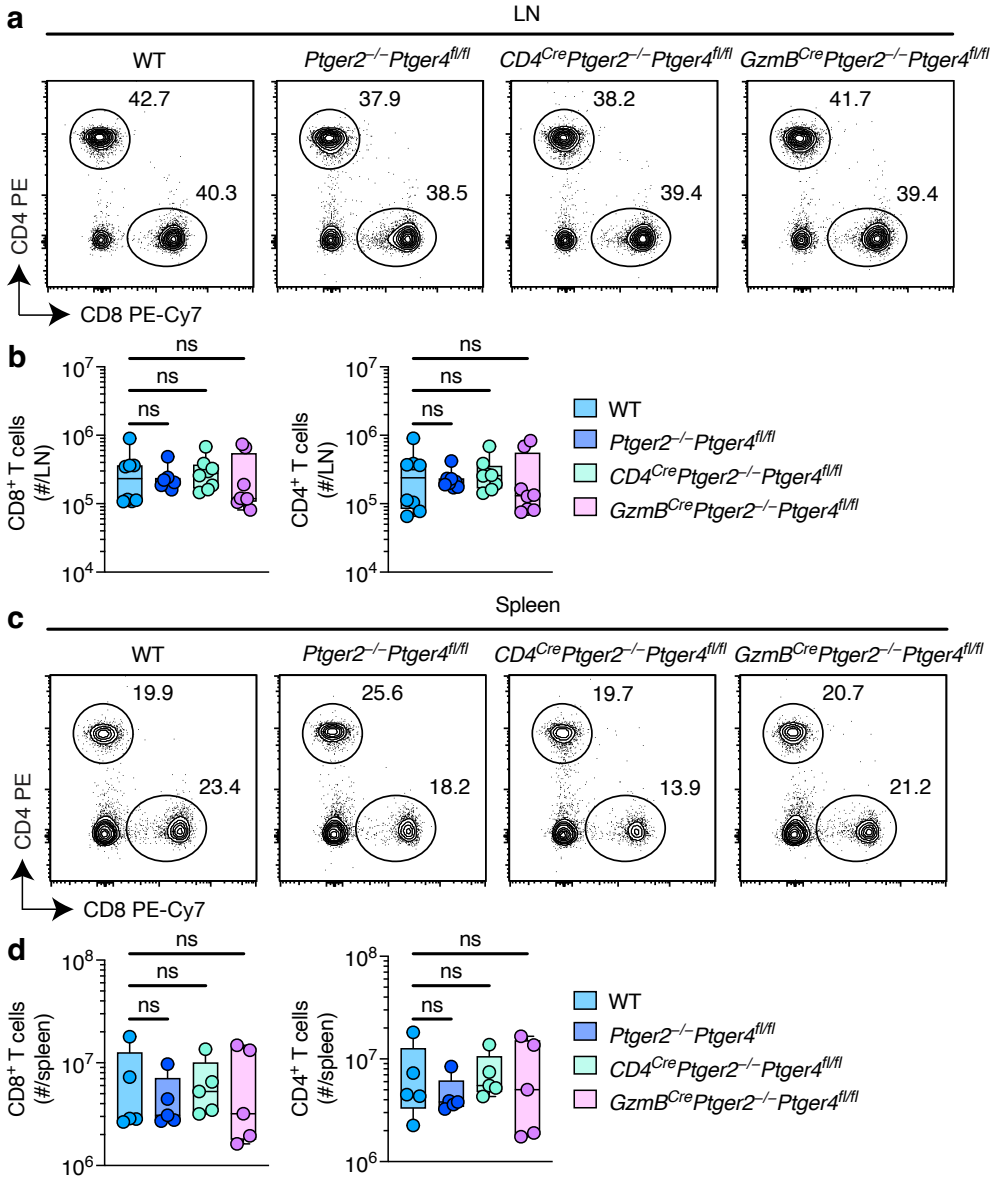


**Figure 4: Characterization of WT, *Ptger2*$^{-/-}$*Ptger4*$^{fl/fl}$, *CD4*$^{Cre}$*Ptger2*$^{-/-}$*Ptger4*$^{fl/fl}$, and *GzmB*$^{Cre}$*Ptger2*$^{-/-}$*Ptger4*$^{fl/fl}$ mice in their T cell numbers. (a)** Representative flow cytometry plots showing frequencies of CD4+ and CD8+ T cells among pre-gated CD45+ immune cells in inguinal lymph nodes of WT, *Ptger2*$^{-/-}$*Ptger4*$^{fl/fl}$, *CD4*$^{Cre}$*Ptger2*$^{-/-}$*Ptger4*$^{fl/fl}$, and *GzmB*$^{Cre}$*Ptger2*$^{-/-}$*Ptger4*$^{fl/fl}$ mice. n=5-8, two independent experiments were pooled. **(b)** Quantification of total numbers of CD4+ and CD8+ T cells per inguinal LN based on **(a)**. **(c)** Representative flow cytometry plots showing frequencies of CD4+ and CD8+ T cells among pre-gated immune cells in spleens of WT, *Ptger2*$^{-/-}$*Ptger4*$^{fl/fl}$, *CD4*$^{Cre}$*Ptger2*$^{-/-}$*Ptger4*$^{fl/fl}$, and *GzmB*$^{Cre}$*Ptger2*$^{-/-}$*Ptger4*$^{fl/fl}$ mice. n=5-8, two independent experiments were pooled. **(d)** Quantification of total numbers of CD4+ and CD8+ T cells per spleen based on **(c)**. Box plots in **(b)** and **(d)** showing the median with corresponding min and max values as whiskers. Statistical significance in **(b)** and **(d)** was determined by one-way ANOVA with Dunnett´s multiple comparison test, $P \geq 0.05$, not significant (ns).

When WT, *Ptger2*$^{-/-}$*Ptger4*$^{fl/fl}$, and *CD4*$^{Cre}$*Ptger2*$^{-/-}$*Ptger4*$^{fl/fl}$ mice were challenged with $PGE_2$-producing (control) BRAF$^{V600E}$ melanoma, *CD4*$^{Cre}$*Ptger2*$^{-/-}$*Ptger4*$^{fl/fl}$ mice exhibited efficient tumor control over time (**Figure 5a**). In contrast, both WT and *Ptger2*$^{-/-}$*Ptger4*$^{fl/fl}$ mice did not show protective tumor control. This suggests that $PGE_2$ signaling on CD8$^+$ T cells leads to tumor immune escape, which the ablation of EP2 and EP4 in T cells can overcome. In line with this, non-$PGE_2$-producing COX1/2-deficient (*Ptgs1/Ptgs2*$^{-/-}$) BRAF$^{V600E}$ tumors were entirely rejected in WT mice, indicating that $PGE_2$ drives the escape from immune surveillance (**Figure 5a**). To determine whether this increased immune response is CD8$^+$ T cell-driven, WT mice and *Rag1*$^{-/-}$ mice (lacking T cells) were challenged with *Ptgs1/Ptgs2*$^{-/-}$ BRAF$^{V600E}$ tumor cells. Furthermore, a subset of WT mice was treated with CD8$^+$ T cell-depleting antibodies (**Figure 5b**). Only fully immune-competent WT mice were able to reject the non-$PGE_2$-producing tumors completely, confirming the pivotal role of CD8$^+$ T cells in mediating protective anti-cancer responses. To validate previous findings that $PGE_2$ drives tumor immune escape, Panc02 cells—a second $PGE_2$-producing tumor cell line—were injected into WT, *Ptger2*$^{-/-}$*Ptger4*$^{fl/fl}$, and *CD4*$^{Cre}$*Ptger2*$^{-/-}$*Ptger4*$^{fl/fl}$ mice (**Figure 5c**).

Consistently, tumors progressively grew in WT and *Ptger2*$^{-/-}$*Ptger4*$^{fl/fl}$ mice, whereas *CD4*$^{Cre}$*Ptger2*$^{-/-}$*Ptger4*$^{fl/fl}$ mice showed full tumor rejection (**Figure 5c**).

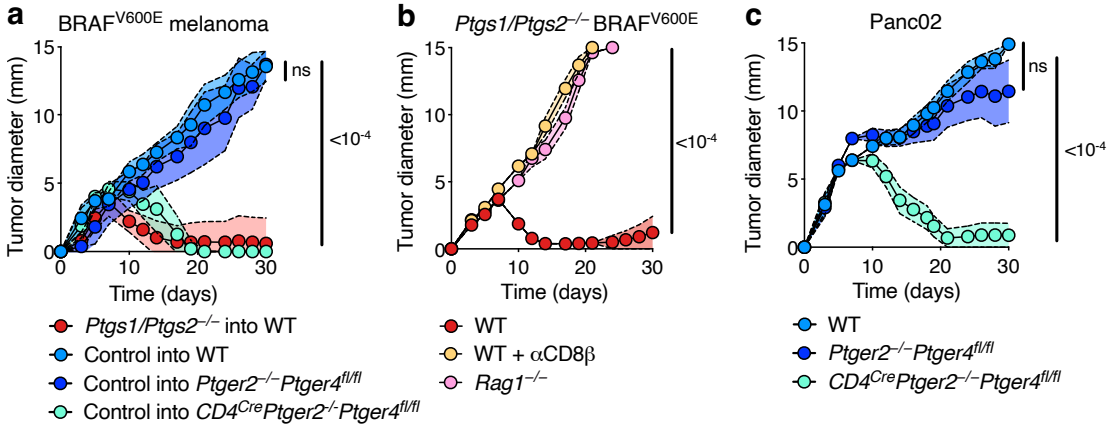


**Figure 5: EP2/EP4 knockout in CD8$^+$ T cells mediates immune control of $PGE_2$-producing tumors.** **(a)** Tumor growth profiles. 2x10$^5$ *Ptgs1/Ptgs2*$^{-/-}$ or control BRAF$^{V600E}$ melanoma cells were injected into the flanks of WT, *Ptger2*$^{-/-}$*Ptger4*$^{fl/fl}$, or *CD4*$^{Cre}$*Ptger2*$^{-/-}$*Ptger4*$^{fl/fl}$ mice. n=10, two independent experiments were pooled. **(b)** Tumor growth profiles. 2x10$^5$ *Ptgs1/Ptgs2*$^{-/-}$ BRAF$^{V600E}$ melanoma cells were injected into the flanks of WT or *Rag1*$^{-/-}$ mice. In some WT mice, CD8$^+$ T cells were depleted by injecting αCD8β depleting antibodies. n=5, two independent experiments were pooled. **(c)** Tumor growth profiles. 2x10$^6$ Panc02 tumor cells were injected into the flanks of WT, *Ptger2*$^{-/-}$*Ptger4*$^{fl/fl}$, or *CD4*$^{Cre}$*Ptger2*$^{-/-}$*Ptger4*$^{fl/fl}$ mice. n=8, two independent experiments were pooled. Data are depicted as mean ± SEM. Statistical significance in **(a)**-**(c)** was determined by one-way ANOVA with Dunnett´s multiple comparison test, $P \geq 0.05$, not significant (ns).

These findings validate that EP2/EP4 ablation in CD8⁺ T cells leads to potent immune control in $PGE_2$-producing tumors.

This increased immune response in *CD4$^{Cre}$Ptger2$^{-/-}$Ptger4$^{fl/fl}$* mice correlated with both increased numbers of tumor-infiltrating CD8⁺ T cells and increased CD8⁺ T cell frequencies among CD45⁺ immune cells (**Figure 6a**). In contrast, no significant differences were observed in the total counts of tumor-infiltrating CD4⁺ T cells and their frequencies among CD45⁺ cells (**Figure 6b**).

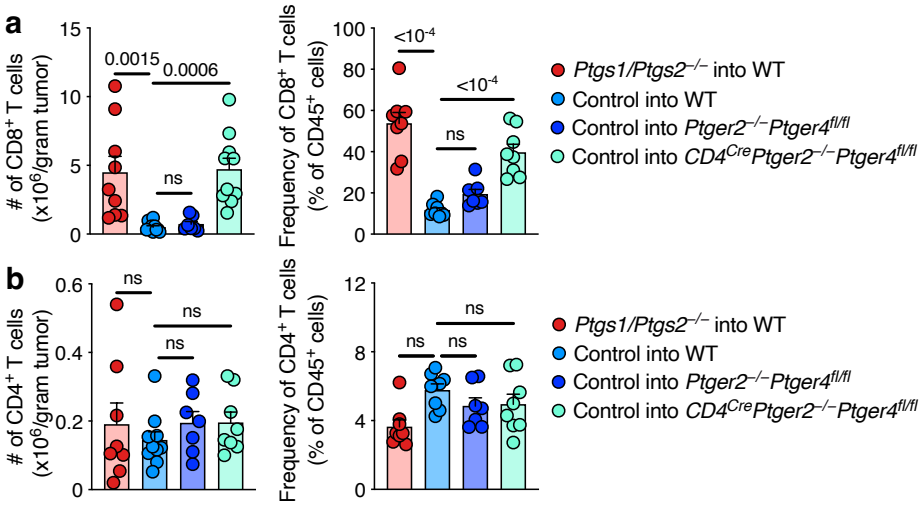


**Figure 6: Ablation of EP2/EP4 in CD8⁺ T cells results in increased CD8⁺ T cell accumulation in $PGE_2$-producing tumors. (a)** WT, *Ptger2$^{-/-}$Ptger4$^{fl/fl}$*, or *CD4$^{Cre}$Ptger2$^{-/-}$Ptger4$^{fl/fl}$* mice received 2x10$^6$ *Ptgs1/Ptgs2$^{-/-}$* or control BRAF$^{V600E}$ melanoma cells and CD8⁺ T cells numbers and frequencies of CD45⁺ cells were determined 11 days post tumor cell inoculation. n=10, two independent experiments were pooled. **(b)** CD4⁺ T cell numbers and frequencies of CD45⁺ cells were determined 11 days post tumor cell inoculation based on **(a)**. Data are depicted as mean ± SEM. Statistical significance was determined by one-way ANOVA with Dunnett´s multiple comparison test, $P \geq 0.05$, not significant (ns).

This implies that $PGE_2$ signaling on CD4⁺ T cells may not play a significant role in immune-mediated tumor control.

In line with these observations, antibody-mediated depletion of CD4⁺ and CD8⁺ T cells in *CD4$^{Cre}$Ptger2$^{-/-}$Ptger4$^{fl/fl}$* mice confirmed the critical role of CD8⁺ but not CD4⁺ T cells in mediating effective anti-cancer immune control (**Figure 7**).

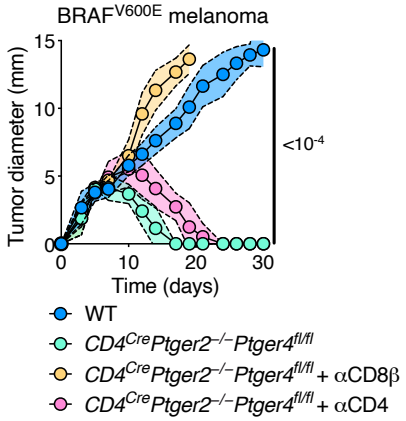


**Figure 7: Elevated tumor immune control in *CD4$^{Cre}$Ptger2$^{-/-}$Ptger4$^{fl/fl}$* mice is mediated by CD8$^{+}$ T cells.** Tumor growth profiles. 2x10$^{5}$ control BRAF$^{V600E}$ melanoma cells were injected into the flanks of *CD4$^{Cre}$Ptger2$^{-/-}$Ptger4$^{fl/fl}$* mice. CD4$^{+}$ and CD8$^{+}$ T cells were depleted with αCD4 and αCD8β depleting antibodies, respectively. n=8-9, two independent experiments were pooled. Data are depicted as mean ± SEM. Statistical significance was determined by two-way ANOVA Bonferroni's correction for multiple testing.

Taken together, these findings underscore the key role of tumor-infiltrating CD8$^{+}$ T cells, as opposed to CD4$^{+}$ T cells, in mediating robust anti-cancer immune responses and that $PGE_2$-EP2/EP4 signaling in CD8$^{+}$ T cells limits their intratumoral accumulation, thereby diminishing the efficacy of CD8$^{+}$ T cell-mediated immunity.

## 4.2 $CD8^+$ T cell priming in distal draining lymph nodes is not affected by tumor-derived $PGE_2$

Within the TME, cDC1s play a key role in initiating anti-cancer immune responses by taking up tumor antigens from their surroundings. This leads to their activation and subsequent migration to tdLNs. Within tdLNs, cDC1s cross-present tumor antigen fragments to naive $CD8^+$ T cells, resulting in T cell activation, which is known as priming. The activated $CD8^+$ T cells then migrate into the TME, where they exert their anti-cancer properties[61,84,185].

To investigate the impact of tumor-derived $PGE_2$ on the cross-presentation by cDC1s to naive $CD8^+$ T cells in tdLNs, WT mice were injected with *Ptgs1/Ptgs2*$^{-/-}$ and control $BRAF^{V600E}$-OVA tumor cells. These cancer cells express the model antigen OVA on their MHC I molecules, which is commonly used as a model for an antigen-specific immune response. Migratory $CD103^+$ cDC1s cross-presenting OVA-associated peptides were identified by flow cytometry using an antibody recognizing OVA-presenting MHC-I (S8:H-2Kb). Mice that received either *Ptgs1/Ptgs2*$^{-/-}$-OVA or control $BRAF^{V600E}$-OVA tumor cells showed increased frequencies of OVA-presenting cDC1s in their tdLNs when compared to mice that were challenged with non-OVA-expressing *Ptgs1/Ptgs2*$^{-/-}$ $BRAF^{V600E}$ tumor cells (**Figure 8a**). Furthermore, no substantial differences in the frequencies of cross-presenting cDC1s within tdLNs between the two experimental groups were observed, suggesting that tumor-derived $PGE_2$ may not affect distal cross-presentation by cDC1s (**Figure 8b**).

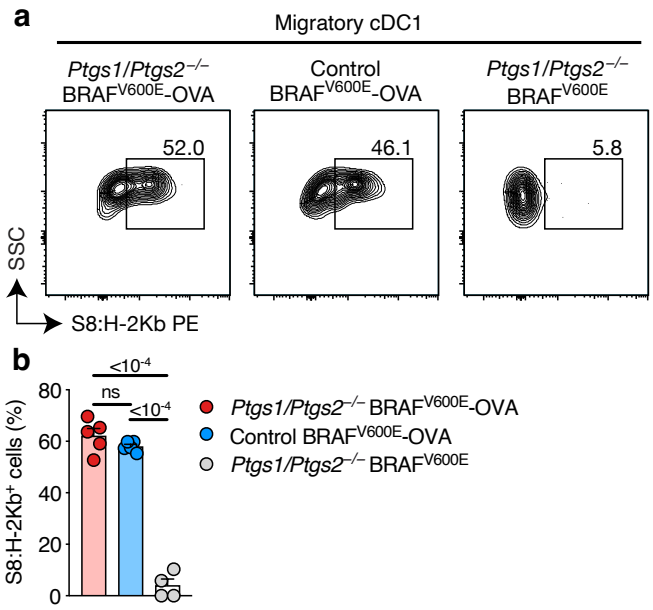


**Figure 8: Tumor-derived $PGE_2$ does not affect cross-presentation of OVA-peptides by cDC1s in tdLNs. (a)** Representative flow cytometry plots showing frequencies of OVA-presenting S8:H-2Kb$^+$ cells among pre-gated migratory cDC1s in tdLNs. **(b)** Frequencies of OVA-presenting cDC1s among pre-gated migratory cDC1s based on **(a)**. n=4-5. Data are depicted as mean ± SEM. Statistical significance in **(b)** was determined by one-way ANOVA with Tukey´s multiple comparison test. $P \geq 0.05$, not significant (ns).

To assess the efficacy of CD8$^+$ T cell priming within tdLNs, naive OT-I T cells were adoptively transferred into WT mice. These mice were then challenged with *Ptgs1/Ptgs2*$^{-/-}$-OVA or control BRAF$^{V600E}$-OVA tumor cells. OT-I T cells are CD8$^+$ T cells that harbor a transgenic TCR, specifically recognizing OVA-derived peptides presented on MHC-I. OT-I T cells in both groups showed an antigen-experienced CD44$^+$TCF1$^+$ phenotype, which was not observed for polyclonal non-antigen-specific CD8$^+$ T cells, which were predominantly naive (**Figure 9a**). Moreover, OT-I T cells efficiently expanded in both groups, indicating that CD8$^+$ T cell priming in distal tdLNs may not be affected by tumor-derived $PGE_2$ (**Figure 9b**).

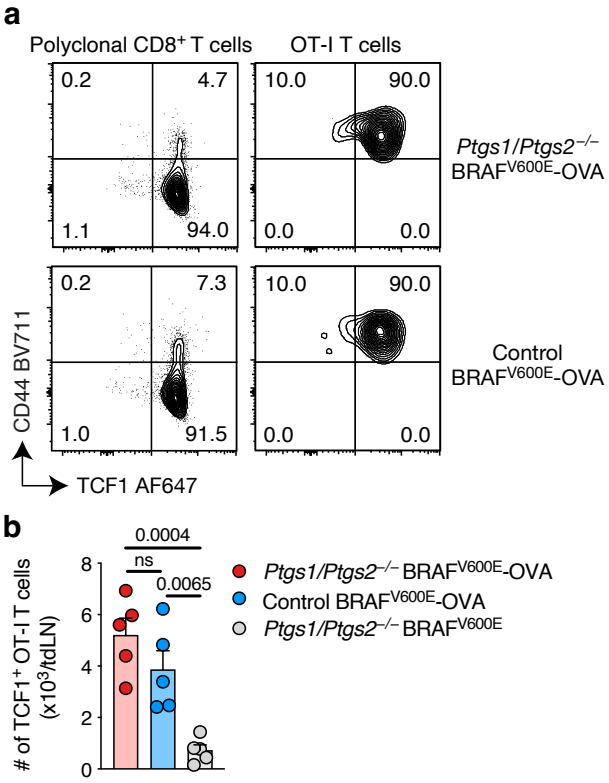


**Figure 9: Tumor-derived $PGE_2$ does not affect priming of $CD8^+$ T cells in tdLNs.**
**(a)** Representative flow cytometry plots showing the expression of TCF1 and CD44 in polyclonal $CD8^+$ T cells and OT-I T cells, pre-gated on $CD8^+$ T cells. **(b)** Quantification of total numbers of $CD44^+TCF1^+$ OT-I T cells corresponding to **(a)**. n=5. Data in **(b)** is depicted as mean ± SEM. Statistical significance in **(b)** was determined by one-way ANOVA with Tukey´s multiple comparison test. $P \geq 0.05$, not significant (ns).

To validate these results, WT mice were challenged with equilaterally transplanted *Ptgs1/Ptgs2*$^{-/-}$ and control $BRAF^{V600E}$ tumors, both sharing the same lymph drainage site. Co-transplanted *Ptgs1/Ptgs2*$^{-/-}$ tumors were rejected in mice while control tumors progressively grew (**Figure 10**).

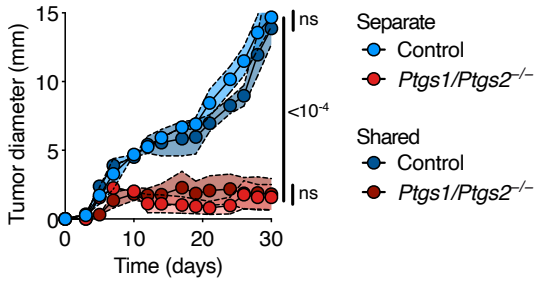


**Figure 10: Tumor-derived $PGE_2$ does not affect tumor control of non-$PGE_2$-producing tumors when the same lymph drainage site is shared.** Tumor growth profiles. WT mice received $2x10^5$ *Ptgs1/Ptgs2*$^{-/-}$ or control $BRAF^{V600E}$ melanoma cells either individually or in an equilateral manner sharing the same drainage lymph site. n=4, two independent experiments were pooled. Data are depicted as mean ± SEM. Statistical significance was determined by two-way ANOVA Bonferroni's correction for multiple testing. $P \geq 0.05$, not significant (ns).

Collectively, these results illustrate that the evasion of immune surveillance mediated by $PGE_2$ is a consequence of local effects without impacting the distal priming of $CD8^+$ T cells in tdLNs.

## 4.3 Tumor-infiltrating CD8$^+$ T cell expansion and differentiation are impaired by $PGE_2$-EP2/EP4 signaling

Recent advances in the cancer field have revealed distinct subtypes of tumor-infiltrating CD8$^+$ T cells which all express exhaustion markers such as PD-1 and TOX. However, despite their exhausted phenotype, these cells are still functional and can mediate protective anti-cancer immune responses[14,114-116]. In this work, 2 distinct populations were classified by their phenotype and functionality. Stem-like TCF1$^+$CD8$^+$ T cells (stem-like or 'exhausted'-like progenitor T cells) exhibit the capability to proliferate and differentiate. In contrast, TIM-3$^+$CD8$^+$(TCF1$^-$) T cells (terminally differentiated effector T cells, intermediate 'exhausted'-like T cells, and terminal 'exhausted'-like T cells) lack proliferative potential but fulfill cytotoxic effector functions. Extensive research has been dedicated to TCF1$^+$CD8$^+$ stem-like T cells, given their pivotal role in the generation of TIM-3$^+$CD8$^+$ effector T cells[122,124,186,187]. This process is crucial for anti-cancer immunity and occurs, at least partially, within the TME[121,122,188].

The previous results raised the question of whether $PGE_2$ might impact the local differentiation of TIM-3$^+$CD8$^+$ T cells originating from tumor-infiltrating stem-like TCF1$^+$CD8$^+$ T cells. To address this question, tumor-infiltrating CD8$^+$ T cells from *Ptger2*$^{-/-}$*Ptger4*$^{fl/fl}$ (as control) and *CD4*$^{Cre}$*Ptger2*$^{-/-}$*Ptger4*$^{fl/fl}$ mice were sorted from control BRAF$^{V600E}$ tumors 11 days post tumor cell injection. Subsequently, these cells were subjected to scRNA-seq and scTCR-seq. Additionally, tumor-infiltrating CD8$^+$ T cells from *GzmB*$^{Cre}$*Ptger2*$^{-/-}$*Ptger4*$^{fl/fl}$ mice were included to assess the influence of $PGE_2$ signaling on effector T cell differentiation. To address the heterogeneity in the analyses, 4 biological replicates were included for each experimental group. scRNA-seq revealed 8 distinct clusters (**Figure 11a**). Each cluster demonstrated an increased expression of the activation markers *Cd44*, *Tox*, and *Pdcd1* (encoding PD-1), which was further confirmed on the protein level, leading to the conclusion that all tumor-infiltrating CD8$^+$ T cells show an antigen-experienced and exhausted phenotype (**Figure 11b,c**).

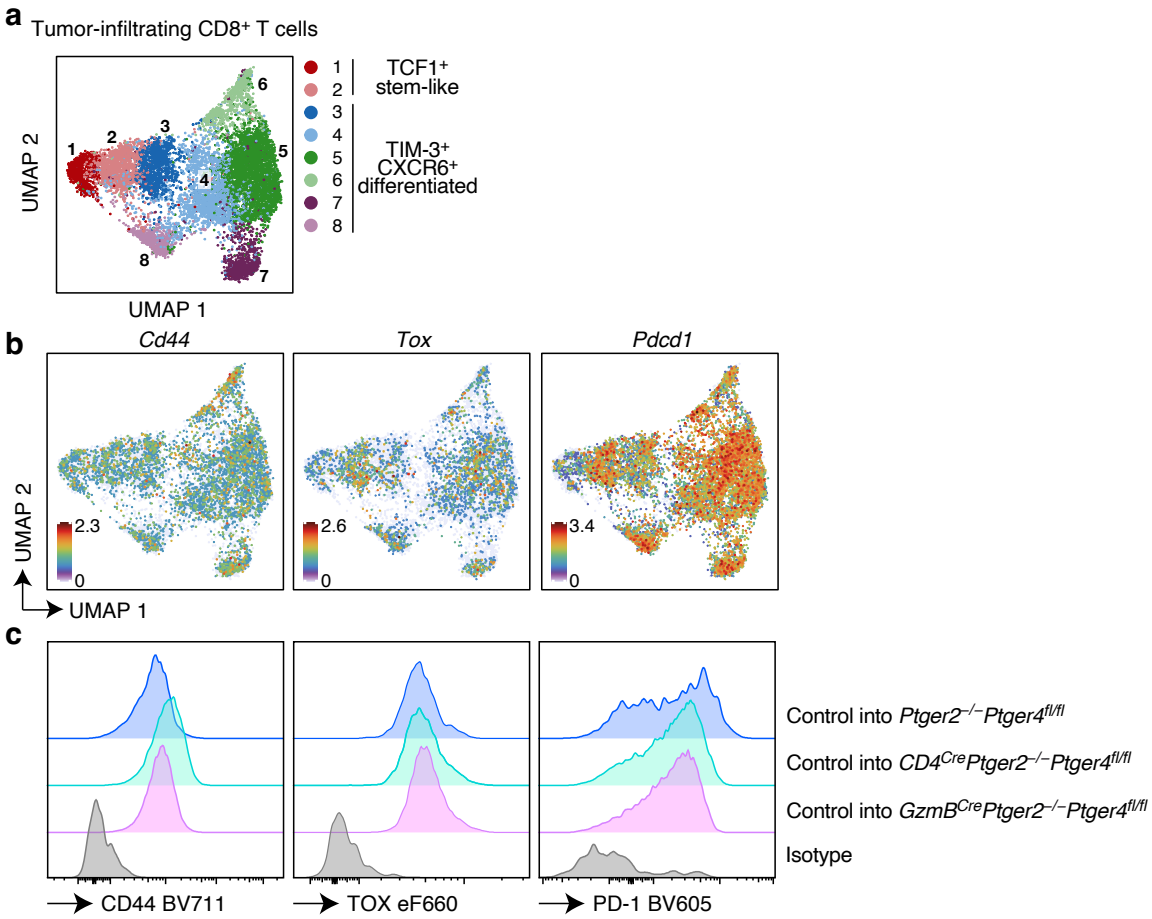


**Figure 11: Single-cell RNA sequencing reveals 8 distinct CD8⁺ T cell clusters.**
**(a)** UMAP plot illustrating 12,516 individual tumor-infiltrating CD8⁺ T cells, color-coded based on their cluster classification. **(b)** UMAP plots showing transcript expression of *Cd44*, *Tox*, and *Pdcd1* (encoding PD-1) based on **(a)**. **(c)** Representative plots showing CD44, TOX, and PD-1 protein expression in tumor-infiltrating CD8⁺ T cells, 11 days post tumor cell injection.

Within clusters 1 and 2, the concatenated scRNA-seq data revealed high expression of stem-like TCF1⁺CD8⁺ T cell markers including *Tcf7* (encoding TCF1), *slamf6*, and *Il7r* (**Figure 12a,b**). To demarcate these stem-like TCF1⁺CD8⁺ T cell clusters from naive T cells, gene sets from Gattinoni et al., 2011 and Prokhnevska et al., 2023 were used to align the obtained gene expression profiles of the TCF1⁺CD8⁺ T cells with the published signatures (**Figure 12c,d**). Notably, both clusters of TCF1⁺CD8⁺ T cells exhibited increased expression of gene signatures distinct from those of naive T cells, suggesting that these cells may have encountered antigens and are not in a naive state. In contrast, clusters 3-8 exhibited no expression of *Tcf7* but displayed a substantial enrichment of markers associated with T cell differentiation and function, including *GzmB, Havcr2* (encoding TIM-3), and *Entpd1* (encoding CD39) (**Figure 12a,b**).

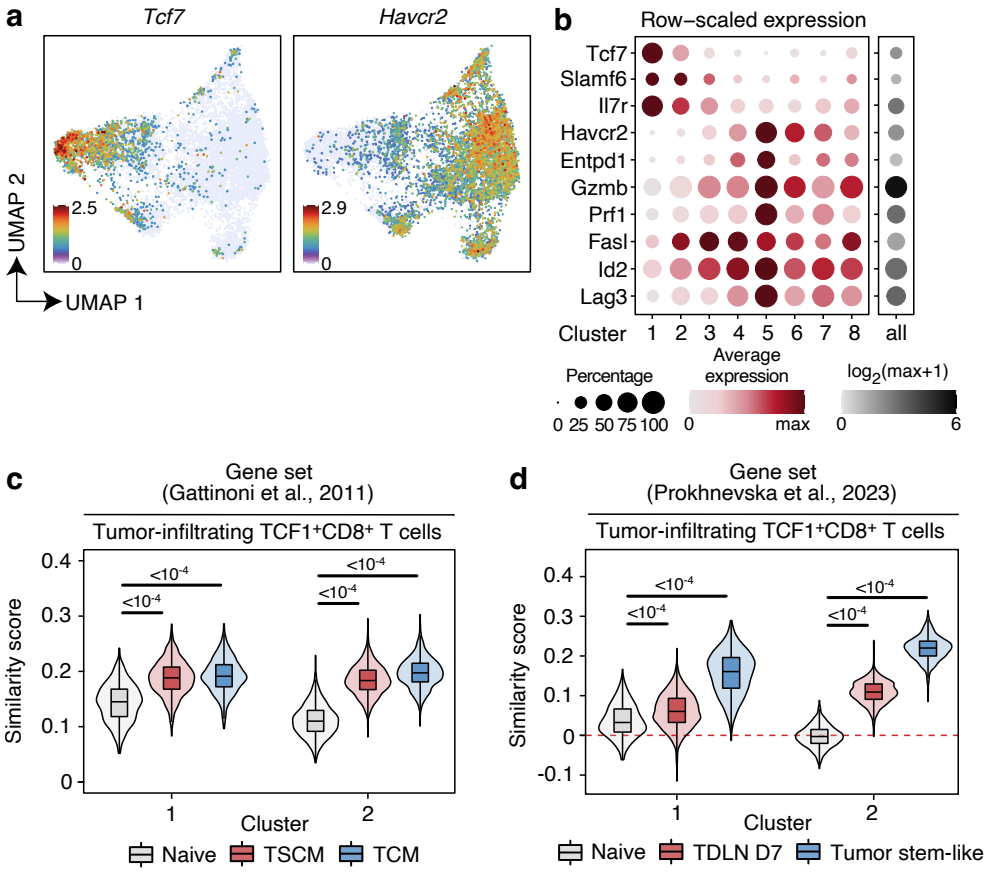


**Figure 12: Stem-like CD8⁺ T cell clusters show a distinct phenotype to naive T cells.**
**(a)** UMAP plot illustrating transcript expression of *Tcf7* and *Havcr2* (encoding TIM-3). **(b)** PCPT plot depicting expression levels of specific genes among clusters. **(c,d)** Correlation between gene expression profiles of tumor-infiltrating TCF1⁺CD8⁺ T cell clusters and the gene signatures of **(c)** naive CD8⁺ T cells, memory stem cell CD8⁺ T cells (TSCM), and central memory CD8⁺ T cells (TCM) as well as **(d)** naive CD8⁺ T cells, tumor antigen-specific CD8⁺ T cells in tdLNs, and tumor-infiltrating stem-like CD8⁺ T cells. Statistical significance in **(c)** and **(d)** was determined using Wilcoxon rank sum test and Bonferroni correction for multiple testing.

This suggests that clusters 3-8 represent the more early differentiated and terminally differentiated CD8⁺ T cell populations.

Moreover, effector CD8⁺ T cells coexpress TIM-3 and CXCR6, serving as overarching markers for distinguishing effectors from stem-like TCF1⁺CD8⁺ T cells (**Figure 13**).

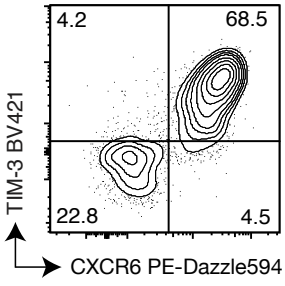


**Figure 13: Tumor-infiltrating TIM-3⁺ CD8⁺ T cells coexpress CXCR6.**
Representative flow cytometry plot showing the coexpression of TIM-3 and CXCR6 in tumor-infiltrating CD8⁺ T cells.

Unsupervised slingshot analysis revealed a tree-shaped developmental trajectory originating from stem-like TCF1⁺CD8⁺ T cells and diverging into separate terminally differentiated T cell populations (**Figure 14**), suggesting that tumor-infiltrating effector T cell populations have their origin in the stem-like T cell compartment.

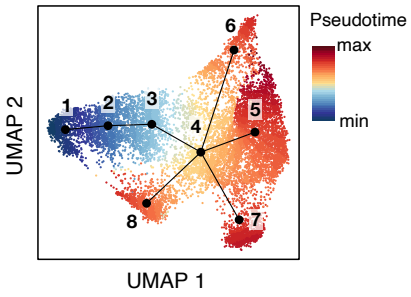


**Figure 14: Effector CD8⁺ T cell differentiation originates from TCF1⁺CD8⁺ T cells within the TME.**
UMAP plot illustrating the predicted developmental trajectory using unsupervised slingshot analysis.

In summary, these findings propose a dynamic pathway of CD8⁺ T cell differentiation within tumors. Initially, tumor-infiltrating stem-like TCF1⁺CD8⁺ T cells proceed in a unidirectional course of effector differentiation, resulting in various smaller branches of terminally differentiated CD8⁺ T cell populations.

To evaluate the influence of $PGE_2$-EP2/EP4 signaling on tumor-infiltrating CD8⁺ T cells, the scRNA-seq data set was divided according to experimental groups. Density analysis uncovered a notable shift towards early effector (clusters 3 and 4) and terminally differentiated CD8⁺ T cell populations (cluster 5) in the data set obtained from *CD4$^{Cre}$Ptger2$^{-/-}$Ptger4$^{fl/fl}$* and *GzmB$^{Cre}$Ptger2$^{-/-}$Ptger4$^{fl/fl}$* mice when compared to those from *Ptger2$^{-/-}$Ptger4$^{fl/fl}$* mice (**Figure 15a)**. Cluster quantification across the 3 experimental groups revealed a distinct lack of effector expansion and differentiation in the *Ptger2$^{-/-}$Ptger4$^{fl/fl}$* cohort (**Figure 15b**). In contrast, *CD4$^{Cre}$Ptger2$^{-/-}$Ptger4$^{fl/fl}$* and *GzmB$^{Cre}$Ptger2$^{-/-}$Ptger4$^{fl/fl}$* mice showed a marked increase of effector expansion and differentiation.

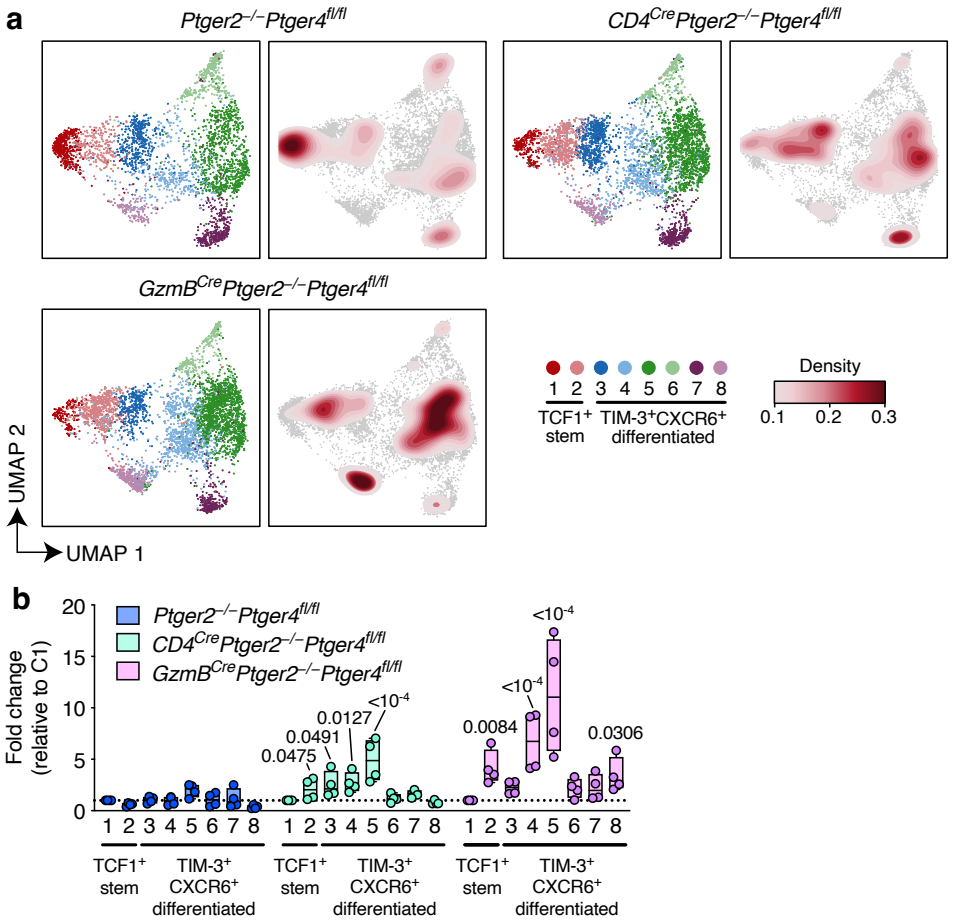


**Figure 15: Tumor-derived $PGE_2$ limits $CD8^+$ T cell effector differentiation and expansion. (a)** Density analysis of tumor-infiltrating $CD8^+$ T cells separated by mouse groups. **(b)** Quantification of $CD8^+$ T cell clusters relative to cluster 1. Box plots in **(b)** showing the median with corresponding min and max values as whiskers. Statistical significance in **(b)** was determined using one-way ANOVA with Bonferroni´s correction for multiple testing.

In line with these observations, the absence of both *Ptger2* and *Ptger4* was confirmed by gene track analysis in tumor-infiltrating stem-like $TCF1^+CD8^+$ T cells derived from *$CD4^{Cre}Ptger2^{-/-}Ptger4^{fl/fl}$* and *$GzmB^{Cre}Ptger2^{-/-}Ptger4^{fl/fl}$* mice (**Figure 16**). In contrast to this, $CD8^+$ T cells from *$Ptger2^{-/-}Ptger4^{fl/fl}$* mice exclusively exhibited the loss of *Ptger2*.

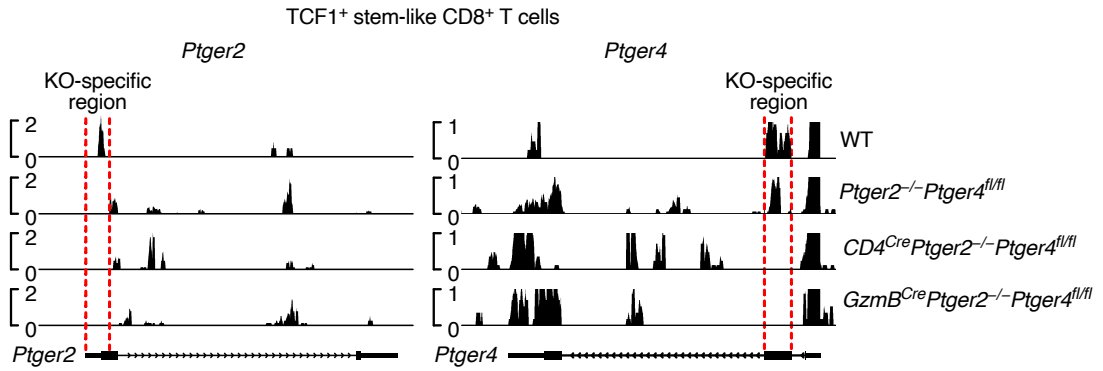


**Figure 16: Tumor-infiltrating $TCF1^+CD8^+$ T cells from *$CD4^{Cre}Ptger2^{-/-}Ptger4^{fl/fl}$* and *$GzmB^{Cre}Ptger2^{-/-}Ptger4^{fl/fl}$* lack of both *Ptger2* and *Ptger4.*** Representative plots for gene tracks illustrating the scRNA-seq read coverage across *Ptger2* and *Ptger4* loci within tumor-infiltrating $TCF1^+CD8^+$ T cells.

Consistent with the increased expansion and proliferation observed in *CD4$^{Cre}$Ptger2$^{-/-}$Ptger4$^{fl/fl}$* and *GzmB$^{Cre}$Ptger2$^{-/-}$Ptger4$^{fl/fl}$* mice, analysis of proliferation signatures revealed an enrichment in gene sets linked to proliferation compared to *Ptger2$^{-/-}$Ptger4$^{fl/fl}$* mice (**Figure 17a**). In line with this finding, both tumor-infiltrating TCF1$^+$ and TIM-3$^+$ CD8$^+$ T cells showed elevated protein expression of the proliferation marker Ki-67 in *CD4$^{Cre}$Ptger2$^{-/-}$Ptger4$^{fl/fl}$* and *GzmB$^{Cre}$Ptger2$^{-/-}$Ptger4$^{fl/fl}$* mice compared to *Ptger2$^{-/-}$Ptger4$^{fl/fl}$* mice (**Figure 17b**). Nevertheless, no significant increase in the expression of gene signatures associated with cytotoxic effector functions was observed among the experimental groups (**Figure 17c**).

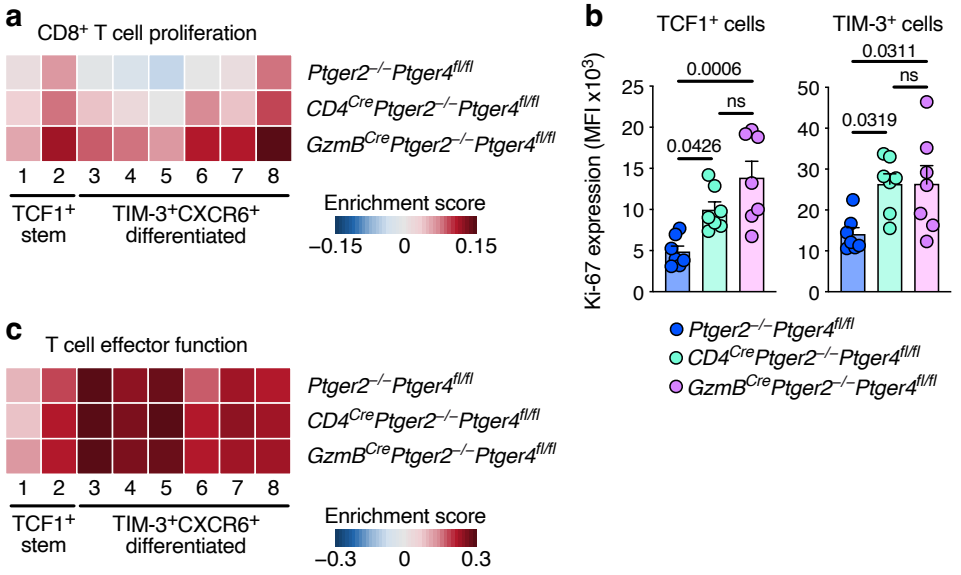


**Figure 17: Tumor-derived PGE$_2$ impairs CD8$^+$ T cell proliferation rather than affecting their effector functions. (a)** CD8$^+$ T cell proliferation signature across tumor-infiltrating CD8$^+$ T cell clusters derived from *Ptger2$^{-/-}$Ptger4$^{fl/fl}$*, *CD4$^{Cre}$Ptger2$^{-/-}$Ptger4$^{fl/fl}$* and *GzmB$^{Cre}$Ptger2$^{-/-}$Ptger4$^{fl/fl}$* mice. **(b)** Expression of the proliferation marker Ki-67 in tumor-infiltrating TCF1$^+$ and TIM-3$^+$ CD8$^+$ T cells from *Ptger2$^{-/-}$Ptger4$^{fl/fl}$*, *CD4$^{Cre}$Ptger2$^{-/-}$Ptger4$^{fl/fl}$* and *GzmB$^{Cre}$Ptger2$^{-/-}$Ptger4$^{fl/fl}$* mice 11 days post tumor cell inoculation with control BRAF$^{V600E}$ melanoma cells. n=7, two independent experiments were pooled. **(c)** CD8$^+$ T cell effector function signature across tumor-infiltrating CD8$^+$ T cell clusters based on **(a)**. Data in **(b)** is depicted as mean ± SEM. Statistical significance in **(b)** was determined using one-way ANOVA with Tukey´s multiple-comparison test.

Moreover, *ex vivo* restimulated intratumoral CD8$^+$ T cells did not show substantial differences in their effector cytokine expression when restimulated with αCD3/CD28 microbeads (**Figure 18a**). Furthermore, to investigate the impact of PGE$_2$ on the specific cytotoxicity of CD8$^+$ T cells, TCF1$^-$ OT-I cells were generated and pre-incubated with or without PGE$_2$. A killing assay revealed no significant differences between PGE$_2$-treated and untreated OT-I cells (**Figure 18b**).

This indicates that $PGE_2$ primarily impairs the expansion and differentiation of intratumoral $CD8^+$ T cells rather than the cytotoxicity of effector $CD8^+$ T cells.

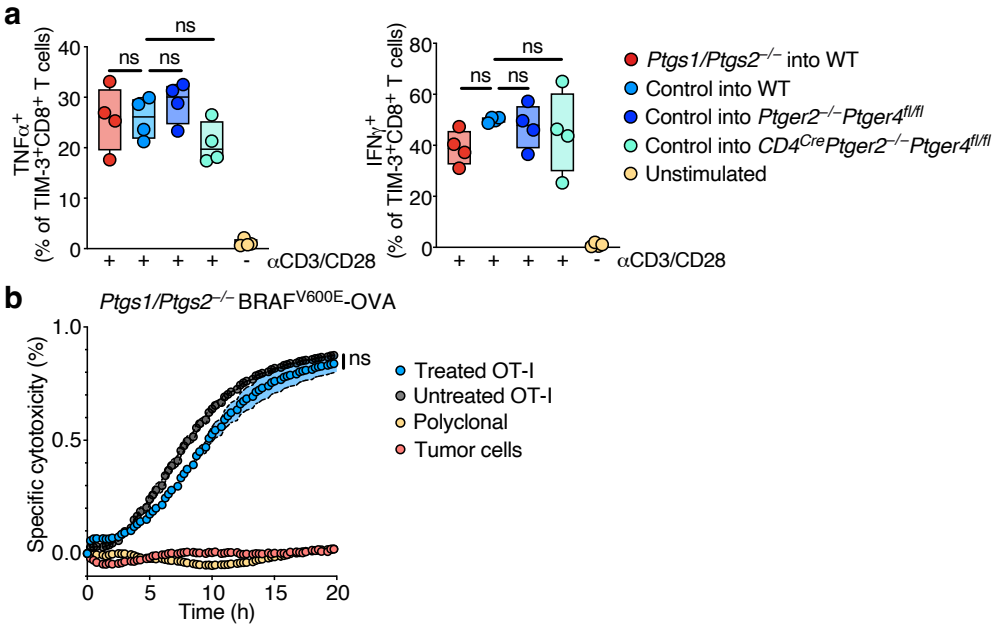


**Figure 18: Tumor-derived $PGE_2$ does not impair CD8+ T cells effector functions.**
**(a)** Tumor-infiltrating $CD8^+$ T cells were sorted from WT, *Ptger2*$^{-/-}$*Ptger4*$^{fl/fl}$, and *CD4*$^{Cre}$*Ptger2*$^{-/-}$*Ptger4*$^{fl/fl}$ mice and restimulated with αCD3/CD28 microbeads for 4 hours. n=4, two independent experiments **(b)** Representative plot for specific cytotoxicity. Repetitively activated OT-I T cells were treated with or without $PGE_2$ for 20 hours and co-cultured with *Ptgs1/Ptgs2*$^{-/-}$ BRAF$^{V600E}$ OVA cells in an effector to target ratio of 1:1. Depicted is one of three independent experiments Box plots in **(a)** showing the median with corresponding min and max values as whiskers. Data in **(b)** is depicted as mean ± SD. Statistical significance was determined using one-way ANOVA with Tukey´s multiple-comparison test.

In summary, these findings collectively suggest that tumor-derived $PGE_2$ hinders both the expansion and differentiation of effector $CD8^+$ T cells originating from intratumoral stem-like $TCF1^+CD8^+$ T cells. Importantly, this impairment can be overcome by the ablation of EP2 and EP4 in stem-like $TCF1^+CD8^+$ T cells.

## 4.4 EP2/EP4 ablation rescues clonal CD8⁺ T cell expansion

The scTCR-seq data uncovered the presence of various clonally expanded tumor-infiltrating CD8⁺ T cells across *Ptger2*$^{-/-}$*Ptger4*$^{fl/fl}$, *CD4*$^{Cre}$*Ptger2*$^{-/-}$*Ptger4*$^{fl/fl}$, and *GzmB*$^{Cre}$*Ptger2*$^{-/-}$*Ptger4*$^{fl/fl}$ mice, demonstrating both tumor specificity and a proliferative expansion (**Figure 19a**). However, while all experimental groups exhibited clonally expanded CD8⁺ T cell clonotypes, this was substantially more pronounced in *CD4*$^{Cre}$*Ptger2*$^{-/-}$*Ptger4*$^{fl/fl}$ and *GzmB*$^{Cre}$*Ptger2*$^{-/-}$*Ptger4*$^{fl/fl}$ mice than in *Ptger2*$^{-/-}$*Ptger4*$^{fl/fl}$ mice (**Figure 19a,b**). These observations were underscored by the presence of hyperexpanded clonotypes, a feature entirely absent in *Ptger2*$^{-/-}$*Ptger4*$^{fl/fl}$ mice (**Figure 19c**). In more detail, *CD4*$^{Cre}$*Ptger2*$^{-/-}$*Ptger4*$^{fl/fl}$ and *GzmB*$^{Cre}$*Ptger2*$^{-/-}$*Ptger4*$^{fl/fl}$ mice showed 22.6% and 35.6% hyperexpanded clonotypes, respectively. In contrast, *Ptger2*$^{-/-}$*Ptger4*$^{fl/fl}$ mice showed a complete absence of hyperexpanded clonotypes.

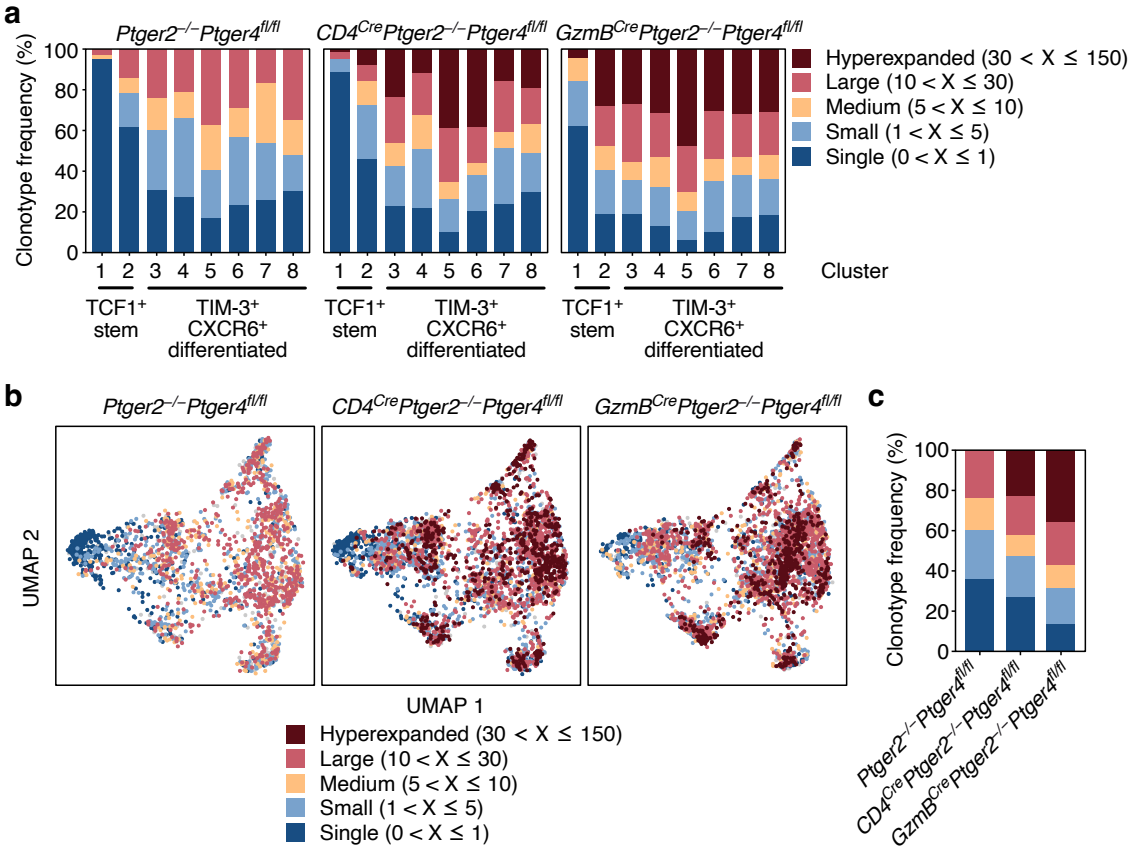


**Figure 19: PGE$_2$-EP2/EP4 signaling limits clonal expansion of tumor-infiltrating CD8⁺ cells.**
**(a)** Clonotype frequencies for each individual CD8⁺ T cell cluster from *Ptger2*$^{-/-}$*Ptger4*$^{fl/fl}$, *CD4*$^{Cre}$*Ptger2*$^{-/-}$*Ptger4*$^{fl/fl}$ *and* *GzmB*$^{Cre}$*Ptger2*$^{-/-}$*Ptger4*$^{fl/fl}$ mice. **(b)** UMAP plots depicting CD8⁺ T cell clonotype distribution among experimental groups. **(c)** Quantification of clonotype frequencies among experimental groups.

In conclusion, $PGE_2$ signaling on tumor-infiltrating $CD8^+$ T cells may suppress their clonal expansion. Notably, this inhibitory effect can be effectively circumvented through the ablation of EP2 and EP4 in $CD8^+$ T cells, resulting in enhanced expansion and differentiation into effector populations within the TME.

## 4.5 $PGE_2$-EP2/EP4 signaling impairs early tumor-infiltrating stem-like $TCF1^+CD8^+$ T cells

To validate the earlier findings indicating the suppressive impact of $PGE_2$ on the local differentiation of intratumoral $CD8^+$ T cells into effector T cells, stem-like $TCF1^+CD8^+$ and $TIM\text{-}3^+CD8^+$ T cells were quantified in *Ptgs1/Ptgs2*$^{-/-}$ and control $BRAF^{V600E}$ tumors derived from WT, *Ptger2*$^{-/-}$*Ptger4*$^{fl/fl}$, and *CD4*$^{Cre}$*Ptger2*$^{-/-}$*Ptger4*$^{fl/fl}$ mice. Interestingly, *CD4*$^{Cre}$*Ptger2*$^{-/-}$*Ptger4*$^{fl/fl}$ mice showed higher frequencies of $TIM\text{-}3^+CD8^+$ T cells in tumors compared to WT and *Ptger2*$^{-/-}$*Ptger4*$^{fl/fl}$ mice (**Figure 20a**). This implies a potential deficiency in the transition from stem-like $TCF1^+CD8^+$ to $TIM\text{-}3^+CD8^+$ T cells in WT and *Ptger2*$^{-/-}$*Ptger4*$^{fl/fl}$ mice. In line with this notion, the numbers of tumor-infiltrating stem-like $TCF1^+CD8^+$ T cells did not show significant differences across experimental groups (**Figure 20b**). This indicates that the generation of $CD8^+$ T cells at tdLNs and their subsequent infiltration into the TME may not be affected by $PGE_2$. In contrast, the quantities of $TIM\text{-}3^+CD8^+$ T cells in tumors derived from *CD4*$^{Cre}$*Ptger2*$^{-/-}$*Ptger4*$^{fl/fl}$ mice exhibited a strong increase compared to those derived from WT and *Ptger2*$^{-/-}$*Ptger4*$^{fl/fl}$ mice (**Figure 20c**).

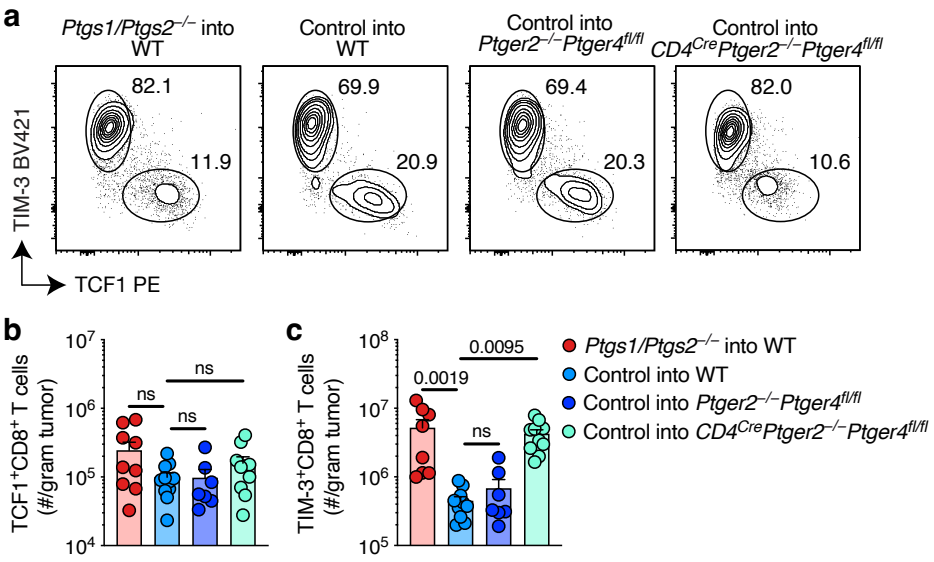


**Figure 20: Ablation of EP2 and EP4 on tumor-infiltrating CD8⁺ T cells leads to effective development of effector CD8⁺ T cells at the tumor site. (a)** 2x10⁶ *Ptgs1/Ptgs2*$^{-/-}$ or control BRAF$^{V600E}$ melanoma cells were injected into the flanks of WT, *Ptger2*$^{-/-}$*Ptger4*$^{fl/fl}$, or *CD4*$^{Cre}$*Ptger2*$^{-/-}$*Ptger4*$^{fl/fl}$ mice. Representative flow cytometry plots depicting the frequencies of intratumoral TCF1⁺ and TIM-3⁺ cells among pre-gated CD44⁺CD8⁺ T cells. **(b)** Quantification of intratumoral TCF1⁺CD8⁺ T cells based on **(a)**. n=7-11, two independent experiments were pooled. **(c)** Quantification of intratumoral TIM-3⁺CD8⁺ T cells based on **(a)**. n=7-11, two independent experiments were pooled. Data in **(b)** and **(c)** is depicted as mean ± SEM. Statistical significance in **(b)** and **(c)** was determined by one-way ANOVA with Tukey´s multiple comparison test. $P \geq 0.05$, not significant (ns).

These findings provide additional evidence that $PGE_2$ might hinder the differentiation and clonal expansion from stem-like TCF1⁺CD8⁺ T cells.

The observation that early infiltrating CD8⁺ T cells on day 6 following tumor cell injection showed a stem-like TCF1⁺ phenotype but not (yet) an effector phenotype made it possible to investigate whether TIM-3⁺CD8⁺ T cells within the TME originate from these early infiltrating stem-like TCF1⁺CD8⁺ T cells (**Figure 21a,b**). *CD4*$^{Cre}$*Ptger2*$^{-/-}$*Ptger4*$^{fl/fl}$ mice were inoculated with control BRAF$^{V600E}$ melanoma cells and treated with FTY720, a potent sphingosine-1-phosphate receptor 1 (S1P1R) antagonist that prevents the egress of lymphocytes—including newly primed CD8⁺ T cells—from draining lymph nodes[189]. Administration of FTY720 from day 6 onward did not impact the development of intratumoral TIM-3⁺CD8⁺ T cells, leading to elevated numbers of CD8⁺ T cells within the TME (**Figure 21c**). Conversely, inhibiting the egress from LNs starting on day 1 lead to decreased numbers of infiltrating CD8⁺ T cells (**Figure 21c**). Remarkably, the proliferative response originating from stem-like TCF1⁺CD8⁺ T cells infiltrated until day 6 proved to be substantial enough to fully control tumor growth (**Figure 21d**).

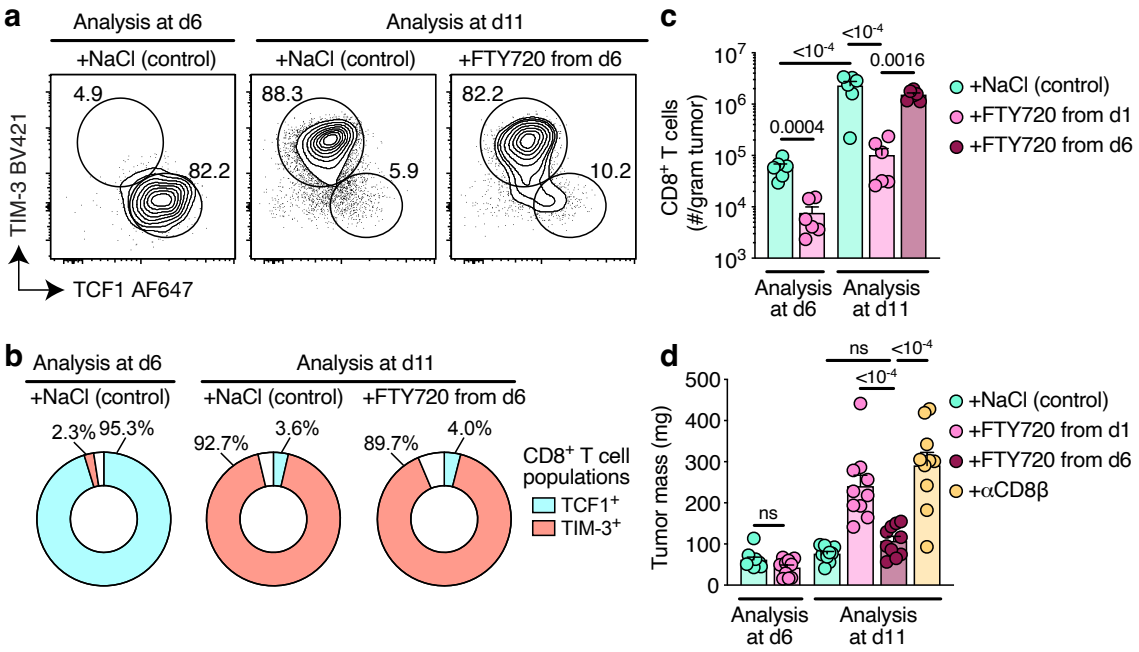


**Figure 21: $PGE_2$ prevents sufficient anti-cancer immune responses by affecting the differentiation of $TCF1^+CD8^+$ T cells into effectors. (a)** Representative flow cytometry plots showing frequencies of intratumoral $TCF1^+$ and $TIM\text{-}3^+$ cells among pre-gated $CD44^+CD8^+$ T cells. **(b)** Donut chart depicting average percentages of $TCF1^+CD8^+$ and effector $TIM\text{-}3^+CD8^+$ T cells across all tumor-infiltrating $CD8^+$ T cells. n=6, pooled from two independent experiments. **(c)** Quantification of intratumoral $CD8^+$ T cell numbers among experimental groups. n=6, pooled from two independent experiments. **(d)** Tumor masses at indicated time points. Antibody-mediated $CD8^+$ T cell depletion in absence of FTY720 treatment was performed using $\alpha CD8\beta$ antibodies. n=10, pooled from two independent experiments. Data in **(c)** and **(d)** is depicted as mean ± SEM. Statistical significance in **(c)** and **(d)** was determined by one-way ANOVA with Tukey´s multiple comparison test. $P \geq 0.05$, not significant (ns).

Taken together, these findings illustrate that the expansion and differentiation of effector $TIM\text{-}3^+CD8^+$ T cells originates from early infiltrating stem-like $TCF1^+CD8^+$ T cells, which ultimately mediate potent anti-cancer immune responses when protected from $PGE_2$ signaling.

## 4.6 $PGE_2$ signaling leads to an IL-2-unresponsive state of stem-like TCF1$^+$CD8$^+$ T cells

To investigate the downstream pathways of $PGE_2$ signaling on tumor-infiltrating stem-like TCF1$^+$CD8$^+$ T cells, transcription factor activity analysis was performed based on the scRNA-seq data. Ablation of EP2 and EP4 on tumor-infiltrating stem-like TCF1$^+$CD8$^+$ T cells led to increased activity of transcription factor networks linked to T cell differentiation (including NFKB1, REL, JUN, and TBX21), stimulatory cytokine signaling (including IRF1, STAT4, JUN, and TBX21), and survival (including RUNX2 and TRP53) (**Figure 22**). Notably, this was observed for both *CD4$^{Cre}$Ptger2$^{-/-}$Ptger4$^{fl/fl}$* and *GzmB$^{Cre}$Ptger2$^{-/-}$Ptger4$^{fl/fl}$* mice. Likewise, an increase in transcription factor network activity associated with elevated IL-2 signaling (STAT1, STAT3, STAT5b, ELK1, and NFATC2) was observed in both *CD4$^{Cre}$Ptger2$^{-/-}$Ptger4$^{fl/fl}$* and *GzmB$^{Cre}$Ptger2$^{-/-}$Ptger4$^{fl/fl}$* mice relative to *Ptger2$^{-/-}$Ptger4$^{fl/fl}$* mice (**Figure 22**).

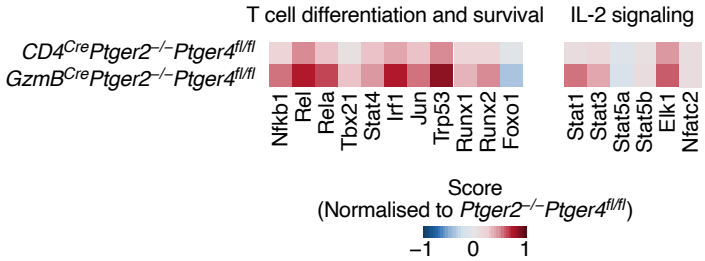


**Figure 22: $PGE_2$ signaling on tumor-infiltrating TCF1$^+$ CD8$^+$ T cells affects transcription factor networks for T cell differentiation and IL-2 signaling.** Transcription factors for T cell differentiation and survival as well as IL-2 signaling from tumor-infiltrating TCF1$^+$CD8$^+$ T cells derived from *CD4$^{Cre}$Ptger2$^{-/-}$Ptger4$^{fl/fl}$* and *GzmB$^{Cre}$Ptger2$^{-/-}$Ptger4$^{fl/fl}$* mice. Normalized to tumor-infiltrating CD8$^+$ T cells derived from *Ptger2$^{-/-}$Ptger4$^{fl/fl}$* mice.

To verify the impact of $PGE_2$ signaling on IL-2-mediated expansion of tumor-infiltrating stem-like TCF1$^+$CD8$^+$ T cells, WT mice were injected with *Ptgs1/Ptgs2$^{-/-}$* BRAF$^{V600E}$ melanoma cells and subsequently, intratumoral stem-like TCF1$^+$CD8$^+$ T cells were sorted (based on the negative expression of TIM-3 and CXCR6). $PGE_2$ significantly blocked the expansion of *ex vivo*-stimulated stem-like TCF1$^+$CD8$^+$ T cells when cultured and activated with high-dose IL-2 and αCD3/CD28 microbeads (**Figure 23a**). To circumvent the limitation of obtaining only a low number of tumor-infiltrating CD8$^+$ T cells from tumor-bearing mice, repetitively activated *in vitro* differentiated

TCF1⁺CD8⁺ T cells were used to investigate the impact of $PGE_2$ signaling in these cells. In line with the *ex vivo* data, repetitively activated TCF1⁺CD8⁺ T cells exhibited comprised expansion upon $PGE_2$ exposure when stimulated with high-dose IL-2 and αCD3/CD28 microbeads (**Figure 23b**). Moreover, the limited T cell expansion was accompanied by reduced DNA replication in $PGE_2$-treated repetitively activated TCF1⁺CD8⁺ T cells (determined by EdU incorporation) (**Figure 23c**).

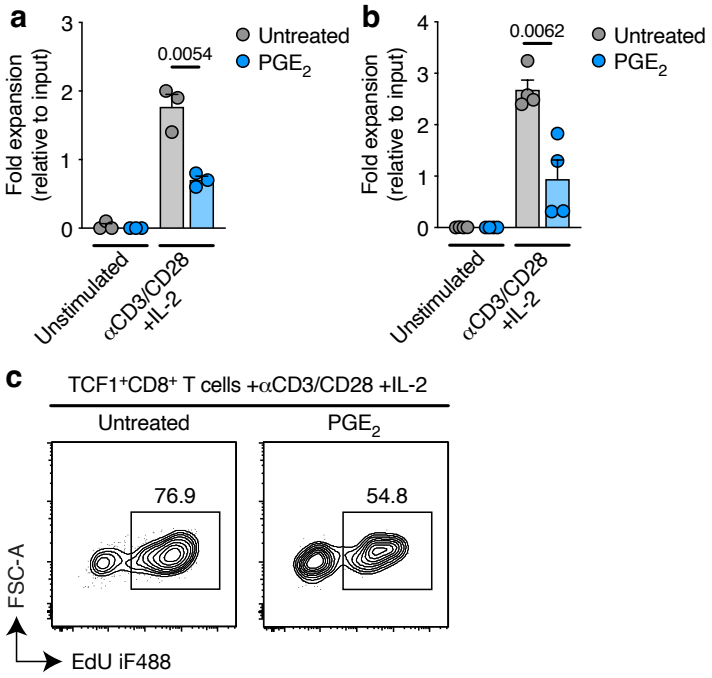


**Figure 23: $PGE_2$-EP2/EP4 signaling impairs IL-2-mediated expansion and proliferation of TCF1⁺CD8⁺ T cells. (a)** Tumor-infiltrating TCF1⁺CD8⁺ T cells were isolated from *Ptgs1/Ptgs2*$^{-/-}$ BRAF$^{V600E}$ tumors and cultured for 3 days in the absence or presence of $PGE_2$ with αCD3/CD28 microbeads and high-dose IL-2. T cell numbers were determined by flow cytometry. n=3, pooled from two independent experiments. **(b)** Repetitively activated *in vitro* differentiated TCF1⁺CD8⁺ T cells were cultured for 3 days in the absence or presence of $PGE_2$ with αCD3/CD28 microbeads and high-dose IL-2. T cell numbers were determined by flow cytometry. n=4, pooled from two independent experiments. **(c)** Representative flow cytometry plots depicting 5-ethynyl-2´-deoxyuridine (EdU) incorporation into the DNA of newly generated CD8⁺ T cells based on **(b)**.Data in **(a)** and **(b)** is depicted as mean ± SEM. Statistical significance in **(a)** and **(b)** was determined by one-way ANOVA with Tukey´s multiple comparison test.

Bulk RNA sequencing uncovered substantial transcriptional changes in both *in vitro* stimulated and non-stimulated repetitively activated TCF1⁺CD8⁺ T cells upon $PGE_2$ treatment (**Figure 24a**). The comparison between stimulated TCF1⁺CD8⁺ $PGE_2$ treated and untreated revealed 294 DEGs ($P$<0.05 with a fold change of ≥2) (**Figure 24b**). GSEA uncovered a significant downregulation of the mammalian target of rapamycin complex 1 (mTORC1) and STAT5 pathways, which are linked to CD8⁺ T cell differentiation, expansion, and IL-2 signaling (**Figure 24c**).

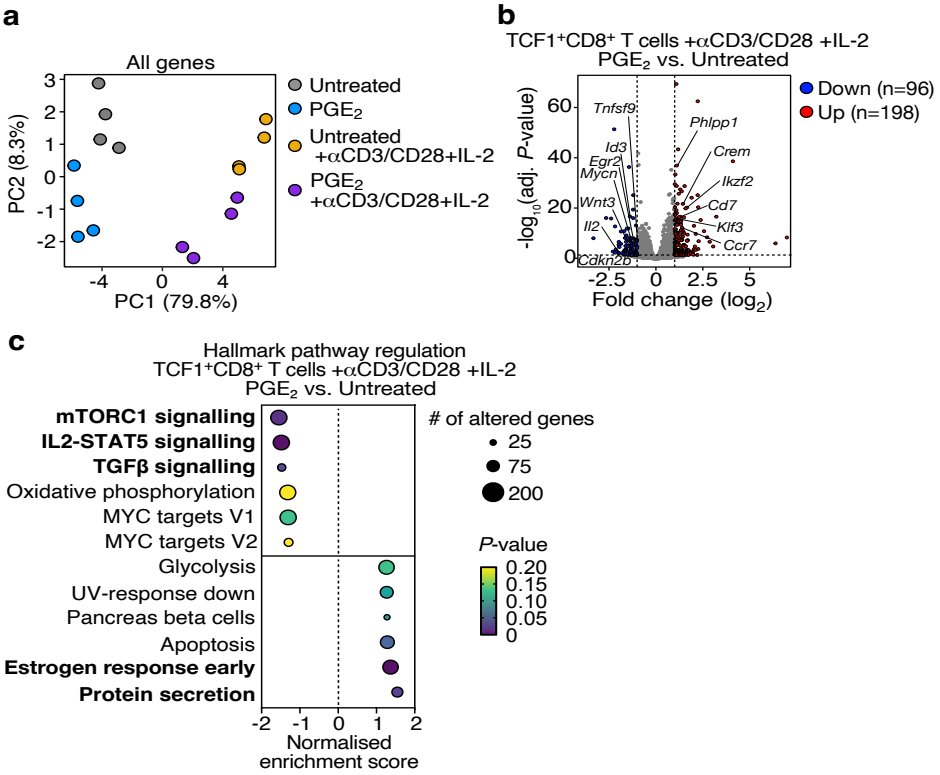


**Figure 24: $PGE_2$ signaling on repetitively activated TCF1⁺CD8⁺ T cells leads to the downregulation of differentiation-associated mTORC1 signaling and IL-2 signaling pathways. (a)** PCA plot based on all DEGs of repetitively activated TCF1⁺CD8⁺ T cells upon $PGE_2$ exposure. **(b)** Volcano plot depicting up- and downregulated genes that were differentially expressed upon $PGE_2$ treatment based on **(a)**. GSEA showing hallmark pathways which are significantly up- and downregulated based on **(a)**.

In line with the inhibitory effect of $PGE_2$ on the IL-2 signaling pathway, repetitively activated TCF1⁺CD8⁺ T cells displayed a diminished capacity to effectively phosphorylate STAT5, a downstream protein that is phosphorylated in response to IL-2 signaling (**Figure 25a**). Accompanied by reduced STAT5 phosphorylation, $PGE_2$-exposed, repetitively activated TCF1⁺CD8⁺ T cells exhibited a significant downregulation of the IL-2Rγc (**Figure 25b**).

This observation suggests that $PGE_2$ signaling on $TCF1^+CD8^+$ T cells may attenuate their responsiveness to IL-2. However, the reduced IL-2 responsiveness could only be partially rescued by very high doses of IL-2 (**Figure 25c**). Consistent with the reduced expression of the IL-2Rγc upon $PGE_2$ exposure, repetitively activated $TCF1^+CD8^+$ T cells failed to efficiently expand when stimulated with other γc cytokines such as IL-7 or IL-15 (**Figure 25d**).

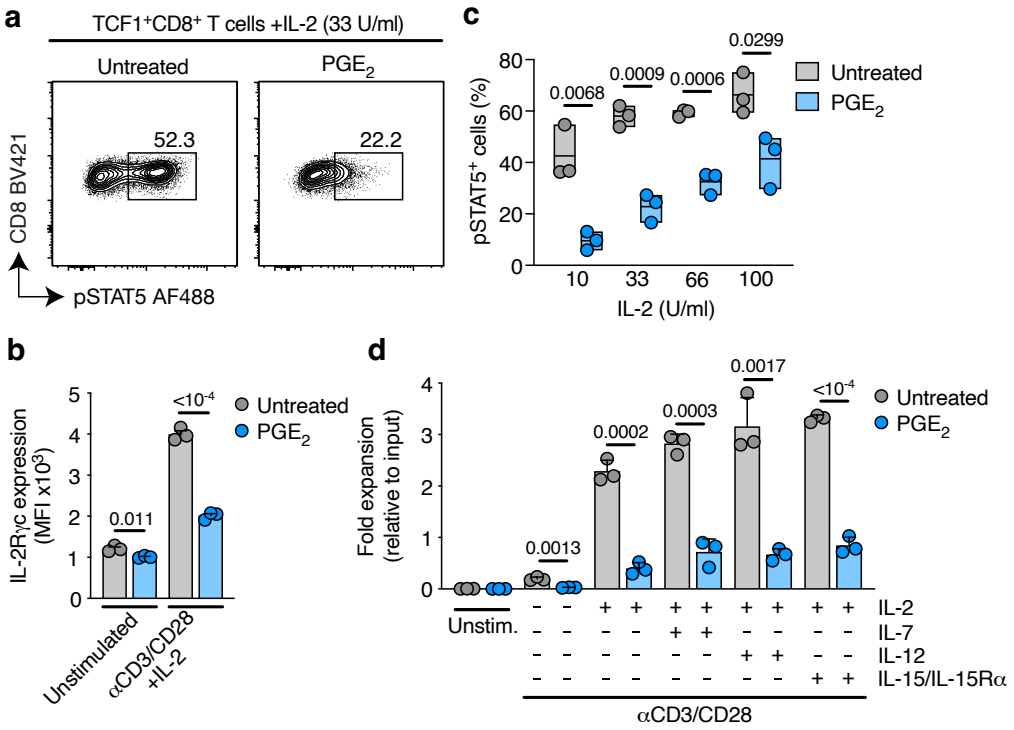


**Figure 25: The $PGE_2$-EP2/EP4 axis impairs IL-2 signaling through the downregulation of IL-2Rγc.** **(a)** Representative flow cytometry plot depicting reduced phosphorylation of STAT5 in repetitively activated $TCF1^+CD8^+$ T cells upon $PGE_2$ exposure. **(b)** Effect of $PGE_2$ exposure on the expression of IL2-Rγc in $TCF1^+CD8^+$ T cells. n=3. **(c)** Frequencies of WT $pSTAT5^+TCF1^+CD8^+$T cells upon stimulation with different concentrations of IL-2 with or without $PGE_2$ treatment based on **(a)**. n=3, representative for n=6 from 3 independent experiments. **(d)** Quantification of $TCF1^+CD8^+$ T cells with indicated stimulation conditions for 3 days. n=3, representative for 3 independent experiments. Data in **(b)** is depicted as mean ± SD. Box plots in **(c)** showing the median with corresponding min and max values as whiskers. Data in **(d)** is depicted as mean ± SEM. Statistical significance in **(b)** was determined by unpaired t-test. Statistical significance in **(c)** and **(d)** was determined by one-way ANOVA with Tukey´s multiple comparison test.

These findings underscore that $PGE_2$ signaling mediates a predominant inhibitory effect on IL-2 signaling by downregulating the IL-2Rγc.

In order to verify that these inhibitory effects are mediated by $PGE_2$-EP2/EP4 signaling on TCF1⁺CD8⁺ T cells, repetitively activated TCF1⁺CD8⁺ T cells from *CD4$^{Cre}$Ptger2$^{-/-}$Ptger4$^{fl/fl}$* mice were used. These T cells efficiently phosphorylated STAT5 when exposed to $PGE_2$ (**Figure 26a**). In alignment with this concept, EP2/EP4 ablated TCF1⁺CD8⁺ T cells expanded into significant numbers upon $PGE_2$ exposure compared to their counterparts with sufficient EP2 and EP4 expression (**Figure 26b**). Consistent with these results, repetitively activated TCF1⁺CD8⁺ T cells derived from *CD4$^{Cre}$Ptger2$^{-/-}$Ptger4$^{fl/fl}$* mice showed no impairment in EdU incorporation when exposed to $PGE_2$ (**Figure 26c**).

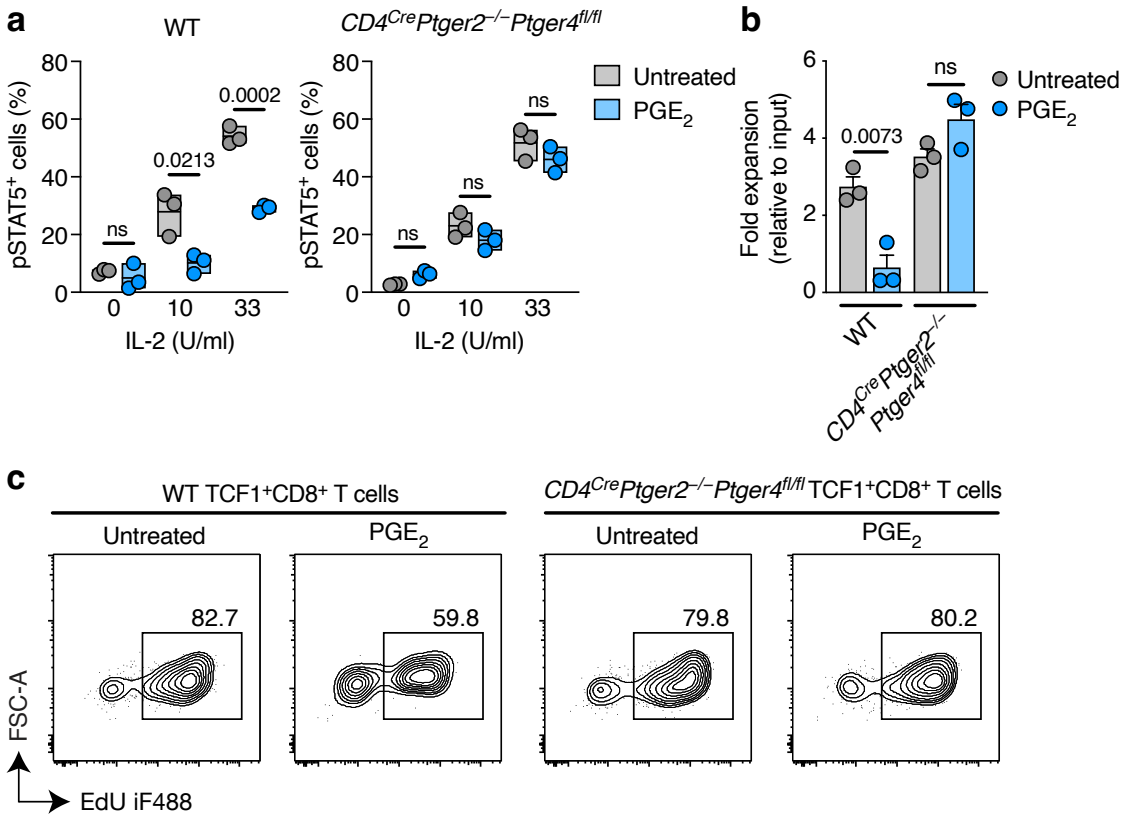


**Figure 26: $PGE_2$-mediated unresponsiveness to IL-2 signaling can be overcome by the ablation of EP2 and EP4. (a)** Frequencies of pSTAT5⁺ repetitively activated TCF1⁺CD8⁺ T cells from WT and *CD4$^{Cre}$Ptger2$^{-/-}$Ptger4$^{fl/fl}$* mice stimulated with different concentrations of IL-2 in the presence or absence of $PGE_2$. n=3, representative for two independent experiments. **(b)** Quantification of TCF1⁺CD8⁺ T cells from WT and *CD4$^{Cre}$Ptger2$^{-/-}$Ptger4$^{fl/fl}$* mice after 3 days of stimulation with high-dose IL-2 and αCD3/CD28 microbeads. n=3, representative for two independent experiments. **(c)** Representative flow cytometry plots illustrating EdU incorporation into newly synthesized DNA of repetitively activated TCF1⁺CD8⁺ stimulated with high-dose IL-2 and αCD3/28 microbeads for 24h based on **(b)**. Box plots in **(a)** showing the median with corresponding min and max values as whiskers. Data in **(d)** is depicted as mean ± SEM. Statistical significance in **(a)** and **(b)** was determined by one-way ANOVA with Tukey´s multiple comparison test. $P \geq 0.05$, not significant (ns).

In summary, these results, combined with the previous scRNA-seq findings, indicate that $PGE_2$-EP2/EP4 signaling in stem-like $TCF1^+CD8^+$ T cells hampers differentiation and expansion, primarily by inhibiting IL-2 signaling. Notably, this inhibitory effect can be reversed by the ablation of EP2 and EP4 on these T cells.

## 4.7 EP2/EP4 ablation in adoptively transferred antigen-specific CD8⁺ T cells permits protective anti-cancer immune responses

To investigate how $PGE_2$ affects antigen-specific CD8⁺ T cell responses, 1x10³ EP2/EP4-sufficient WT and *CD4$^{Cre}$Ptger2$^{-/-}$Ptger4$^{fl/fl}$* OT-I T cells were adoptively co-transferred into WT recipient mice and subsequently challenged with MC38-OVA tumor cells. Based on the expression of the congenic markers CD45.1 and CD45.2, WT (CD45.1/CD45.1) OT-I and *CD4$^{Cre}$Ptger2$^{-/-}$Ptger4$^{fl/fl}$* (CD45.1/CD45.2) OT-I T cells could be distinguished from each other as well as from the WT (CD45.2/CD45.2) recipient T cells in both tdLNs and tumors (**Figure 27a**). OT-I T cells derived from both WT OT-I and *CD4$^{Cre}$Ptger2$^{-/-}$Ptger4$^{fl/fl}$* OT-I mice demonstrated efficient expansion within tdLNs (**Figure 27b**).

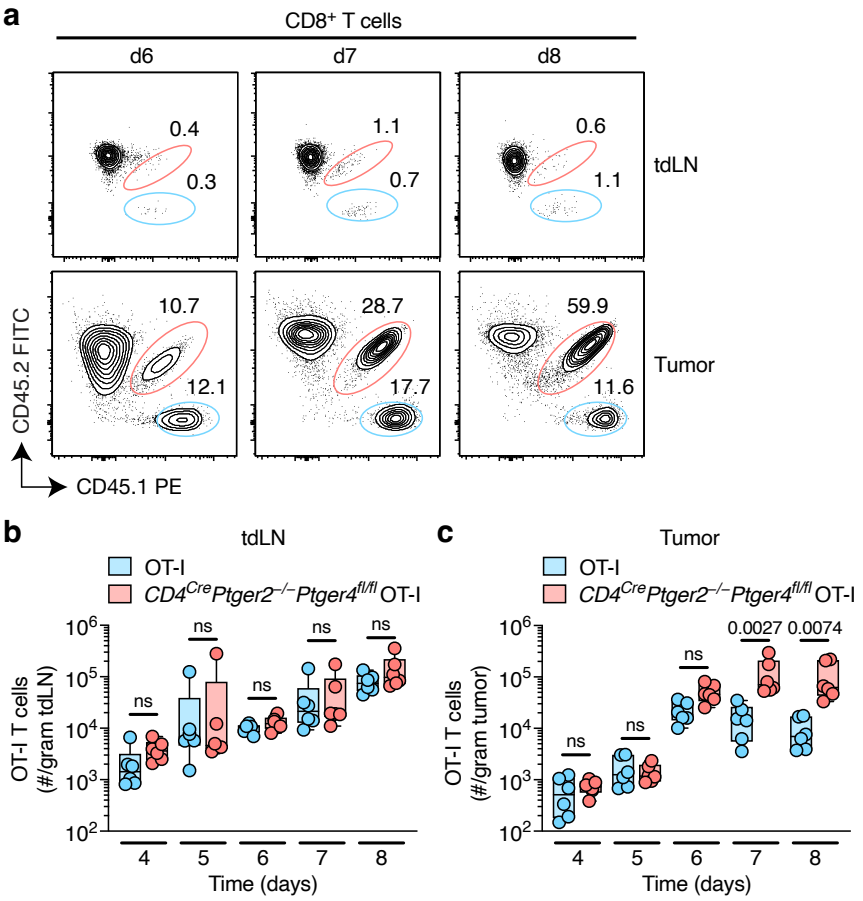


**Figure 27: EP2/EP4 ablation on adoptively transferred tumor-specific CD8⁺ T cells leads to increased T cell expansion at the tumor site. (a)** Representative flow cytometry plots illustrating adoptively transferred WT (EP2/EP4 sufficient, CD45.1/CD45.1) and *CD4$^{Cre}$Ptger2$^{-/-}$Ptger4$^{fl/fl}$* (CD45.1/CD45.2) OT-I T cells in tdLNs and MC38-OVA tumors at indicated time points after tumor cell inoculation. **(b)** Quantification of WT OT-I and *CD4$^{Cre}$Ptger2$^{-/-}$Ptger4$^{fl/fl}$* OT-I T cells in tdLNs based on **(a)**. n=6, pooled from two independent experiments. **(c)** Quantification of WT OT-I and *CD4$^{Cre}$Ptger2$^{-/-}$Ptger4$^{fl/fl}$* OT-I T cells in MC38-OVA tumors based on **(a)**. n=6, pooled from two independent experiments. Box plots in **(b)** and **(c)** showing the median with corresponding min and max values as whiskers. Data in **(b)** and **(c)** is depicted as mean ± SEM. Statistical significance in **(b)** and **(c)** was determined by one-way ANOVA with Tukey´s multiple comparison test. $P \geq 0.05$, not significant (ns).

In contrast, following an initial phase of proliferation, WT OT-I T cells experienced a collapse within the TME, while *CD4$^{Cre}$Ptger2$^{-/-}$Ptger4$^{fl/fl}$* OT-I T cells expanded substantially (**Figure 27c**).

Similarly, OT-I T cells from *Ptger2$^{-/-}$Ptger4$^{fl/fl}$* OT-I mice exhibited compromised CD8$^{+}$ T cell expansion compared to *CD4$^{Cre}$Ptger2$^{-/-}$Ptger4$^{fl/fl}$* OT-I T cells (**Figure 28**).

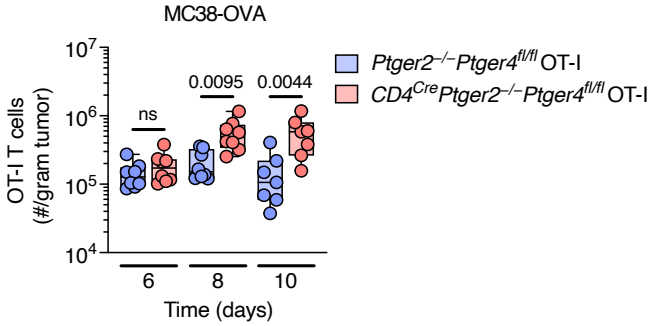


**Figure 28: Only double deficiency of EP2 and EP4 in adoptively transferred OT-I T cells protects from PGE$_2$-mediated impairment of expansion.** Quantification of OT-I T cells after the co-transfer of 1x10$^3$ OT-I T cells from *Ptger2$^{-/-}$Ptger4$^{fl/fl}$* and *CD4$^{Cre}$Ptger2$^{-/-}$Ptger4$^{fl/fl}$* OT-I mice into WT mice that were subsequently challenged with 2x10$^6$ MC38-OVA tumor cells. n=7-8, pooled from two independent experiments. Box plots showing the median with corresponding min and max values as whiskers. Data is depicted as mean ± SEM. Statistical significance was determined by one-way ANOVA with Tukey´s multiple comparison test. $P \geq 0.05$, not significant (ns).

These results suggest that only the deficiency of both EP2 and EP4 in adoptively transferred OT-I T cells is sufficient for expansion, overcoming the influence of PGE$_2$ signaling.

Notably, the phenotype of early tumor-infiltrating OT-I T cells deficient in EP2 and EP4 undergoes dynamic changes over time. Initially characterized by CD44$^{high}$ and TCF1$^{+}$TIM-3$^{low}$CXCR6$^{-}$Ki-67$^{low}$ expression, these cells transition to a TCF1$^{-}$TIM-3$^{high}$CXCR6$^{+}$Ki-67$^{high}$ phenotype, indicating a distinct differentiation process (**Figure 29a**). Moreover, tumor-infiltrating OT-I T cells deficient in EP2 and EP4 analyzed at later time points (day 8) exhibited a diverse array of stem-like and differentiated effector T cell subpopulations. These include CD62L$^{+}$ and CD62L$^{-}$ T cells within the TCF1$^{+}$CD8$^{+}$ (TIM-3$^{-}$CXCR6$^{-}$) T cell population, as well as early CX$_3$CR1$^{+}$ and late CX$_3$CR1$^{-}$ TIM-3$^{+}$CXCR6$^{+}$ cells, illustrating a diverse spectrum of T cell differentiation occurring within the TME (**Figure 29b**).

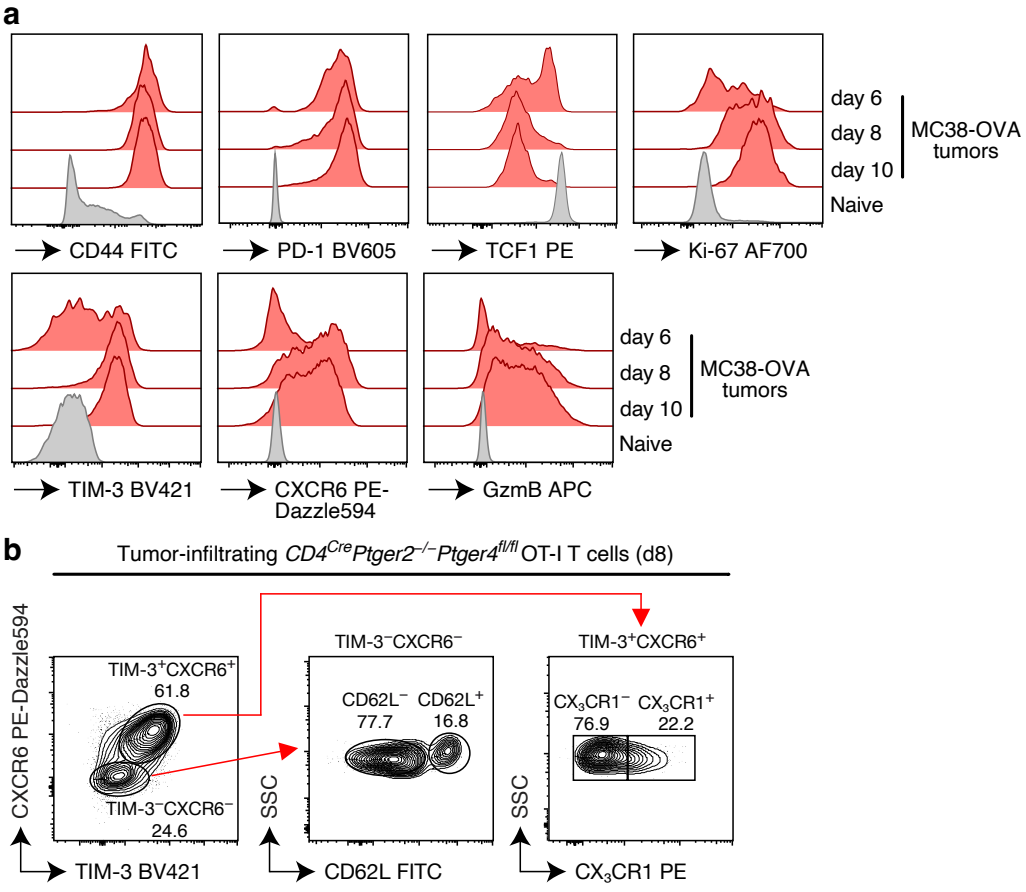


**Figure 29: Adoptively transferred *CD4$^{Cre}$Ptger2$^{-/-}$Ptger4$^{fl/fl}$* OT-I T cells into MC38-OVA bearing mice give rise to distinct effector CD8$^{+}$ T cell populations. (a)** Flow cytometry plots illustrating the expression of indicated markers in tumor-infiltrating *CD4$^{Cre}$Ptger2$^{-/-}$Ptger4$^{fl/fl}$* OT-I T cells in MC38-OVA tumors. Naive WT OT-I T cells served as control. **(b)** Representative flow cytometry plots depicting subpopulation composition among tumor-infiltrating *CD4$^{Cre}$Ptger2$^{-/-}$Ptger4$^{fl/fl}$* OT-I T cells based on **(a)**.

To verify the lineage of effector TIM-3$^{+}$CD8$^{+}$ T cells originating from the stem-like TCF1$^{+}$CD8$^{+}$ (TIM-3$^{-}$CXCR6$^{-}$) population, these two distinct OT-I T cell subsets were sorted from mice bearing MC38-OVA tumors 8 days after the adoptive T cell transfer of 1x10$^{3}$ naive OT-I T cells. Subsequently, 2 days post tumor cell inoculation, the obtained tumor-infiltrating TIM-3$^{-}$CXCR6$^{-}$ and TIM-3$^{+}$CXCR6$^{+}$ populations were retransferred into MC38-OVA-bearing *Rag1*$^{-/-}$ mice. TIM-3$^{-}$CXCR6$^{-}$ OT-I T cells exhibited significant expansion in recipient mice, whereas their TIM-3$^{+}$CXCR6$^{+}$ counterparts did not undergo substantial proliferation (**Figure 30a,b**). Moreover, TIM-3$^{-}$CXCR6$^{-}$ OT-I T cells underwent differentiation, giving rise to TIM-3$^{+}$CXCR6$^{+}$ OT-I T cells (**Figure 30c**).

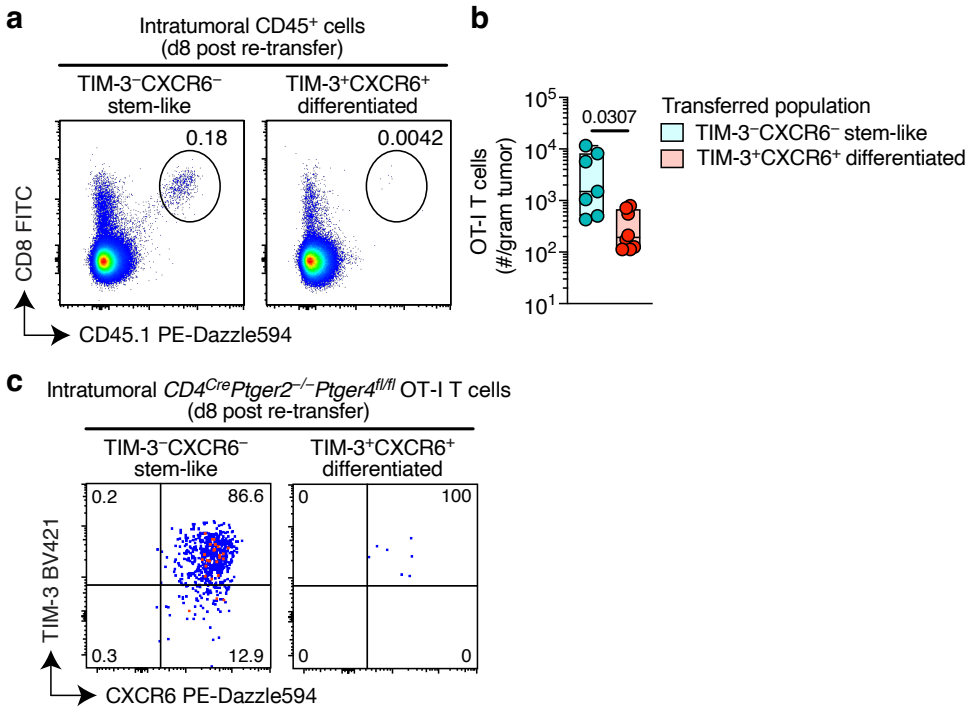


**Figure 30: Intratumoral TIM-3$^{-}$CXCR6$^{-}$ OT-I T cells expand and give rise to TIM-3$^{+}$CXCR6$^{+}$ OT-I T cells after a retransfer. (a)** Representative flow cytometry plot showing the frequencies of expanded intratumoral OT-I T cells in recipient mice among CD45$^{+}$ immune cells on day 8 after retransfer. **(b)** Quantification of intratumoral OT-I T cells in recipient mice based on **(a)**. n=7-8, pooled from two independent experiments. **(c)** Representative flow cytometry plots depicting the expression of TIM-3 and CXCR6 among expanded OT-I T cells based on **(a)**. Box plots in **(b)** showing the median with corresponding min and max values as whiskers. Data in **(b)** is depicted as mean ± SEM. Statistical significance was determined by an unpaired t-test.

Consistent with these findings, the differentiation of TCF1⁺ OT-I T cells into TIM-3⁺ OT-I cells was exclusively observed at the tumor site and not within tdLNs (**Figure 31a,b**). In tdLNs, the OT-I T cells maintained their TCF1⁺CD44⁺ expression, while at the tumor site, OT-I T cells progressively underwent differentiation into TCF1⁻CXCR6⁺ OT-I T cells.

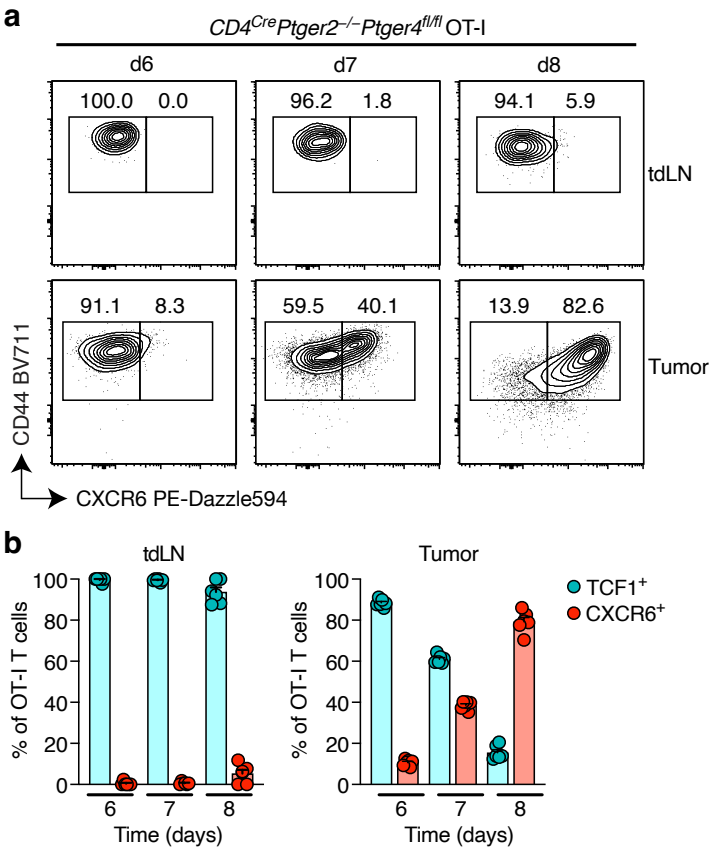


**Figure 31: Development of TIM-3⁺CXCR6⁺ effectors exclusively occurs within the tumor.**
**(a)** Representative flow cytometry plots illustrating CD44 and CXCR6 expression among pre-gated OT-I T cells in tdLNs and tumors at specified time points following the transfer of naive OT-I T cells. **(b)** Quantification of TCF1⁺ and effector CXCR6⁺ OT-I T cells in tdLNs and tumors based on **(a)**. n=6, pooled from two independent experiments.

In line with these observations and the previous FTY720 experiments, blocking the egress of newly primed antigen-specific OT-I T cells from tdLNs starting from day 6 onward did not impact the expansion of OT-I T cells at the tumor site (**Figure 32**).

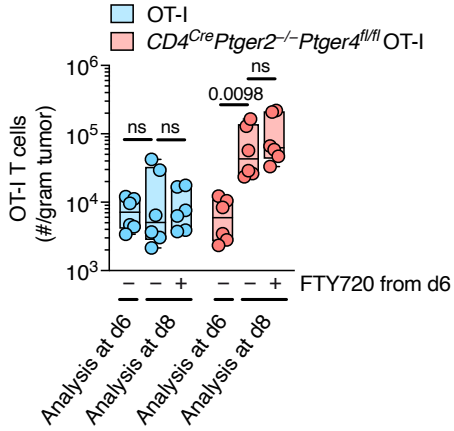


**Figure 32: Early tumor-infiltrating TCF1⁺ OT-I T cells efficiently expand within the TME.** Quantification of OT-I T cells 8 days after the adoptive transfer of 1x10³ naive OT-I T cells and the injection of MC38-OVA tumor cells. Mice received FTY720 treatment 6 days post tumor cell injections. n=6, pooled from two independent experiments. Box plots showing the median with corresponding min and max values as whiskers. Data is depicted as mean ± SEM. Statistical significance was determined by one-way ANOVA with Tukey´s multiple comparison test. $P \geq 0.05$, not significant (ns).

Collectively, these findings underscore the crucial role of stem-like TCF1⁺CD8⁺ T cells, which infiltrate the TME early and undergo local expansion and differentiation, ultimately giving rise to TIM-3⁺CD8⁺ T cells.

In line with previous findings indicating that $PGE_2$ signaling induces a non-responsive phenotype to IL-2, inhibiting the IL-2 pathway in antigen-specific OT-I T cells within mice bearing *Ptgs1/Ptgs2*$^{-/-}$ BRAF$^{V600E}$-OVA melanoma using αIL-2Rβ (αCD122) and αIL-2Rγc (αCD132) blocking antibodies (on day 6 and 7 post tumor cell injections) resulted in a significant reduction in OT-I T cell numbers (**Figure 33a,b**). Moreover, consistent observations were noted upon blocking the IL-2Rβ and IL-2Rγc in *CD4*$^{Cre}$*Ptger2*$^{-/-}$*Ptger4*$^{fl/fl}$ OT-I T cells in mice harboring MC38-OVA tumors (**Figure 33c,d**).

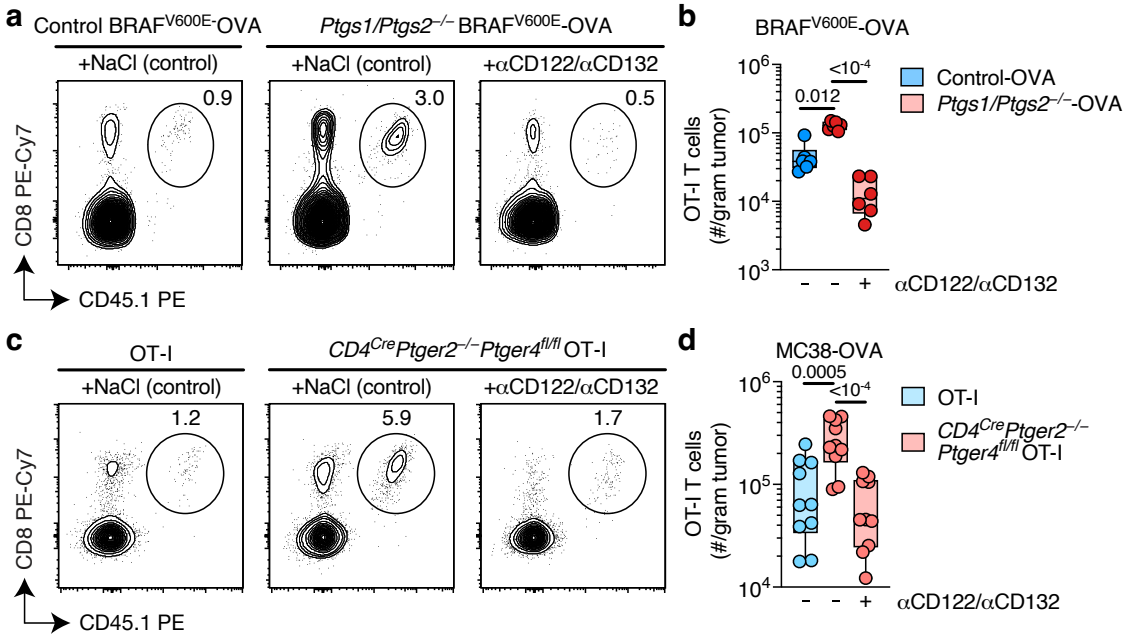


**Figure 33: Blocking the IL-2 pathway in OT-I T cells results in decreased CD8⁺ T cell numbers within the TME. (a)** Representative flow cytometry plots depicting the frequencies of OT-I T cells after blockage of the IL-2R signaling in *Ptgs1/Ptgs2*$^{-/-}$ BRAF$^{V600E}$-OVA tumors. **(b)** Quantification of tumor-infiltrating OT-I T cells 8 days post OT-I T cell transfer and tumor cell inoculation based on **(a)**. n=6, pooled from two independent experiments. **(c)** Representative flow cytometry plots depicting the frequencies of OT-I T cells after blockage of the IL-2R signaling in MC38-OVA tumors. **(d)** Quantification of tumor-infiltrating OT-I T cells 8 days post OT-I T cell transfer and tumor cell inoculation based on **(c)**. n=10, pooled from two independent experiments. Box plots in **(b)** and **(d)** showing the median with corresponding min and max values as whiskers. Data in **(b)** and **(d)** is depicted as mean ± SEM. Statistical significance for **(b)** and **(d)** was determined by one-way ANOVA with Tukey´s multiple comparison test.

Additionally, the co-transfer of mock-treated control *CD4*$^{Cre}$*Ptger2*$^{-/-}$*Ptger4*$^{fl/fl}$ (CD45.1/CD45.1) and *Cd122*$^{-/-}$-*CD4*$^{Cre}$*Ptger2*$^{-/-}$*Ptger4*$^{fl/fl}$ (CD45.1/CD45.2) OT-I T cells into WT recipient mice (CD45.2/CD45.2), initiated 2 days after tumor cell inoculation with MC38-OVA cells, confirmed reduced IL-2 mediated expansion and effector differentiation of tumor-infiltrating OT-I T cells (**Figure 34a,b**).

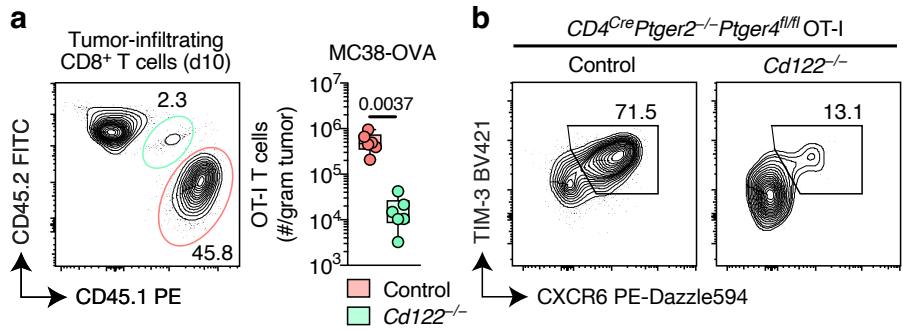


**Figure 34: Ablation of IL-2Rβ results in a substantial decrease in tumor-infiltrating expansion and effector differentiation. (a)** Representative flow cytometry plot and Quantification of adoptively transferred mock-*CD4*$^{Cre}$*Ptger2*$^{-/-}$*Ptger4*$^{fl/fl}$ (CD45.1/CD45.1) and *Cd122*$^{-/-}$-*CD4*$^{Cre}$*Ptger2*$^{-/-}$*Ptger4*$^{fl/fl}$ (CD45.1/CD45.2) OT-I T cells in MC38-OVA tumors 8 days post adoptive T cell transfer. n=6, pooled from two independent experiments. **(b)** Representative flow cytometry plot illustrating the expression of CXCR6 and TIM-3 among tumor-infiltrating OT-I T cells on day 8 post T cell transfer based on **(a)**. Box plot in **(a)** showing the median with corresponding min and max values as whiskers. Data in **(a)** is depicted as mean ± SEM. Statistical significance for **(a)** was determined by a paired t-test.

Collectively, these findings suggest that $PGE_2$-EP2/EP4 signaling hinders the IL-2 responsiveness of intratumoral $CD8^+$ T cells, consequently impeding their expansion and effector differentiation. This impairment can be overcome by the ablation of EP2 and EP4.

Finally, to assess whether the ablation of EP2 and EP4 on adoptively transferred OT-I T cells leads to protective $CD8^+$ T cell-mediated anti-cancer immune responses, WT mice received either $1x10^3$ naive WT OT-I or *CD4*$^{Cre}$*Ptger2*$^{-/-}$*Ptger4*$^{fl/fl}$ OT-I T cells, followed by the injection of either $2x10^6$ MC38-OVA or D4M.3A-pOVA tumor cells (**Figure 35**). Mice that received *CD4*$^{Cre}$*Ptger2*$^{-/-}$*Ptger4*$^{fl/fl}$ OT-I T cells were able to reject tumors completely, which was not observed for mice that received WT OT-I T cells (**Figure 35a,b**). In line with previous findings, *CD4*$^{Cre}$*Ptger2*$^{-/-}$*Ptger4*$^{fl/fl}$ OT-I T cell numbers were substantially increased within D4M.3A-pOVA tumors compared to their WT counterparts (**Figure 35c**). This indicates that, in the context of this tumor model, the protective anti-cancer immune response once again originates from the expanded population of EP2/EP4 ablated OT-I T cells.

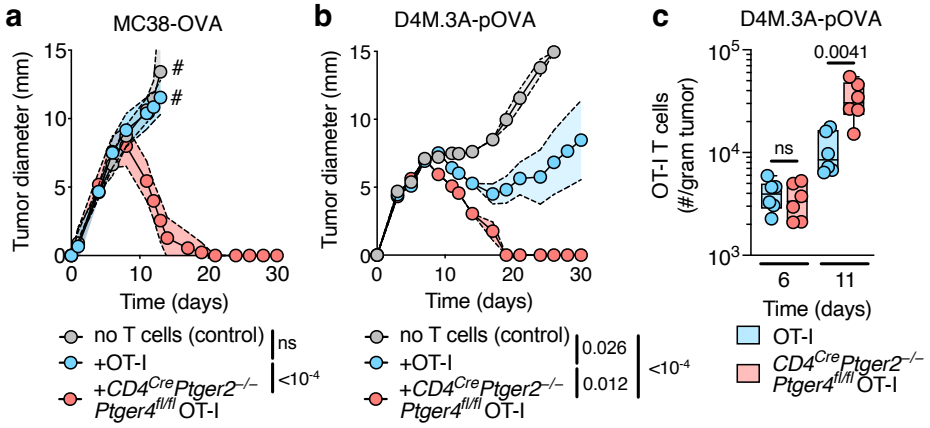


**Figure 35: Ablation of EP2 and EP4 on adoptively transferred OT-I T cells mounts protective anti-cancer immune responses. (a)** Tumor growth profiles. WT mice received either 1x10$^3$ naive WT OT-I or *CD4$^{Cre}$Ptger2$^{-/-}$Ptger4$^{fl/fl}$* OT-I T cells and subsequently were injected with 2x10$^6$ MC38-OVA tumor cells. **(b)** Tumor growth profiles. WT mice received either 1x10$^3$ naive OT-I or *CD4$^{Cre}$Ptger2$^{-/-}$Ptger4$^{fl/fl}$* OT-I T cells and subsequently were injected with 2x10$^6$ D4M.3A-pOVA tumor cells. **(c)** WT mice received both 1x10$^3$ naive OT-I and *CD4$^{Cre}$Ptger2$^{-/-}$Ptger4$^{fl/fl}$* OT-I T cells and subsequently were injected with 2x10$^6$ D4M.3A-pOVA tumor cells. n=6, pooled from two independent experiments. Box plots in **(c)** showing the median with corresponding min and max values as whiskers. Data is depicted as mean ± SEM. Statistical significance for **(a)** and **(b)** was determined by two-way ANOVA with Bonferroni´s correction for multiple testing and statistical significance for **(c)** was determined by an unpaired t-test.

In summary, these findings collectively demonstrate that disrupting the $PGE_2$-EP2/EP4 axis in tumor-specific CD8$^+$ T cells promotes their intratumoral expansion and differentiation into effector CD8$^+$ T cells, ultimately fostering protective T cell-mediated anti-cancer immune responses.

# 5 Discussion

$CD8^+$ T cells play a pivotal role in orchestrating anti-cancer immunity in both mice and humans. Recent advancements have highlighted the significance of stem-like $TCF1^+CD8^+$ T cells in mediating effective $CD8^+$ T cell responses against viral infections and cancer through their capacity to generate effector $CD8^+$ T cells[113,121,122]. Despite this recognition, our understanding of the differentiation process of these stem-like $TCF1^+CD8^+$ T cells and the factors influencing their regulation remains limited.

Many human and mouse cancers exhibit a profound expression of prostaglandin E2, which has been recognized to mediate immunosuppressive effects, leading to cancer immune escape[57–59,62,65]. $PGE_2$ is widely acknowledged for its impact on myeloid cells, affecting macrophages, monocytes, and dendritic cells[59,62]. In line with this, $PGE_2$ also exerts effects on lymphocytes, including NK cells and T cells[50,60,91,92]. Nevertheless, our understanding of the specific effects of $PGE_2$ signaling in T cells remains limited, underscoring the need for comprehensive investigation and further exploration. This study aimed to elucidate the impact of tumor-derived $PGE_2$ on stem-like $TCF1^+CD8^+$ T cells using a novel mouse model in which T cells were ablated in their expression of the two $PGE_2$ receptors, EP2 and EP4. This model provided profound insights into the direct impact of $PGE_2$ signaling in tumor-infiltrating $CD8^+$ T cells, thereby unraveling its subsequent downstream effects. This study revealed that $PGE_2$ signaling in stem-like $TCF1^+CD8^+$ T cells impairs their local differentiation and expansion into effector $CD8^+$ T cells, thus impeding effective anti-cancer immune responses. This effect is, at least in part, mediated by the downregulation of IL-2 responsiveness and the consequent decrease in mTORC1 signaling in stem-like $TCF1^+CD8^+$ T cells. Hence, the findings outlined in this work reveal a novel checkpoint that the immune system must overcome to orchestrate potent anti-cancer $CD8^+$ T cell responses, ultimately influencing the determination between tumor escape and tumor control.

## 5.1 The role of tumor-derived $PGE_2$ in regulating anti-cancer T cell responses

Remarkably, the specific contribution of $PGE_2$ signaling in anti-cancer $CD8^+$ T cells has been poorly characterized until now. Consequently, the mechanisms through which $PGE_2$ signaling in $CD8^+$ T cells leads to a diminished anti-cancer immune response remain poorly understood. In this study, enhanced tumor control was observed when *Ptgs1/Ptgs2*$^{-/-}$ and control $BRAF^{V600E}$ tumor cells were transplanted into WT and *CD4*$^{Cre}$*Ptger2*$^{-/-}$*Ptger4*$^{fl/fl}$ mice, respectively. This phenomenon could be attributed to increased numbers of intratumoral effector $CD8^+$ T cells, an observation not found in WT and *Ptger2*$^{-/-}$*Ptger4*$^{fl/fl}$ mice challenged with $PGE_2$-producing control $BRAF^{V600E}$ tumor cells. Consistently, prior investigations have correlated favorable clinical prognoses in human cancer patients with a significant abundance of tumor-infiltrating $CD8^+$ T cells, with terminally differentiated effector $CD8^+$ T cells being the most prevalent[107,121,122]. These findings highlight the direct inhibitory effect of $PGE_2$ on $CD8^+$ T cells and the development of potent anti-cancer immune responses mediated by $CD8^+$ T cells.

Given the pivotal role of the priming event in the early immune response to cancer in tdLNs, this study aimed to explore the potential influence of tumor-derived $PGE_2$ on this process[11,188,190]. Both the cross-presentation of tumor-derived antigens by cDC1s, as well as the activated phenotype and expansion of antigen-specific $TCF1^+CD8^+$ T cells in tdLNs, occurred independently of tumor-derived $PGE_2$. In line with this, *Ptgs1/Ptgs2*$^{-/-}$ tumors that shared the same lymph drainage site with control $BRAF^{V600E}$ melanoma were effectively rejected by WT mice. Notably, primed $CD8^+$ T cells demonstrated a distinct phenotype compared to naive counterparts, initiating alterations in both their gene expression profile and epigenetic signature as noted by others[122,188,191]. Concurrently, these $CD8^+$ T cells began to upregulate CD44 early after TCR engagement while maintaining their $TCF1^+$ phenotype, indicating their status as antigen-experienced cells[122,188,192]. This aligns with previous research indicating that $PGE_2$ does not influence cDC1-mediated

priming of naive antigen-specific $CD8^+$ T cells in tdLNs[62]. Primed $CD8^+$ T cells then migrated into the TME, exhibiting a stem-like $TCF1^+CD8^+$ phenotype[121,188]. These results, coupled with the observation that $PGE_2$ did not impact T cell migration to the tumor site, conclusively demonstrate that tumor-derived $PGE_2$ shows no influence on T cell priming, expansion in secondary lymphoid organs, and the infiltration of antigen-specific stem-like $TCF1^+CD8^+$ T cells into the TME.

These findings indicate the urgent need for a comprehensive understanding of the local effects of tumor-derived $PGE_2$ on $CD8^+$ T cell biology within the tumor. Studying anti-cancer immune responses in *CD4$^{Cre}$Ptger2$^{-/-}$Ptger4$^{fl/fl}$* mice, as well as the adoptive T cell transfers, provided compelling evidence that $PGE_2$ has a direct effect on $CD8^+$ T cells within the TME. Notably, several studies have demonstrated that within the TME, the stem-like $TCF1^+CD8^+$ T cells experience reactivation by APCs, including cDC1s, providing essential costimulatory signals and making them potential contributors to T cell-mediated anti-cancer immunity[11,61,62]. Tumor-derived $PGE_2$ has been noted to affect NK cell-mediated recruitment of cDC1s into the TME, which is essential for T cell restimulation, by reducing the expression of the chemokine ligands CCL5 and XCL1[60,87]. Additionally, it has been observed that $PGE_2$ impedes the cytokine-mediated modulation of tumor-infiltrating $CD8^+$ T cells by cDC1s, as indicated by their reduced expression of IL-12[62]. However, according to recently published data, the capacity of intratumoral cDC1s to perform cross-presentation and deliver essential costimulatory signals to tumor-infiltrating stem-like $TCF1^+CD8^+$ T cells appears unaltered by $PGE_2$[62]. This observation suggests that $PGE_2$ might reduce the infiltration of cDC1s into the TME rather than directly impacting the restimulation of intratumoral stem-like $TCF1^+CD8^+$ T cells. However, in this study, a comprehensive analysis to assess the direct impact of $PGE_2$ on tumor-infiltrating $CD8^+$ T cells in the context of local reactivation has not been addressed, leaving the need for future investigation. Furthermore, it is worth noting that the cDC1-mediated assistance in T cell responses might be less crucial than anticipated for anti-cancer

immunity in specific types of cancer as demonstrated by others[193,194]. Nevertheless, the direct effects of $PGE_2$ signaling in $CD8^+$ T cells seem to surpass any potential decrease in their reactivation by cDC1s within the TME. This suggests that the suppressive influence of $PGE_2$ on $CD8^+$ T cells extends beyond its effects on NK cells or DCs, prominently affecting the functionality of tumor-infiltrating $CD8^+$ T cells directly.

Given the absence of $PGE_2$-EP2/EP4 signaling in *CD4$^{Cre}$Ptger2$^{-/-}$Ptger4$^{fl/fl}$* mice in both $CD4^+$ and $CD8^+$ T cells, this study aimed to investigate the contribution of $CD4^+$ T cells in the used tumor and mouse models. $PGE_2$ signaling on $CD4^+$ T cells did not impact their recruitment or abundance at the tumor site. Moreover, $CD4^+$ T cell-targeted depletion did not alter the outcome of complete tumor control in *CD4$^{Cre}$Ptger2$^{-/-}$Ptger4$^{fl/fl}$* mice. However, $CD4^+$ T cell-depleted mice exhibited a slight delay in tumor control compared to non-depleted mice. These results indicate that $PGE_2$ signaling in $CD4^+$ T cells may only play a minor role in mediating robust anti-cancer immune responses, at least in the models studied in this work. Nonetheless, $CD4^+$ T cells are recognized as significant contributors to anti-tumor immunity. They provide $CD8^+$ T cells with supportive cytokines like IFN$\gamma$ and TNF$\alpha$, and they activate DCs, indirectly enhancing cross-presentation to anti-cancer $CD8^+$ T cells[195,196]. Moreover, EP2/EP4 signaling in $CD4^+$ T cells has been demonstrated to impede differentiation towards pro-inflammatory anti-cancer $T_{h1}$ cells while promoting polarization into non-inflammatory $T_{h2}$ cells[73]. Consequently, the observed slight delay in tumor control in $CD4^+$ T cell-depleted *CD4$^{Cre}$Ptger2$^{-/-}$Ptger4$^{fl/fl}$* mice may be attributed to the absence of IFN$\gamma$- and TNF$\alpha$-producing $CD4^+$ T cells along with the depletion of $T_{h1}$ cells. Nonetheless, further investigation is needed to understand the precise influence of $PGE_2$ on the differentiation and function of $CD4^+$ T cells and, subsequently, its impact on $CD8^+$ T cell-mediated anti-cancer immunity.

Only very little is known about the effects of $PGE_2$-EP2/EP4 signaling in $CD8^+$ T cells. In this study, $PGE_2$ signaling on intratumoral TIM-$3^+CD8^+$ T cells did not impair their gene signatures associated with effector functions or their potential to upregulate effector molecules such as IFNγ and TNFα. Furthermore, $PGE_2$ did not show an effect on the direct killing of tumor cells by effector $CD8^+$ T cells. These data indicate that $PGE_2$ may not mediate its suppressive effects on anti-cancer immunity by impairing $CD8^+$ T cell effector functions. In contrast to this, previous studies suggested that $PGE_2$ signaling in $CD8^+$ T cells negatively impairs the production of effector cytokines and molecules, including TNFα, IFNγ, GzmB, and perforin, whereas others have demonstrated that the engagement of the $PGE_2$-EP2/EP4 axis may lead to suppressed cytotoxicity[184,197]. For example, elevated levels of $PGE_2$ in patients with chronic hepatitis B virus infection were associated with increased viral loads and decreased levels of perforin and GzmB in $CD8^+$ T cells[184,197]. However, further investigation is required to determine whether these elevated $PGE_2$ levels directly affect the production of effector molecules and the cytotoxicity of $CD8^+$ T cells or exert their influence indirectly through other mechanisms[197]. Moreover, studies have shown that $PGE_2$ signaling in virus-specific P14 $CD8^+$ T cells can decrease the production of perforin, TNFα, and IFNγ upon restimulation with virus-peptide *ex vivo*. However, it is worth noting that in these studies, a very high concentration of $PGE_2$ (40 μM) was used for restimulation, which may not be physiologically relevant, considering that 3 μM (the concentration employed in this study and representative of what is found within the TME; data not shown in this work) already demonstrated significant effects on $CD8^+$ T cells. Hence, further investigation is necessary to determine whether there are differences in effector molecule production among effector $CD8^+$ T cells between viral infections and cancers under physiological concentrations of $PGE_2$.

In summary, these findings suggest that $PGE_2$ signaling on $CD8^+$ T cells does not influence T cell priming in distal secondary lymphoid organs and subsequent infiltration of stem-like $TCF1^+CD8^+$ T cells into the TME. Moreover, $CD4^+$ T cells appear to play only a minor role in mediating anti-cancer immunity in the models examined in this study. Finally, the results suggest that $PGE_2$ has no substantial effect on the functionality of cancer-specific effector $CD8^+$ T cells. Consequently, this raises the question of how $PGE_2$ exerts its suppressive effects on tumor-infiltrating $CD8^+$ T cells and their function to mediate effective anti-cancer immunity.

## 5.2 The local effects of $PGE_2$ on tumor-infiltrating $CD8^+$ T cells

This study revealed that early tumor-infiltrating stem-like $TCF1^+CD8^+$ T cells, which are phenotypically distinct from naive cells, give rise to diverse populations of terminally differentiated $CD8^+$ T cells directly within the TME as previously suggested by Prokhnevska et al. (2023). This groundbreaking discovery highlights that stem-like $TCF1^+CD8^+$ T cells differentiate and proliferate into clonally related $CD8^+$ T cells directly within the TME, underscoring their pivotal role as a primary source of anti-cancer effector $CD8^+$ T cells. This observation aligns with earlier findings that depleting stem-like $TCF1^+CD8^+$ T cells substantially reduces the accumulation of effector $CD8^+$ T cells[198,199]. In line with this, inhibiting the influx of newly primed $TCF1^+CD8^+$ T cells after their prior tumor infiltration resulted in the generation of effector cells, thereby ultimately contributing to tumor control[122]. These findings have also been described in the field of chronic infection, where TCF1-expressing $CD8^+$ T cells differentiate and expand into progeny cells, thereby maintaining the anti-virus immune response[108,118]. However, the developmental trajectory in the context of tumors has not been demonstrated until now and emphasizes that, in contrast to established perspectives for chronic LCMV infections, the signals for the differentiation of stem-like $TCF1^+CD8^+$ T cells into effector $CD8^+$ T cells do not exclusively occur initially within secondary lymphoid organs but instead may also manifest directly at the tumor site[120,123,127,128]. This raises the question of which environmental factors and stimulatory signals contribute to the local differentiation and expansion of stem-like $TCF1^+CD8^+$ T cells into their progeny.

Results from this work revealed that despite similar intratumoral stem-like $TCF1^+CD8^+$ T cell numbers at early time points following tumor cell inoculation, the presence of tumor-derived $PGE_2$ results in a significant reduction in the quantity of differentiated $TIM\text{-}3^+CD8^+$ T cells. Consistently, studies have shown that $PGE_2$ acts locally and may hinder the differentiation and proliferation of $CD8^+$ T cells[62,92,94–96,200,201]. However, this study demonstrated that $PGE_2$ signaling directly impacts

stem-like TCF1$^{+}$CD8$^{+}$ T cells, independent of indirect mechanisms, such as interactions with other immune cells. This suggests that $PGE_2$ signaling on tumor-infiltrating stem-like TCF1$^{+}$CD8$^{+}$ T cells impairs their local differentiation and proliferation into effector CD8$^{+}$ T cells, consequently impacting the establishment of robust anti-cancer immune response mediated by CD8$^{+}$ T cells. In line with this, previous research has underscored the significant influence of $PGE_2$ signaling not only on CD4$^{+}$ T cell but also on TAM differentiation, promoting the development of anti-inflammatory cell subsets[73,81,93]. Nevertheless, a comprehensive understanding of the T cell-intrinsic mechanisms triggered by $PGE_2$ signaling in CD8$^{+}$ T cells remains elusive until now.

Furthermore, it is worth noting that *GzmB$^{Cre}$Ptger2$^{-/-}$Ptger4$^{fl/fl}$* mice showed an even more pronounced differentiation and expansion signature within the TME when compared to *CD4$^{Cre}$Ptger2$^{-/-}$Ptger4$^{fl/fl}$* mice. This can be explained by an increased presence of NK cell-recruited cross-presenting cDC1s at the tumor site[11,60,62]. This may lead to elevated cluster formation with stem-like TCF1$^{+}$CD8$^{+}$ T cells, resulting in enhanced differentiation and expansion of intratumoral effector CD8$^{+}$ T cells (elaborated in more detail in section 5.1)[61,62].

Together, these findings strongly support the idea that effector T cell differentiation takes place within the TME. Moreover, tumor-derived $PGE_2$ seems to directly affect intratumoral stem-like TCF1$^{+}$CD8$^{+}$ T cells in their expansion and differentiation, leading to reduced numbers of effector CD8$^{+}$ T cells and ultimately affecting the development of robust anti-cancer immune responses. However, the precise T cell-intrinsic mechanisms triggered by $PGE_2$ signaling in stem-like TCF1$^{+}$CD8$^{+}$ T cells remain unknown and will be discussed in section 5.3.

## 5.3 Molecular T cell-intrinsic mechanism underlying $PGE_2$-mediated impairment of anti-cancer T cell responses in tumors

This work revealed that $PGE_2$ signaling in intratumoral stem-like $TCF1^+CD8^+$ T cells induces a reduced gene expression signature associated with differentiation and IL-2 signaling. Moreover, the engagement of the $PGE_2$-EP2/EP4 axis in $CD8^+$ T cells led to the downregulation of the IL-2-STAT5 signaling pathway, which was further accompanied by the reduction of the mTROC1 signaling cascade. Finally, $PGE_2$ signaling significantly downregulated the IL-2Rγc-expression in stem-like $TCF1^+CD8^+$ T cells. These findings underscore the substantial impact of $PGE_2$ signaling on intratumoral stem-like $TCF1^+CD8^+$ T cells, attenuating their responsiveness to IL-2. This discovery offers a potential explanation for the observed deficiency in differentiation and expansion into effector $CD8^+$ T cells originating from stem-like $TCF1^+CD8^+$ T cells directly within the TME. This is further supported by the downregulation of TBX21, previously identified as one of the primary drivers for the differentiation of stem-like $TCF1^+CD8^+$ T cells[113,126]. In line with this, numerous studies have previously demonstrated the association of $PGE_2$ with the impairment of early $CD8^+$ T cell activation, leading to reduced IL-2 production and sensitivity to exogenous IL-2[95,202,203]. Moreover, it has been demonstrated that $PGE_2$ can dampen cytokine and chemokine signaling in cDC1s, monocytes, $CD4^+$ T cells, and NK cells[60,62,73]. However, a detailed explanation for this phenomenon in $CD8^+$ T cells remained elusive until now. The downregulation of IL-2Rγc and the subsequent failure to respond to IL-2 upon $PGE_2$ signaling is a significant breakthrough as it has not been described previously for intratumoral stem-like $TCF1^+CD8^+$ T cells and provides new insights into the $PGE_2$-mediated immune suppressive effects in anti-cancer immunity. In recent years, there has been an increasing emphasis on investigating IL-2 signaling, driven by the development of novel classes of IL-2R agonists for cancer therapy[43,45,148]. Understanding the role of IL-2 signaling is crucial for fostering productive anti-cancer responses, particularly with the emerging recognition of the significant function played by tumor-infiltrating stem-like $TCF1^+CD8^+$ T cells[45,204]. Therefore, the knowledge obtained from this

study enhances our understanding of the complexities of IL-2-mediated $CD8^+$ T cell responses to $PGE_2$-producing tumors.

Notably, the downregulation of IL-2Rγc suggests that $PGE_2$ signaling may not only restrict IL-2 sensing but also impact the signaling of other common gamma chain cytokines. In line with this, extensive research has lately concentrated on elucidating the significance of the common gamma chain cytokines IL-7 and IL-15 in the development, maintenance, and exhaustion of various T cell subsets, as well as their pivotal role in cancer immunotherapy[205–208].

Taken together, these findings demonstrate that $PGE_2$ signaling in tumor-infiltrating stem-like $TCF1^+CD8^+$ T cells limits their responsiveness to IL-2, thereby affecting their local differentiation into effector $CD8^+$ T cells. Moreover, the observed downregulation of the IL-2Rγc indicates that $PGE_2$ may also influence other gamma chain cytokine-mediated pathways. Hence, exploring this dimension, which remains elusive in the current study, might be of great interest in finding novel therapeutic options for anti-cancer immunotherapy besides the IL-2 axis.

## 5.4 Implication for our understanding of T cell biology and for T cell targeted therapy

Studies have shown that stem-like TCF1$^+$CD8$^+$ T cells, which initially respond to ICB in tumors and chronic infections, demonstrate prognostic value for positive clinical outcomes, yet despite their robust initial response, they fail to mediate robust T cell immunity, most likely through exhaustion-related pathway induction, the development of a quiescent phenotype, and a suppressive TME[113,131,132]. Therefore, understanding the biology of stem-like TCF1$^+$CD8$^+$ T cells is crucial for advancing targeted therapies, particularly in addressing challenges related to increased T cell responses post-treatment. The need to potentiate the capacity of stem-like TCF1$^+$CD8$^+$ T cells to generate effector CD8$^+$ T cells without compromising their long-term persistence remains a significant challenge, highlighting the necessity for research focused on unraveling the biology of stem-like TCF1$^+$CD8$^+$ T cells in the context of targeted therapy. Hence, there is considerable interest in targeting the $PGE_2$-EP2/EP4 pathway on these cells to promote robust differentiation and expansion of effector CD8$^+$ T cells, thereby facilitating potent CD8$^+$ T cell responses.

One of those targeted therapies is the chimeric antigen receptor (CAR) T cell therapy, which has been proven largely effective in hematological malignancies like myeloma and non-Hodgkin B cell lymphomas[209–211]. This study revealed that an adoptive T cell transfer of EP2/EP4-ablated CD8$^+$ T cells can facilitate curative anti-cancer responses through enhanced proliferation at the tumor site compared to CD8$^+$ T cells with intact $PGE_2$-EP2/EP4 signaling. These findings suggest that adoptively transferred CD8$^+$ T cells are capable of infiltrating the TME and that EP2/EP4 knockout CD8$^+$ T cells can overcome the tumor-suppressive environment, leading to potent anticancer responses. Yet, implementing CAR T cell therapy to target solid cancers encounters several challenges beyond the immunosuppressive environment. These include limitations in trafficking and infiltration, on-target restrictions, and the risk of off-tumor toxicity[209,210]. Nonetheless, EP2/EP4 ablation on adoptively

transferred $CD8^+$ T cells represents a step towards overcoming immunosuppressive factors that might otherwise attenuate robust anti-cancer $CD8^+$ T cell responses. However, it remains to be determined whether these findings will extend to more established tumors, and further investigation is needed to assess the potential of EP2/EP4 ablation on CAR T cells within the context of human therapeutic approaches.

Another promising strategy targeting $CD8^+$ T cells involves employing ADCs. These innovative compounds consist of monoclonal antibodies covalently linked to cytotoxic drugs via a chemical or biochemical linker. They are currently employed to deliver their cytotoxic payloads into cancer cells, thereby initiating their elimination. Nevertheless, these drugs exhibit significant side effects, such as neutropenia, thrombocytopenia, hepatotoxicity, nephrotoxicity, and gastrointestinal reactions. These adverse effects are attributed to the premature release of cytotoxic payloads into the bloodstream before reaching its target cell[166]. This underscores the urgent need for approaches to mitigate off-target effects.

One promising strategy could involve the use of ADCs in $CD8^+$ T cell-targeted therapy. Two promising small molecules specifically targeting EP2 (TG6-129) and EP4 (LY3127760) have been shown to exhibit low cytotoxicity *in vivo* with highly selective binding to the $G\alpha_s$ subunits of EP2 and EP4, leading to effective blockade of EP2/EP4 signaling[212,213]. This study demonstrated that the global EP2 knockout and the combined knockout with EP4 in T cells in mice did not lead to any pathologies or changes in the composition of $CD4^+$ and $CD8^+$ T cells under physiological conditions. This implies that the release of potential EP2 and EP4 inhibitors into the bloodstream before reaching its target cell may result in reduced side effects, as these drugs would not exert cytotoxic effects on non-target cells. However, it has to be considered that non-steroidal anti-inflammatory drugs (NSAIDs), intended to inhibit COX enzymes and thereby $PGE_2$ synthesis, have been associated with severe side effects such as cardiovascular diseases and central nervous system disorders in patients, implying that blocking the $PGE_2$-EP2/EP4 axis may have an impact on

physiological functions and potentially on the body's homeostasis[214–216]. Nevertheless, the results from this study highlight ADCs as a promising and innovative avenue for modification to target $CD8^+$ T cells rather than cancer cells. Nevertheless, this hypothesis requires detailed investigation, especially regarding whether the premature release and the subsequent simultaneous blockade of EP2 and EP4 in cells other than $CD4^+$ and $CD8^+$ T cells may have any pathophysiological implications.

Another limitation of ADCs is that these drugs have a much bigger molecular weight than conventional cytotoxic drugs, limiting the infiltration into the TME[165]. Considering that stem-like $TCF1^+CD8^+$ T cells start to display a PD-1 positive phenotype in draining lymph nodes and in blood in both the context of tumors and chronic infections, targeting PD-1 with ADCs emerges as a promising strategy to specifically address antigen-experienced stem-like $TCF1^+CD8^+$ T cells to effectively overcome the challenge of diminished drug infiltration into the TME[113,128,217].

Moreover, it is worth noting that the efficacy of drugs may be influenced by ATP-binding cassette transporters (ABC), as $CD8^+$ T cells also express these molecules that actively pump drugs out of cells. However, current evidence suggests that these ABC transporters play a more prominent role in cancer cells[218–220]. Nevertheless, further investigation is necessary to determine whether EP2/EP4-blocked stem-like $TCF1^+CD8^+$ T cells can effectively infiltrate more established tumors and whether the blockade of EP2/EP4 is adequate to protect these cells from $PGE_2$ signaling. Moreover, the applicability of this targeted $CD8^+$ T cell therapeutic approach for humans needs to be validated in future research.

Taken together, focusing on the EP2/EP4 signaling pathway in $CD8^+$ T cells shows promise for clinical treatment. An encouraging and novel approach might involve developing ADCs to specifically target stem-like $TCF1^+CD8^+$ T cells. Future research might investigate selective EP2/EP4 inhibitors and tailored drug delivery methods for the stem-like $TCF1^+CD8^+$ T cell population, potentially revolutionizing targeted $CD8^+$ T cell treatment options.

In summary, this study revealed a novel mechanism wherein tumor-derived $PGE_2$ impacts the localized expansion and effector differentiation of stem-like $TCF1^+CD8^+$ T cells within the TME, a critical process for evading the immune response in cancer. This inhibitory effect depends on T cell-intrinsic signaling through the $PGE_2$ receptors EP2 and EP4. $PGE_2$ signaling does not impact distal naive $CD8^+$ T cell priming at tdLNs or the infiltration of activated $TCF1^+CD8^+$ T cells at the tumor site. These stem-like $TCF1^+CD8^+$ T cells undergo differentiation and expansion into effector cells, a process in which $PGE_2$, at least in part, interferes with the downregulation of IL-2 responsiveness, resulting in reduced mTORC1 signaling and reduced effector $CD8^+$ T cell numbers within the TME. Disrupting the $PGE_2$-EP2/EP4 axis in stem-like $TCF1^+CD8^+$ T cells enhances their sensitivity to IL-2, thereby inducing an accumulation of effector $CD8^+$ T cells and a robust and protective anti-cancer immune response (**Figure 36**).

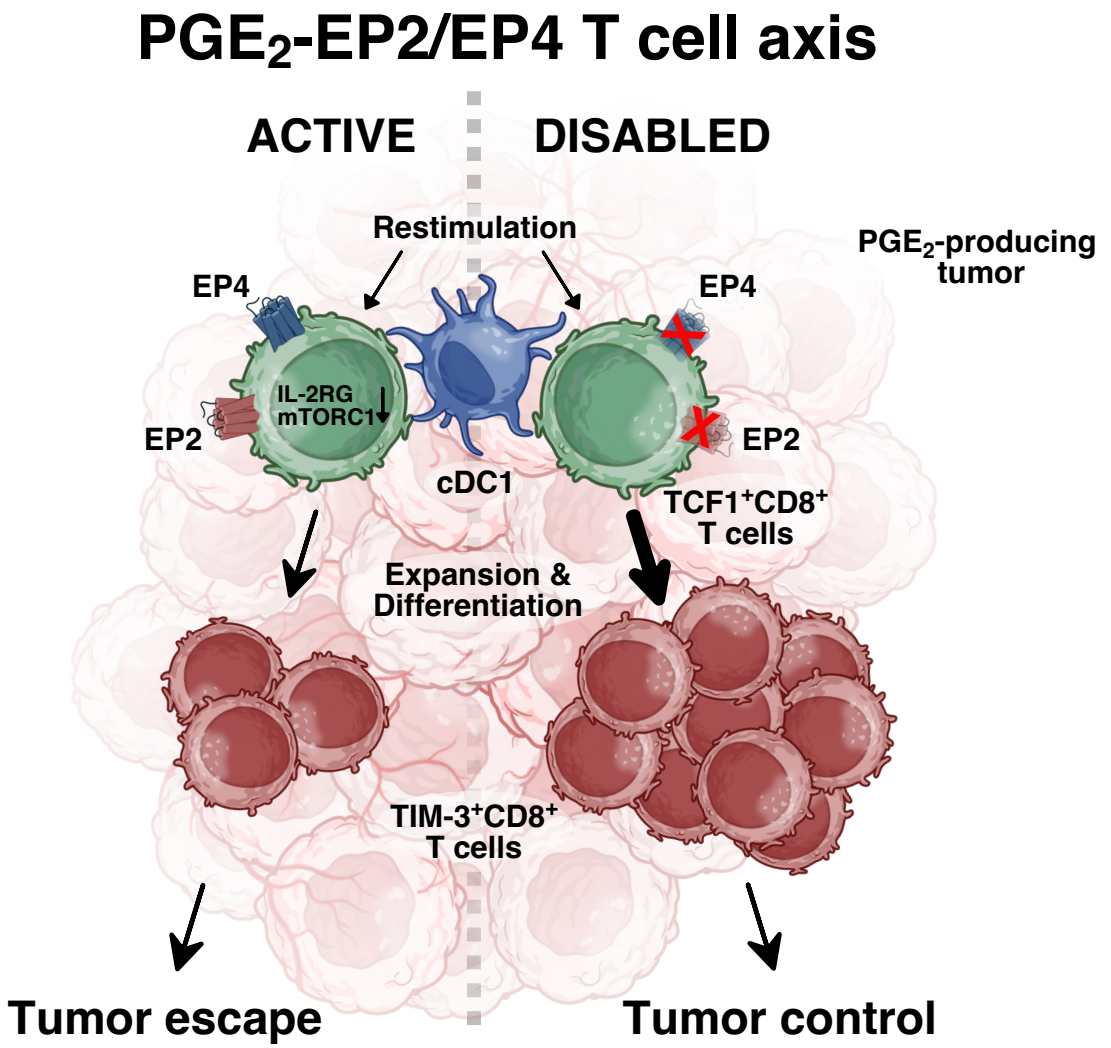


**Figure 36: Schematic illustration of the effects of $PGE_2$ signaling on tumor-infiltrating $CD8^+$ T cells.** Created with BioRender.com.

The study indicates that inhibiting the $PGE_2$-EP2/EP4 signaling axis shows promise in enhancing $CD8^+$ T cell immune therapy for cancer patients, as evidenced by the observed effect when EP2/EP4-ablated $CD8^+$ T cells were adoptively transferred into tumor-bearing mice. Furthermore, these findings underscore the urgent need to gain a deeper understanding of the dynamics of stem-like $TCF1^+CD8^+$ T cell-mediated immune responses and how extrinsic factors regulate them. This knowledge may offer novel therapeutic approaches to target stem-like $TCF1^+CD8^+$ T cells in cancers and chronic infections. Such approaches may involve CAR T cell therapy and ADCs, contributing to the enhancement of existing treatment modalities.

# References


1. Murphy, K. & Weaver, C. *Janeway Immunologie*. *Janeway Immunologie* (Springer Berlin Heidelberg, 2018). doi:10.1007/978-3-662-56004-4.
2. Şenel, S. An overview of physical, microbiological and immune barriers of oral mucosa. *International Journal of Molecular Sciences* vol. 22 Preprint at https://doi.org/10.3390/ijms22157821 (2021).
3. Marshall, J. S., Warrington, R., Watson, W. & Kim, H. L. An introduction to immunology and immunopathology. *Allergy, Asthma and Clinical Immunology* vol. 14 Preprint at https://doi.org/10.1186/s13223-018-0278-1 (2018).
4. Laskowski, T. J., Biederstädt, A. & Rezvani, K. Natural killer cells in antitumour adoptive cell immunotherapy. *Nature Reviews Cancer* vol. 22 557–575 Preprint at https://doi.org/10.1038/s41568-022-00491-0 (2022).
5. Chaplin, D. D. Overview of the immune response. *Journal of Allergy and Clinical Immunology* 125, (2010).
6. Beutler, B. Not 'molecular patterns' but molecules. *Immunity* 19, 155–156 (2003).
7. Germain, R. N. t-cell development and the CD4-CD8 lineage decision. *Nature Reviews Immunology* vol. 2 309–322 Preprint at https://doi.org/10.1038/nri798 (2002).
8. Takahama, Y. Journey through the thymus: Stromal guides for T-cell development and selection. *Nature Reviews Immunology* vol. 6 127–135 Preprint at https://doi.org/10.1038/nri1781 (2006).
9. Liu, K. Dendritic Cells. in *Encyclopedia of Cell Biology* vol. 3 741–749 (Elsevier Inc., 2016).
10. Banchereau, J. *et al. IMMUNOBIOLOGY OF DENDRITIC CELLS*. *Annu. Rev. Immunol* vol. 18 www.annualreviews.org (2000).
11. Böttcher, J. P. & Reis e Sousa, C. The Role of Type 1 Conventional Dendritic Cells in Cancer Immunity. *Trends in Cancer* vol. 4 784–792 Preprint at https://doi.org/10.1016/j.trecan.2018.09.001 (2018).
12. Chen, L. & Flies, D. B. Molecular mechanisms of T cell co-stimulation and co-inhibition. *Nature Reviews Immunology* vol. 13 227–242 Preprint at https://doi.org/10.1038/nri3405 (2013).
13. Cox, M. A., Kahan, S. M. & Zajac, A. J. Anti-viral CD8 T cells and the cytokines that they love. *Virology* vol. 435 157–169 Preprint at https://doi.org/10.1016/j.virol.2012.09.012 (2013).
14. Giles, J. R., Globig, A. M., Kaech, S. M. & Wherry, E. J. CD8+ T cells in the cancer-immunity cycle. *Immunity* vol. 56 2231–2253 Preprint at https://doi.org/10.1016/j.immuni.2023.09.005 (2023).
15. Chao, R. *et al.* Nutrient Condition in the Microenvironment Determines Essential Metabolisms of CD8+ T Cells for Enhanced IFNγ Production by Metformin. *Front Immunol* 13, (2022).
16. Heintzman, D. R., Fisher, E. L. & Rathmell, J. C. Microenvironmental influences on T cell immunity in cancer and inflammation. *Cellular and Molecular Immunology* vol. 19 316–326 Preprint at https://doi.org/10.1038/s41423-021-00833-2 (2022).
17. Chang, C. H. *et al.* Metabolic Competition in the Tumor Microenvironment Is a Driver of Cancer Progression. *Cell* 162, 1229–1241 (2015).
18. Sinclair, L. V. *et al.* Control of amino-acid transport by antigen receptors coordinates the metabolic reprogramming essential for T cell differentiation. *Nat Immunol* 14, 500–508 (2013).
19. Dustin, M. L., Chakraborty, A. K. & Shaw, A. S. Understanding the structure and function of the immunological synapse. *Cold Spring Harbor perspectives in biology* vol. 2 Preprint at https://doi.org/10.1101/cshperspect.a002311 (2010).
20. Hay, Z. L. Z. & Slansky, J. E. Granzymes: The Molecular Executors of Immune-Mediated Cytotoxicity. *International Journal of Molecular Sciences* vol. 23 Preprint at https://doi.org/10.3390/ijms23031833 (2022).
21. Krensky, A. M. & Clayberger, C. Biology and clinical relevance of granulysin: REVIEW ARTICLE. *Tissue Antigens* vol. 73 193–198 Preprint at https://doi.org/10.1111/j.1399-0039.2008.01218.x (2009).

22. Mor, G., Abrahams, V. M. & Kamsteeg, M. *The Fas/Fas Ligand System and Cancer Immune Privilege and Apoptosis*. *MOLECULAR BIOTECHNOLOGY* vol. 25 (2003).

23. Hoekstra, M. E., Vijver, S. V. & Schumacher, T. N. Modulation of the tumor micro-environment by CD8+ T cell-derived cytokines. *Current Opinion in Immunology* vol. 69 65–71 Preprint at https://doi.org/10.1016/j.coi.2021.03.016 (2021).

24. Bhat, M. Y. *et al.* Comprehensive network map of interferon gamma signaling. *J Cell Commun Signal* 12, 745–751 (2018).

25. Schoenborn, J. R. & Wilson, C. B. Regulation of Interferon-γ During Innate and Adaptive Immune Responses. *Advances in Immunology* vol. 96 41–101 Preprint at https://doi.org/10.1016/S0065-2776(07)96002-2 (2007).

26. Su, Z., Dhusia, K. & Wu, Y. Understanding the functional role of membrane confinements in TNF-mediated signaling by multiscale simulations. *Commun Biol* 5, (2022).

27. Yang, S. *et al.* Differential roles of TNFα-TNFR1 and TNFα-TNFR2 in the differentiation and function of CD4 + Foxp3 + induced Treg cells in vitro and in vivo periphery in autoimmune diseases. *Cell Death Dis* 10, (2019).

28. Wajant, H. & Siegmund, D. TNFR1 and TNFR2 in the control of the life and death balance of macrophages. *Frontiers in Cell and Developmental Biology* vol. 7 Preprint at https://doi.org/10.3389/fcell.2019.00091 (2019).

29. Faustman, D. & Davis, M. TNF receptor 2 pathway: Drug target for autoimmune diseases. *Nature Reviews Drug Discovery* vol. 9 482–493 Preprint at https://doi.org/10.1038/nrd3030 (2010).

30. Perdomo-Celis, F., Taborda, N. A. & Rugeles, M. T. CD8+ T-cell response to HIV infection in the era of antiretroviral therapy. *Frontiers in Immunology* vol. 10 Preprint at https://doi.org/10.3389/fimmu.2019.01896 (2019).

31. Kalia, V. & Sarkar, S. Regulation of Effector and Memory CD8 T Cell Differentiation by IL-2—A Balancing Act. *Frontiers in Immunology* vol. 9 Preprint at https://doi.org/10.3389/fimmu.2018.02987 (2018).

32. Malek, T. R. The biology of interleukin-2. *Annual Review of Immunology* vol. 26 453–479 Preprint at https://doi.org/10.1146/annurev.immunol.26.021607.090357 (2008).

33. Jain, J., Loh, C. & Rao, A. *Transcriptional Regulation of the IL-2 Gene*. *Current Opinion in Immunology* vol. 7 (1995).

34. Tullia Lindsten, Carl H. June, Jeffrey A. Ledbetter, Gregory Stella & Craig B. Thompson. Regulation of Lymphokine Messenger RNA Stability by a Surface-Mediated T Cell Activator Pathway. *Science (1979)* 244, 339–343 (1989).

35. Gong, D. & Malek, T. R. Cytokine-Dependent Blimp-1 Expression in Activated T Cells Inhibits IL-2 Production. *The Journal of Immunology* 178, 242–252 (2007).

36. Villarino, A. V. *et al.* Helper T cell IL-2 production is limited by negative feedback and STAT-dependent cytokine signals. *Journal of Experimental Medicine* 204, 65–71 (2007).

37. Spolski, R., Li, P. & Leonard, W. J. Biology and regulation of IL-2: from molecular mechanisms to human therapy. *Nature Reviews Immunology* vol. 18 648–659 Preprint at https://doi.org/10.1038/s41577-018-0046-y (2018).

38. Stauber, D. J., Debler, E. W., Horton, P. A., Smith, K. A. & Wilson, I. A. *Crystal Structure of the IL-2 Signaling Complex: Paradigm for a Heterotrimeric Cytokine Receptor*. www.pnas.orgcgidoi10.1073pnas.0511161103 (2006).

39. Rickert, M., Wang, X., Boulanger, M. J., Goriatcheva, N. & Garcia, K. C. Structural Biology: The structure of interleukin-2 complexed with its alpha receptor. *Science (1979)* 308, 1477–1480 (2005).

40. Gaffen, S. L. Signaling domains of the interleukin 2 receptor. *Cytokine* 14, 63–77 (2001).

41. Nelson, B. H. & Willerford, D. M. Biology of the interleukin-2 receptor. *Adv Immunol* 70, 1–81 (1998).

42. Niederlova, V., Tsyklauri, O., Kovar, M. & Stepanek, O. IL-2-driven CD8+ T cell phenotypes: implications for immunotherapy. *Trends in Immunology* vol. 44 890–901 Preprint at https://doi.org/10.1016/j.it.2023.09.003 (2023).

43. Codarri Deak, L. *et al.* PD-1-cis IL-2R agonism yields better effectors from stem-like CD8+ T cells. *Nature 2022 610:7930* 610, 161–172 (2022).

44. Tichet, M. *et al.* Bispecific PD1-IL2v and anti-PD-L1 break tumor immunity resistance by enhancing stem-like tumor-reactive CD8+ T cells and reprogramming macrophages. *Immunity* 56, 162-179.e6 (2023).

45. Hashimoto, M. *et al.* PD-1 combination therapy with IL-2 modifies CD8+ T cell exhaustion program. *Nature* 610, 173–181 (2022).

46. Dunn, G. P., Old, L. J. & Schreiber, R. D. The three Es of cancer immunoediting. *Annual Review of Immunology* vol. 22 329–360 Preprint at https://doi.org/10.1146/annurev.immunol.22.012703.104803 (2004).

47. Dunn, G. P., Bruce, A. T., Ikeda, H., Old, L. J. & Schreiber, R. D. *Cancer Immunoediting: From Immuno-Surveillance to Tumor Escape*. http://www.nature.com/natureimmunology (2002).

48. Bhatia, A. & Kumar, Y. Cancer-immune equilibrium: Questions unanswered. *Cancer Microenvironment* vol. 4 209–217 Preprint at https://doi.org/10.1007/s12307-011-0065-8 (2011).

49. Lengauer, C. & Kinzler, K. W. *Genetic Instabilities in Human Cancers*. *NATURE* vol. 396 www.nature.com (1998).

50. Phipps, R. P., Stein, S. H. & Roper, R. L. *A New View of Prostaglandin E Regulation of the Immune Response*. (1991).

51. Mirlekar, B. Tumor promoting roles of IL-10, TGF-β, IL-4, and IL-35: Its implications in cancer immunotherapy. *SAGE Open Med* 10, (2022).

52. Finetti, F. *et al.* Prostaglandin E2 and cancer: Insight into tumor progression and immunity. *Biology* vol. 9 1–26 Preprint at https://doi.org/10.3390/biology9120434 (2020).

53. Thumkeo, D. *et al.* PGE2-EP2/EP4 signaling elicits immunosuppression by driving the mregDC-Treg axis in inflammatory tumor microenvironment. *Cell Rep* 39, (2022).

54. Zhang, X. *et al.* Cyclooxygenase 2 Promotes Proliferation and Invasion in Ovarian Cancer Cells via the PGE2/NF-κB Pathway. *Cell Transplant* 28, 1S-13S (2019).

55. Wang, D. & Dubois, R. N. Eicosanoids and cancer. *Nature Reviews Cancer* vol. 10 181–193 Preprint at https://doi.org/10.1038/nrc2809 (2010).

56. Hubbard, W. C. & Hopkins Medicine, J. *Profiles of Prostaglandin Biosynthesis in Normal Lung and Tumor Tissue from Lung Cancer Patients*. http://cancerres.aacrjournals.org/content/48/11/3140 (1988).

57. Hambek, M. *et al.* Inverse correlation between serum PGE2 and T classification in head and neck cancer. *Head Neck* 29, 244–248 (2007).

58. Wang, D. & DuBois, R. N. Cyclooxygenase-2: A Potential Target in Breast Cancer. *Semin Oncol* 31, 64–73 (2004).

59. Zelenay, S. *et al.* Cyclooxygenase-Dependent Tumor Growth through Evasion of Immunity. *Cell* 162, 1257–1270 (2015).

60. Böttcher, J. P. *et al.* NK Cells Stimulate Recruitment of cDC1 into the Tumor Microenvironment Promoting Cancer Immune Control. *Cell* 172, 1022-1037.e14 (2018).

61. Meiser, P. *et al.* A distinct stimulatory cDC1 subpopulation amplifies CD8+ T cell responses in tumors for protective anti-cancer immunity. *Cancer Cell* 41, 1498-1515.e10 (2023).

62. Bayerl, F. *et al.* Tumor-derived prostaglandin E2 programs cDC1 dysfunction to impair intratumoral orchestration of anti-cancer T cell responses. *Immunity* 56, 1341-1358.e11 (2023).

63. DuBois, R. N. *et al.* Cyclooxygenase in biology and disease. *The FASEB Journal* 12, 1063–1073 (1998).

64. Park, J. Y., Pillinger, M. H. & Abramson, S. B. Prostaglandin E2 synthesis and secretion: The role of PGE2 synthases. *Clinical Immunology* 119, 229–240 (2006).

65. Wang, D. & Dubois, R. N. Eicosanoids and cancer. *Nature Reviews Cancer* vol. 10 181–193 Preprint at https://doi.org/10.1038/nrc2809 (2010).

66. Dannenberg, A. J. & Subbaramaiah, K. Targeting cyclooxygenase-2 in human neoplasia: Rationale and promise. *Cancer Cell* 4, 431–436 (2003).

67. O'Callaghan, G. & Houston, A. Prostaglandin E2 and the EP receptors in malignancy: Possible therapeutic targets? *British Journal of Pharmacology* vol. 172 5239–5250 Preprint at https://doi.org/10.1111/bph.13331 (2015).

68. Narumiya, S., Sugimoto, Y. & Ushikubi, F. *Prostanoid Receptors: Structures, Properties, and Functions*. (1999).

69. Sugimoto, Y. & Narumiya, S. Prostaglandin E receptors. *Journal of Biological Chemistry* vol. 282 11613–11617 Preprint at https://doi.org/10.1074/jbc.R600038200 (2007).

70. Fujino, H., West, K. A. & Regan, J. W. Phosphorylation of glycogen synthase kinase-3 and stimulation of T-cell factor signaling following activation of EP2 and EP4 prostanoid receptors by prostaglandin E2. *Journal of Biological Chemistry* 277, 2614–2619 (2002).

71. Woodward, D. F., Jones, R. L. & Narumiya, S. International union of basic and clinical pharmacology. LXXXIII: Classification of prostanoid receptors, updating 15 years of progress. *Pharmacol Rev* 63, 471–538 (2011).

72. Namba, T. *et al.* Alternative splicing of C-terminal tail of prostaglandin E receptor subtype EP3 determines G-protein specificity. *Nature* 365, 166–170 (1993).

73. An, Y., Yao, J. & Niu, X. The Signaling Pathway of PGE2and Its Regulatory Role in T Cell Differentiation. *Mediators of Inflammation* vol. 2021 Preprint at https://doi.org/10.1155/2021/9087816 (2021).

74. Condamine, T. & Gabrilovich, D. I. Molecular mechanisms regulating myeloid-derived suppressor cell differentiation and function. *Trends in Immunology* vol. 32 19–25 Preprint at https://doi.org/10.1016/j.it.2010.10.002 (2011).

75. Porta, C. *et al.* Tumor-derived prostaglandin E2 promotes p50 NF-kB-dependent differentiation of monocytic MDSCs. *Cancer Res* 80, 2874–2888 (2020).

76. Travelli, C. *et al.* Nicotinamide phosphoribosyltransferase acts as a metabolic gate for mobilization of myeloid-derived suppressor cells. *Cancer Res* 79, 1938–1951 (2019).

77. Sinha, P., Clements, V. K., Fulton, A. M. & Ostrand-Rosenberg, S. Prostaglandin E2 promotes tumor progression by inducing myeloid-derived suppressor cells. *Cancer Res* 67, 4507–4513 (2007).

78. Yu, S. *et al. Tumor Exosomes Inhibit Differentiation of Bone Marrow Dendritic Cells 1 The Journal of Immunology*. www.jimmunol.org (2007).

79. Xiang, X. *et al.* Induction of myeloid-derived suppressor cells by tumor exosomes. *Int J Cancer* 124, 2621–2633 (2009).

80. Obermajer, N., Muthuswamy, R., Lesnock, J., Edwards, R. P. & Kalinski, P. Positive feedback between PGE2 and COX2 redirects the differentiation of human dendritic cells toward stable myeloid-derived suppressor cells. *Blood* 118, 5498–5505 (2011).

81. Mizuno, R., Kawada, K. & Sakai, Y. Prostaglandin E2/EP signaling in the tumor microenvironment of colorectal cancer. *International Journal of Molecular Sciences* vol. 20 Preprint at https://doi.org/10.3390/ijms20246254 (2019).

82. Zhou, J. *et al.* Tumor-Associated Macrophages: Recent Insights and Therapies. *Frontiers in Oncology* vol. 10 Preprint at https://doi.org/10.3389/fonc.2020.00188 (2020).

83. Sato, T. *et al.* Interleukin 10 in the tumor microenvironment: A target for anticancer immunotherapy. *Immunol Res* 51, 170–182 (2011).

84. Spranger, S., Bao, R. & Gajewski, T. F. Melanoma-intrinsic β-catenin signalling prevents anti-tumour immunity. *Nature* 523, 231–235 (2015).

85. Willingham, S. B. *et al.* The CD47-signal regulatory protein alpha (SIRPa) interaction is a therapeutic target for human solid tumors. *Proc Natl Acad Sci U S A* 109, 6662–6667 (2012).

86. Ruffell, B. *et al.* Macrophage IL-10 Blocks CD8+ T Cell-Dependent Responses to Chemotherapy by Suppressing IL-12 Expression in Intratumoral Dendritic Cells. *Cancer Cell* 26, 623–637 (2014).

87. Wculek, S. K. *et al.* Dendritic cells in cancer immunology and immunotherapy. *Nature Reviews Immunology* vol. 20 7–24 Preprint at https://doi.org/10.1038/s41577-019-0210-z (2020).

88. Holt, D., Ma, X., Kundu, N. & Fulton, A. Prostaglandin E 2 (PGE 2) suppresses natural killer cell function primarily through the PGE 2 receptor EP4. *Cancer Immunology, Immunotherapy* 60, 1577–1586 (2011).

89. Frumento, G. *et al.* Tryptophan-derived catabolites are responsible for inhibition of T and natural killer cell proliferation induced by indoleamine 2,3-dioxygenase. *Journal of Experimental Medicine* 196, 459–468 (2002).

90. Klöss, S. *et al.* Cetuximab reconstitutes pro-inflammatory cytokine secretions and tumor-infiltrating capabilities of sMICA-inhibited NK cells in HNSCC tumor spheroids. *Front Immunol* 6, (2015).

91. Hilkens, C. M., Snijders, A., Snijdewint, F. G., Wierenga, E. A. & Kapsenberg, M. L. Modulation of T-cell cytokine secretion by accessory cell-derived products. *Eur Respir J Suppl* 22, 90s–94s (1996).

92. Harris, S. G., Padilla, J., Koumas, L., Ray, D. & Phipps, R. P. *Prostaglandins as Modulators Of. TRENDS in Immunology* vol. 23 http://immunology.trends.com1471-4906/02/$-seefrontmatter (2002).

93. Bryn, T. *et al.* LPS-activated monocytes suppress T-cell immune responses and induce FOXP3+ T cells through a COX-2-PGE2-dependent mechanism. *Int Immunol* 20, 235–245 (2008).

94. Khan, M. M., Tran, A.-C. & Keaney, K. M. *Forskolin and Prostaglandin E2 Regulate the Generation of Human Cytolytic T Lymphocytes*. (1990).

95. Vercammen, C. & Ceuppens', J. L. *Prostaglandin E2 Inhibits Human T-Cell Proliferation after Crosslinking of the CD3-Ti Complex by Directly Affecting T Cells at an Early Step of the Activation Process'. CELLULARIMMUNOIDGY* vol. 104 (1987).

96. Rahmouni, S. *et al. Cyclo-Oxygenase Type 2-Dependent Prostaglandin E 2 Secretion Is Involved in Retrovirus-Induced T-Cell Dysfunction in Mice. Biochem. J* vol. 384 (2004).

97. Kim, S. H. *et al.* The COX2 effector microsomal PGE2 synthase 1 is a regulator of immunosuppression in cutaneous melanoma. *Clinical Cancer Research* 25, 1650–1663 (2019).

98. Wang, Q., Morris, R. J., Bode, A. M. & Zhang, T. Prostaglandin Pathways: Opportunities for Cancer Prevention and Therapy. *Cancer Research* vol. 82 949–965 Preprint at https://doi.org/10.1158/0008-5472.CAN-21-2297 (2022).

99. Kaech, S. M. *et al.* Selective expression of the interleukin 7 receptor identifies effector CD8 T cells that give rise to long-lived memory cells. *Nat Immunol* 4, 1191–1198 (2003).

100. Joshi, N. S. *et al. Inflammation Directs Memory Precursor and Short-Lived Effector CD8(+) T Cell Fates via the Graded Expression of T-Bet Transcription Factor*.

101. Jameson, S. C. & Masopust, D. Understanding Subset Diversity in T Cell Memory. *Immunity* vol. 48 214–226 Preprint at https://doi.org/10.1016/j.immuni.2018.02.010 (2018).

102. Schietinger, A. *et al.* Tumor-Specific T Cell Dysfunction Is a Dynamic Antigen-Driven Differentiation Program Initiated Early during Tumorigenesis. *Immunity* 45, 389–401 (2016).

103. Khan, O. *et al.* TOX transcriptionally and epigenetically programs CD8+ T cell exhaustion. *Nature* 571, 211–218 (2019).

104. Mclane, L. M., Abdel-Hakeem, M. S. & Wherry, E. J. CD8 T Cell Exhaustion During Chronic Viral Infection and Cancer. (2019) doi:10.1146/annurev-immunol-041015.

105. Wherry, E. J. *et al.* Molecular Signature of CD8+ T Cell Exhaustion during Chronic Viral Infection. *Immunity* 27, 670–684 (2007).

106. Speiser, D. E. *et al. T Cell Differentiation in Chronic Infection and Cancer: Functional Adaptation or Exhaustion?* www.nature.com/reviews/immunol (2014).

107. Sade-Feldman, M. *et al.* Defining T Cell States Associated with Response to Checkpoint Immunotherapy in Melanoma. *Cell* 175, 998-1013.e20 (2018).

108. Beltra, J. C. *et al.* Developmental Relationships of Four Exhausted CD8+ T Cell Subsets Reveals Underlying Transcriptional and Epigenetic Landscape Control Mechanisms. *Immunity* 52, 825-841.e8 (2020).

109. Hudson, W. H. *et al.* Proliferating Transitory T Cells with an Effector-like Transcriptional Signature Emerge from PD-1+ Stem-like CD8+ T Cells during Chronic Infection. *Immunity* 51, 1043-1058.e4 (2019).

110. Rahim, M. K. *et al.* Dynamic CD8+ T cell responses to cancer immunotherapy in human regional lymph nodes are disrupted in metastatic lymph nodes. *Cell* 186, 1127-1143.e18 (2023).

111. Magen, A. *et al.* Intratumoral dendritic cell-CD4+ T helper cell niches enable CD8+ T cell differentiation following PD-1 blockade in hepatocellular carcinoma. *Nat Med* 29, 1389–1399 (2023).

112. Zander, R. *et al.* CD4+ T Cell Help Is Required for the Formation of a Cytolytic CD8+ T Cell Subset that Protects against Chronic Infection and Cancer. *Immunity* 51, 1028-1042.e4 (2019).

113. Zehn, D., Thimme, R., Lugli, E., de Almeida, G. P. & Oxenius, A. 'Stem-like' precursors are the fount to sustain persistent CD8+ T cell responses. *Nature Immunology* vol. 23 836–847 Preprint at https://doi.org/10.1038/s41590-022-01219-w (2022).

114. Quezada, L. K. *et al.* Early transcriptional and epigenetic divergence of CD8+ T cells responding to acute versus chronic infection. *PLoS Biol* 21, (2023).

115. Giles, J. R. *et al.* Shared and distinct biological circuits in effector, memory and exhausted CD8+ T cells revealed by temporal single-cell transcriptomics and epigenetics. *Nat Immunol* 23, 1600–1613 (2022).

116. Daniel, B. *et al.* Divergent clonal differentiation trajectories of T cell exhaustion. *Nat Immunol* 23, 1614–1627 (2022).

117. Kasmani, M. Y. *et al.* Clonal lineage tracing reveals mechanisms skewing CD8+ T cell fate decisions in chronic infection. *Journal of Experimental Medicine* 220, (2023).

118. Utzschneider, D. T. *et al.* T Cell Factor 1-Expressing Memory-like CD8+ T Cells Sustain the Immune Response to Chronic Viral Infections. *Immunity* 45, 415–427 (2016).

119. He, R. *et al.* Follicular CXCR5-expressing CD8+ T cells curtail chronic viral infection. *Nature* 537, 412–416 (2016).

120. Im, S. J. *et al.* Defining CD8+ T cells that provide the proliferative burst after PD-1 therapy. *Nature* 537, 417–421 (2016).

121. Jansen, C. S. *et al.* An intra-tumoral niche maintains and differentiates stem-like CD8 T cells. *Nature* 576, 465–470 (2019).

122. Siddiqui, I. *et al.* Intratumoral Tcf1 + PD-1 + CD8 + T Cells with Stem-like Properties Promote Tumor Control in Response to Vaccination and Checkpoint Blockade Immunotherapy. *Immunity* 50, 195-211.e10 (2019).

123. Eberhardt, C. S. *et al.* Functional HPV-specific PD-1+ stem-like CD8 T cells in head and neck cancer. *Nature* 597, 279 (2021).

124. Miller, B. C. *et al.* Subsets of exhausted CD8+ T cells differentially mediate tumor control and respond to checkpoint blockade. *Nat Immunol* 20, 326–336 (2019).

125. Im, S. J. & Ha, S. J. Re-defining T-Cell Exhaustion: Subset, Function, and Regulation. *Immune Netw* 20, (2020).

126. Chen, Y. *et al.* BATF regulates progenitor to cytolytic effector CD8+ T cell transition during chronic viral infection. *Nat Immunol* 22, 996 (2021).

127. Im, S. J. *et al.* Characteristics and anatomic location of PD-1+TCF1+ stem-like CD8 T cells in chronic viral infection and cancer. *Proc Natl Acad Sci U S A* 120, (2023).

128. Im, J., Konieczny, B. T., Hudson, W. H., Masopust, D. & Ahmed, R. PD-1+ stemlike CD8 T cells are resident in lymphoid tissues during persistent LCMV infection. 117, 4292–4299 (2020).

129. Alfei, F. *et al.* TOX reinforces the phenotype and longevity of exhausted T cells in chronic viral infection. *Nature* 571, 265–269 (2019).

130. Scott, A. C. *et al.* TOX is a critical regulator of tumour-specific T cell differentiation. *Nature* 571, 270–274 (2019).

131. Utzschneider, D. T. *et al.* T cells maintain an exhausted phenotype after antigen withdrawal and population reexpansion. *Nat Immunol* 14, 603–610 (2013).

132. Pauken, K. E. *et al.* Epigenetic stability of exhausted T cells limits durability of reinvigoration by PD-1 blockade. *Science (1979)* 354, 1160–1165 (2016).

133. Rosenberg, S. A. IL-2: The First Effective Immunotherapy for Human Cancer. *J Immunol* 192, 5451 (2014).

134. Hernandez, R., Põder, J., LaPorte, K. M. & Malek, T. R. Engineering IL-2 for immunotherapy of autoimmunity and cancer. *Nat Rev Immunol* 22, 614–628 (2022).

135. Niederlova, V., Tsyklauri, O., Kovar, M. & Stepanek, O. IL-2-driven CD8+ T cell phenotypes: implications for immunotherapy. *Trends Immunol* 44, 890–901 (2023).

136. Raeber, M. E., Sahin, D., Karakus, U. & Boyman, O. A systematic review of interleukin-2-based immunotherapies in clinical trials for cancer and autoimmune diseases. *EBioMedicine* 90, (2023).

137. Saadoun, D. *et al.* Regulatory T-cell responses to low-dose interleukin-2 in HCV-induced vasculitis. *N Engl J Med* 365, 2067–2077 (2011).

138. Klatzmann, D. & Abbas, A. K. The promise of low-dose interleukin-2 therapy for autoimmune and inflammatory diseases. *Nat Rev Immunol* 15, 283–294 (2015).

139. Donohue, J., (Baltimore, S. R.-J. of immunology & 1983, undefined. The fate of interleukin-2 after in vivo administration. *journals.aai.orgJH Donohue, SA RosenbergJournal of immunology (Baltimore, Md.: 1950), 1983•journals.aai.org* (2010) doi:10.4049/jimmunol.130.5.2203.

140. Maeda, M. *et al.* IL-2/IL-2 Receptor Pathway Plays a Crucial Role in the Growth and Malignant Transformation of HTLV-1-Infected T Cells to Develop Adult T-Cell Leukemia. *Front Microbiol* 11, (2020).

141. Atkins, M. B. *et al.* High-dose recombinant interleukin 2 therapy for patients with metastatic melanoma: analysis of 270 patients treated between 1985 and 1993. *J Clin Oncol* 17, 2105–2116 (1999).

142. Yu, H., Lee, H., Herrmann, A., Buettner, R. & Jove, R. Revisiting STAT3 signalling in cancer: new and unexpected biological functions. *Nat Rev Cancer* 14, 736–746 (2014).

143. Carmenate, T. *et al.* Human IL-2 mutein with higher antitumor efficacy than wild type IL-2. *J Immunol* 190, 6230–6238 (2013).

144. Chen, X. *et al.* A novel human IL-2 mutein with minimal systemic toxicity exerts greater antitumor efficacy than wild-type IL-2. *Cell Death Dis* 9, (2018).

145. Klein, C. *et al.* Cergutuzumab amunaleukin (CEA-IL2v), a CEA-targeted IL-2 variant-based immunocytokine for combination cancer immunotherapy: Overcoming limitations of aldesleukin and conventional IL-2-based immunocytokines. *Oncoimmunology* 6, (2017).

146. Silva, D. A. *et al.* De novo design of potent and selective mimics of IL-2 and IL-15. *Nature* 565, 186–191 (2019).

147. Piper, M. *et al.* Simultaneous targeting of PD-1 and IL-2Rβγ with radiation therapy inhibits pancreatic cancer growth and metastasis. *Cancer Cell* 41, 950-969.e6 (2023).

148. Ren, Z. *et al.* Selective delivery of low-affinity IL-2 to PD-1+ T cells rejuvenates antitumor immunity with reduced toxicity. *J Clin Invest* 132, (2022).

149. Tichet, M. *et al.* Bispecific PD1-IL2v and anti-PD-L1 break tumor immunity resistance by enhancing stem-like tumor-reactive CD8+ T cells and reprogramming macrophages. *Immunity* 56, 162-179.e6 (2023).

150. Burge, C., Vanguru, V. & Ho, P. J. Chimeric Antigen Receptor T-Cell Therapy. *Aust Prescr* 46, 36–39 (2022).

151. Maalej, K. M. *et al.* CAR-cell therapy in the era of solid tumor treatment: current challenges and emerging therapeutic advances. *Molecular Cancer 2023 22:1* 22, 1–54 (2023).

152. Abramson, J. S. *et al.* Lisocabtagene maraleucel for patients with relapsed or refractory large B-cell lymphomas (TRANSCEND NHL 001): a multicentre seamless design study. *The Lancet* 396, 839–852 (2020).

153. O'Leary, M. C. *et al.* FDA Approval summary: Tisagenlecleucel for treatment of patients with relapsed or refractory b-cell precursor acute lymphoblastic leukemia. *Clinical Cancer Research* 25, 1142–1146 (2019).

154. Mishra, A. K. *et al.* CAR-T-Cell Therapy in Multiple Myeloma: B-Cell Maturation Antigen (BCMA) and Beyond. *Vaccines (Basel)* 11, 1721 (2023).

155. Siddiqui, I., Erreni, M., Van Brakel, M., Debets, R. & Allavena, P. Enhanced recruitment of genetically modified CX3CR1-positive human T cells into Fractalkine/CX3CL1 expressing tumors: Importance of the chemokine gradient. *J Immunother Cancer* 4, 1–12 (2016).

156. Thadi, A. *et al.* Early Investigations and Recent Advances in Intraperitoneal Immunotherapy for Peritoneal Metastasis. *Vaccines (Basel)* 6, (2018).

157. Wei, X. *et al.* PSCA and MUC1 in non-small-cell lung cancer as targets of chimeric antigen receptor T cells. *Oncoimmunology* 6, (2017).

158. Feng, K. chao *et al.* Cocktail treatment with EGFR-specific and CD133-specific chimeric antigen receptor-modified T cells in a patient with advanced cholangiocarcinoma. *J Hematol Oncol* 10, 1–11 (2017).

159. Giavridis, T. *et al.* CAR T cell-induced cytokine release syndrome is mediated by macrophages and abated by IL-1 blockade. *Nat Med* 24, 731–738 (2018).

160. Dinarello, C. A., Simon, A. & Van Der Meer, J. W. M. Treating inflammation by blocking interleukin-1 in a broad spectrum of diseases. *Nat Rev Drug Discov* 11, 633–652 (2012).

161. Trédan, O., Galmarini, C. M., Patel, K. & Tannock, I. F. Drug resistance and the solid tumor microenvironment. *J Natl Cancer Inst* 99, 1441–1454 (2007).

162. Safarzadeh Kozani, P., Safarzadeh Kozani, P. & Rahbarizadeh, F. Addressing the obstacles of CAR T cell migration in solid tumors: wishing a heavy traffic. *Crit Rev Biotechnol* 42, 1079–1098 (2022).

163. Huang, Y. *et al.* Interleukin-armed chimeric antigen receptor-modified T cells for cancer immunotherapy. *Gene Ther* 25, 192–197 (2018).

164. Zimmermann, K. *et al.* Design and Characterization of an 'All-in-One' Lentiviral Vector System Combining Constitutive Anti-GD2 CAR Expression and Inducible Cytokines. *Cancers (Basel)* 12, (2020).

165. Fu, Z., Li, S., Han, S., Shi, C. & Zhang, Y. Antibody drug conjugate: the "biological missile" for targeted cancer therapy. *Signal Transduction and Targeted Therapy* vol. 7 Preprint at https://doi.org/10.1038/s41392-022-00947-7 (2022).

166. Mahalingaiah, P. K. *et al.* Potential mechanisms of target-independent uptake and toxicity of antibody-drug conjugates. *Pharmacol Ther* 200, 110–125 (2019).

167. Onda, M., Kobayashi, K. & Pastan, I. Depletion of regulatory T cells in tumors with an anti-CD25 immunotoxin induces CD8 T cell-mediated systemic antitumor immunity. *Proc Natl Acad Sci U S A* 116, 4575–4582 (2019).

168. Zammarchi, F. *et al.* ADCT-402, a PBD dimer-containing antibody drug conjugate targeting CD19-expressing malignancies. *Blood* 131, 1094–1105 (2018).

169. Yang, J. & Bae, H. Drug conjugates for targeting regulatory T cells in the tumor microenvironment: guided missiles for cancer treatment. *Experimental & Molecular Medicine 2023 55:9* 55, 1996–2004 (2023).

170. Lahoz, E. G., De Haro, M. A. L. & Esponda, P. Use of puromycin N-acetyltransferase (PAC) as a new reporter gene in transgenic animals. *Nucleic Acids Res* 19, 3465 (1991).

171. Wübbenhorst, D. *et al.* Tetracycline-regulated bone morphogenetic protein 2 gene expression in lentivirally transduced primary rabbit chondrocytes for treatment of cartilage defects. *Arthritis Rheum* 62, 2037–2046 (2010).

172. Di Pilato, M. *et al.* Targeting the CBM complex causes Treg cells to prime tumours for immune checkpoint therapy. *Nature 2019 570:7759* 570, 112–116 (2019).

173. Di Pilato, M. *et al.* CXCR6 positions cytotoxic T cells to receive critical survival signals in the tumor microenvironment. *Cell* 184, 4512-4530.e22 (2021).

174. Oh, S. A., Seki, A. & Rutz, S. Ribonucleoprotein Transfection for CRISPR/Cas9-Mediated Gene Knockout in Primary T Cells. *Curr Protoc Immunol* 124, (2019).

175. Kaech, S. M., Hemby, S., Kersh, E. & Ahmed, R. Molecular and functional profiling of memory CD8 T cell differentiation. *Cell* 111, 837–851 (2002).

176. Hao, Y. *et al.* Integrated analysis of multimodal single-cell data. *Cell* 184, 3573-3587.e29 (2021).

177. Ramírez, F. *et al.* deepTools2: a next generation web server for deep-sequencing data analysis. *Nucleic Acids Res* 44, W160–W165 (2016).

178. Ou, J. & Zhu, L. J. trackViewer: a Bioconductor package for interactive and integrative visualization of multi-omics data. *Nature Methods* vol. 16 453–454 Preprint at https://doi.org/10.1038/s41592-019-0430-y (2019).

179. Danecek, P. *et al.* Twelve years of SAMtools and BCFtools. *Gigascience* 10, (2021).

180. Gatto, F., Schulze, A. & Nielsen, J. Systematic Analysis Reveals that Cancer Mutations Converge on Deregulated Metabolism of Arachidonate and Xenobiotics. *Cell Rep* 16, 878–895 (2016).

181. Kalinski, P. Regulation of Immune Responses by Prostaglandin E2. *The Journal of Immunology* 188, 21–28 (2012).

182. Mosenden, R. *et al.* Mice with Disrupted Type I Protein Kinase A Anchoring in T Cells Resist Retrovirus-Induced Immunodeficiency. *The Journal of Immunology* 186, 5119–5130 (2011).

183. Lone, A. M. & Taskén, K. Phosphoproteomics-based characterization of prostaglandin E2 signaling in T cells. *Mol Pharmacol* 99, 370–382 (2021).

184. Chen, J. H. *et al.* Prostaglandin E2 and programmed cell death 1 signaling coordinately impair CTL function and survival during chronic viral infection. *Nat Med* 21, 327–334 (2015).

185. Roberts, E. W. *et al.* Critical Role for CD103+/CD141+ Dendritic Cells Bearing CCR7 for Tumor Antigen Trafficking and Priming of T Cell Immunity in Melanoma. *Cancer Cell* 30, 324–336 (2016).

186. Liu, B. *et al.* Temporal single-cell tracing reveals clonal revival and expansion of precursor exhausted T cells during anti-PD-1 therapy in lung cancer. *Nat Cancer* 3, 108–121 (2022).

187. Kurtulus, S. *et al.* Checkpoint Blockade Immunotherapy Induces Dynamic Changes in PD-1 – CD8 + Tumor-Infiltrating T Cells. *Immunity* 50, 181-194.e6 (2019).

188. Prokhnevska, N. *et al.* CD8+ T cell activation in cancer comprises an initial activation phase in lymph nodes followed by effector differentiation within the tumor. *Immunity* 56, 107-124.e5 (2023).

189. Mandala, S. *et al.* Alteration of lymphocyte trafficking by sphingosine-1-phosphate receptor agonists. *Science* 296, 346–349 (2002).

190. Chen, D. S. & Mellman, I. Oncology meets immunology: The cancer-immunity cycle. *Immunity* vol. 39 1–10 Preprint at https://doi.org/10.1016/j.immuni.2013.07.012 (2013).

191. Miron, M. *et al.* Human Lymph Nodes Maintain TCF-1hi Memory T Cells with High Functional Potential and Clonal Diversity throughout Life. *The Journal of Immunology* 201, 2132–2140 (2018).

192. CD44 activation and associated primary adhesion is inducible via T cell receptor stimulation - PubMed. https://pubmed.ncbi.nlm.nih.gov/9300670/.

193. Duong, E. *et al.* Type I interferon activates MHC class I-dressed CD11b+ conventional dendritic cells to promote protective anti-tumor CD8+ T cell immunity. *Immunity* 55, 308-323.e9 (2022).

194. Asano, K. *et al.* CD169-positive macrophages dominate antitumor immunity by crosspresenting dead cell-associated antigens. *Immunity* 34, 85–95 (2011).

195. Tay, R. E., Richardson, E. K. & Toh, H. C. Revisiting the role of CD4+ T cells in cancer immunotherapy—new insights into old paradigms. *Cancer Gene Therapy* vol. 28 5–17 Preprint at https://doi.org/10.1038/s41417-020-0183-x (2021).

196. Hor, J. L. *et al.* Spatiotemporally Distinct Interactions with Dendritic Cell Subsets Facilitates CD4+ and CD8+ T Cell Activation to Localized Viral Infection. *Immunity* 43, 554–565 (2015).

197. Li, X. *et al.* Prostaglandin E2 facilitates Hepatitis B virus replication by impairing CTL function. *Mol Immunol* 103, 243–250 (2018).

198. Welten, S. P. M. *et al.* Tcf1+ cells are required to maintain the inflationary T cell pool upon MCMV infection. *Nature Communications 2020 11:1* 11, 1–14 (2020).

199. Chen, L. *et al.* Stem cell-like T cell depletion in the recurrent head and neck cancer immune microenvironment. *Oncoimmunology* 12, (2023).

200. Sreeramkumar, V., Fresno, M. & Cuesta, N. Prostaglandin E2 and T cells: friends or foes? *Immunol Cell Biol* 90, 579–586 (2012).

201. Zhang, Y. & Daaka, Y. PGE2 promotes angiogenesis through EP4 and PKA Cγ pathway. *Blood* 118, 5355 (2011).

202. Rincón, M. *et al.* Prostaglandin E2 and the increase of intracellular cAMP inhibit the expression of interleukin 2 receptors in human T cells. *Eur J Immunol* 18, 1791–1796 (1988).

203. Maca, R. D. *The Effects of Prostaglandins on the Proliferation of Cultured Human T Lymphocytes*.

204. Corria-Osorio, J. *et al.* Orthogonal cytokine engineering enables novel synthetic effector states escaping canonical exhaustion in tumor-rejecting CD8+ T cells. *Nat Immunol* 24, 869–883 (2023).

205. Rubinstein, M. P. *et al.* IL-7 and IL-15 differentially regulate CD8+ T-cell subsets durina contraction of the immune response. *Blood* 112, 3704–3712 (2008).

206. Hirakawa, M. *et al.* IL-2, IL-7, IL-15 and IL-6 Induce Differential Activation of Naive and Memory T Cell Subsets. *Blood* 126, 3425–3425 (2015).

207. Sheikh, A. *et al.* Selective dependence on IL-7 for antigen-specific CD8 T cell responses during airway influenza infection. *Sci Rep* 12, (2022).

208. Zhang, S., Zhao, J., Bai, X., Handley, M. & Shan, F. Biological effects of IL-15 on immune cells and its potential for the treatment of cancer. *International Immunopharmacology* vol. 91 Preprint at https://doi.org/10.1016/j.intimp.2020.107318 (2021).

209. Guzman, G., Reed, M. R., Bielamowicz, K., Koss, B. & Rodriguez, A. CAR-T Therapies in Solid Tumors: Opportunities and Challenges. *Current Oncology Reports* vol. 25 479–489 Preprint at https://doi.org/10.1007/s11912-023-01380-x (2023).

210. Maalej, K. M. *et al.* CAR-cell therapy in the era of solid tumor treatment: current challenges and emerging therapeutic advances. *Molecular Cancer* vol. 22 Preprint at https://doi.org/10.1186/s12943-023-01723-z (2023).

211. Sabatino, M. *et al.* Generation of clinical-grade CD19-specific CAR-modified CD8+ memory stem cells for the treatment of human B-cell malignancies. *Blood* 128, 519 (2016).

212. Sluter, M. N. *et al.* EP2 Antagonists (2011-2021): A Decade's Journey from Discovery to Therapeutics. *Journal of Medicinal Chemistry* vol. 64 11816–11836 Preprint at https://doi.org/10.1021/acs.jmedchem.1c00816 (2021).

213. Jin, Y. *et al.* LY3127760, a Selective Prostaglandin E4 (EP4) Receptor Antagonist, and Celecoxib: A Comparison of Pharmacological Profiles. *Clin Transl Sci* 11, 46–53 (2018).

214. Wen, B., Wei, Y. T., Mu, L. L., Wen, G. R. & Zhao, K. The molecular mechanisms of celecoxib in tumor development. *Medicine (United States)* vol. 99 Preprint at https://doi.org/10.1097/MD.0000000000022544 (2020).

215. Fraser, D. M., Sullivan, F. M., Thompson, A. M. & McCowan, C. Aspirin use and survival after the diagnosis of breast cancer: a population-based cohort study. *Br J Cancer* 111, 623–627 (2014).

216. Tomić, T., Domínguez-López, S. & Barrios-Rodríguez, R. Non-aspirin non-steroidal anti-inflammatory drugs in prevention of colorectal cancer in people aged 40 or older: A systematic review and meta-analysis. *Cancer Epidemiol* 58, 52–62 (2019).

217. Connolly, K. A. *et al.* A reservoir of stem-like CD8+ T cells in the tumor-draining lymph node preserves the ongoing antitumor immune response. *Sci Immunol* 6, (2021).

218. Sipos, G. & Kuchler, K. Fungal ATP-Binding Cassette (ABC) Transporters in Drug Resistance & Detoxification. *Curr Drug Targets* 7, 471–481 (2006).

219. Buongervino, S. *et al.* Antibody-Drug Conjugate Efficacy in Neuroblastoma: Role of Payload, Resistance Mechanisms, Target Density, and Antibody Internalization. *Mol Cancer Ther* 20, 2228–2239 (2021).

220. Thurm, C., Schraven, B. & Kahlfuss, S. Review abc transporters in t cell-mediated physiological and pathological immune responses. *Int J Mol Sci* 22, (2021).

## Publication of this doctoral thesis

Acknowledgment: Reproduced with permission from Springer Nature

Excerpts from this work were included in the following publication:

**Sebastian B. Lacher***, Janina Dörr*, Gustavo P. de Almeida, Julian Hönninger, Felix Bayerl, Anna Hirschberger, Anna-Marie Pedde, Philippa Meiser, Lukas Ramsauer, Thomas J. Rudolph, Nadine Spranger, Matteo Morotti, Alizee J. Grimm, Sebastian Jarosch, Arman Oner, Lisa Gregor, Stefanie Lesch, Stefanos Michaelides, Luisa Fertig, Daria Briukhovetska, Lina Majed2, Sophia Stock, Dirk H. Busch, Veit R. Buchholz, Percy A. Knolle, Dietmar Zehn, Denarda Dangaj Laniti, Sebastian Kobold & Jan P. Böttcher. $PGE_2$ limits effector expansion of tumour-infiltrating stem-like $CD8^+$ T cells.

Nature 629, 417–425 (2024). https://doi.org/10.1038/s41586-024-07254-x

## Publications

Matteo Morotti*, Alizee J. Grimm*, Helen Carrasco Hope, Marion Arnaud, Mathieu Desbuisson, Nicolas Rayroux, David Barras, Maria Masid, Baptiste Murgues, Bovannak S. Chap, Marco Ongaro, Ioanna A. Rota,Catherine Ronet, Aspram Minasyan, Johanna Chiffelle, **Sebastian B. Lacher**, Sara Bobisse, Clément Murgues, Eleonora Ghisoni, Khaoula Ouchen, Ribal Bou Mjahed, Fabrizio Benedetti, Naoill Abdellaoui, Riccardo Turrini, Philippe O. Gannon, Khalil Zaman, Patrice Mathevet, Loic Lelievre, Isaac Crespo, Marcus Conrad, Gregory Verdeil, Lana E. Kandalaft, Julien Dagher, Jesus Corria-Osorio, Marie-Agnes Doucey, Ping-Chih Ho, Alexandre Harari, Nicola Vannini, Jan P. Böttcher,Denarda Dangaj Laniti & George Coukos. $PGE_2$ inhibits TIL expansion by disrupting IL-2 signalling and mitochondrial function.

Nature 629, 426–434 (2024). https://doi.org/10.1038/s41586-024-07352-w

Felix Bayerl*, Philippa Meiser, Sainitin Donakonda, Anna Hirschberger, **Sebastian B. Lacher**, Anna-Marie Pedde, Chris D. Hermann, Anais Elewaut, Moritz Knolle, Lukas Ramsauer, Thomas J. Rudolph, Simon Grassmann, Rupert Öllinger, Nicole Kirchhammer, Marcel Trefny, Martina Anton, Dirk Wohlleber, Bastian Höchst, Anne Zaremba, Achim Krüger, Roland Rad, Anna C. Obenauf, Dirk Schadendorf, Alfred Zippelius, Veit R. Buchholz,
Barbara U. Schraml, and Jan P. Böttcher. Tumor-derived prostaglandin E2 programs cDC1 dysfunction to impair intratumoral orchestration of anti-cancer T cell responses.
Immunity. 2023;56(6):1341-1358.e11. doi:10.1016/j.immuni.2023.05.011

Philippa Meiser*, Moritz A. Knolle*, Anna Hirschberger, Gustavo P. de Almeida, Felix Bayerl, **Sebastian Lacher**, Anna-Marie Pedde, Sophie Flommersfeld, Julian Hönninger, Leonhard Stark, Fabian Stögbauer, Martina Anton, Markus Wirth, Dirk Wohlleber, Katja Steiger, Veit R. Buchholz, Barbara Wollenberg, Christina E. Zielinski, Rickmer Braren, Daniel Rueckert, Percy A. Knolle, Georgios Kaissis, and Jan P. Böttcher. A distinct stimulatory cDC1 subpopulation amplifies $CD8^+$ T cell responses in tumors for protective anti-cancer immunity.
Cancer Cell. 2023;41(8):1498-1515.e10. doi:10.1016/j.ccell.2023.06.008

## List of figures

## List of tables

## List of abbreviations

| | |
|---|---|
| α | anti |
| 15-PGDH | 15-hydroxyprostaglandin dehydrogenase |
| ABC | ATP-binding cassette transporter |
| ACK | Ammonium-chloride-potassium |
| ADC | Antibody-drug conjugate |
| AICD | Activation-induced cell death |
| AIRE | Autoimmune regulator |
| APC | Antigen-presenting cell |
| BATF | Basic leucine zipper transcription factor |
| BCR | B cell receptor |
| BLIMP-1 | B lymphocyte maturation protein 1 |
| cAMP | Cyclic adenosine monophosphate |
| CAR | Chimeric antigen receptor |
| CCL | C-C motif chemokine ligand |
| CCR | C-C motif chemokine receptor |
| cDC1 | Type 1 conventional dendritic cell |
| CIN | Chromosomal instability |
| cl. | Cluster |
| conc. | Concentration |
| control | $BRAF^{V600E}$ melanoma |
| COX | Cyclooxygenase |
| CREB | cAMP-responsive element binding protein |
| cTEC | Cortical thymic epithelial cell |
| CXCL | C-X-C motif chemokine ligand |
| CXCR | C-X-C motif chemokine receptor |
| DC | Dendritic cell |
| DD | Fas-containing death domain |
| DEG | Differentially expressed gene |
| DMEM | Dulbecco´s Modified Eagle´s Medium |

| | |
|---|---|
| EDTA | Ethylenediaminetetraacetic acid |
| EDU | 5-Ethynyl-2´-deoxyuridine |
| EGFR | Epidermal growth factor receptor |
| EMT | Epithelial-mesenchymal transition |
| EP | $PGE_2$ receptor |
| ERK | Extracellular signal-regulator kinase |
| FasL | Fas ligand |
| FCS | Fetal calf serum |
| FLT3L | FMS-like tyrosine kinase 3 ligand |
| FPKMs | Transcript sequence per Million mapped reads |
| g | Gramm |
| *g* | Gravitational force equivalent |
| GEM | Gel bead-in-emulsion |
| GEO | Gene Expression Omnibus |
| GPCR | G-protein coupled receptor |
| GSEA | Gene set enrichment analysis |
| GzmB | Granzyme B |
| HPRT | Hypoxanthine-phosphoribosyl-transferase 1 |
| i.p. | Intraperitoneal |
| i.v. | Intravenous |
| ICB | Immune checkpoint blockade |
| ICOS | Inducible T cell costimulator |
| IDO | Indoleamine 2,3-dioxygenase |
| IFNγ | Interferon gamma |
| IL | Interleukin |
| IL-2R | High-affinity IL-2 receptor |
| IL-2Rγc | Interleukin 2 receptor gamma chain, common gamma chain |
| IRES | Internal ribosome entry site |
| IRF | Interferon regulatory factor |
| JAK | Janus kinase |

| | |
|---|---|
| KNN | K-nearest neighbors |
| LAG3 | Lymphocyte-activation gene 3 |
| LCMV | Lymphocytic choriomeningitis virus |
| LN | Lymph node |
| MAPK | Mitogen-activated protein kinase |
| MDSC | Myeloid-derived suppressor cell |
| MHC | Major histocompatibility complex |
| N/A | Not available |
| ml | Milliliter |
| mRNA | messenger ribonucleic acid |
| mTEC | Medullary thymic epithelial cell |
| mTOR | Mammalian target of rapamycin |
| n | nano |
| NES | Normalized enrichment score |
| NF-κB | Nuclear factor kappa-light-chain-enhancer of activated B cells |
| NFAT | Nuclear factor of activated T cell |
| NK | Natural killer cell |
| NKT | Natural killer T cell |
| NSAID | Non-steroidal anti-inflammatory drug |
| NSCLC | Non-small cell lung cancer |
| OVA | Ovalbumin, model antigen |
| *P* | *P*-value |
| PAC | Puromycin-N-acetyltransferase |
| PBS | Phosphate-buffered saline |
| PCA | Principal component analysis |
| PD-1 | Programmed cell death protein 1 |
| $PGE_2$ | Prostaglandin E2 |
| $PGH_2$ | Prostaglandin H2 |
| PGK | Phosphoglycerate kinase |
| PI3K | Phospho-inositide 3-kinase |

| | |
|---|---|
| PKA | Protein kinase A |
| PKC | Protein kinase C |
| RPMI | Roswell Park Memorial Institute |
| RT | Room temperature |
| s.c. | Subcutaneous |
| S1P1R | Sphingosine-1-phosphate receptor 1 |
| scRNA-seq | Single-cell RNA sequencing |
| scTCR-seq | Single-cell TCR sequencing |
| SD | Standard deviation |
| SEM | Standard error of the mean |
| Shc | SH2 domain-containing transforming protein |
| SIRP$\alpha$ | Signal regulatory protein-$\alpha$ |
| SMAC | Supramolecular activation complex |
| SNN | Shared nearest neighbor |
| STAT | Signal transducer and activator of transcription |
| TACE | TNF$\alpha$-converting enzyme |
| TAM | Tumor-associated macrophage |
| TBX21 | T-box transcription factor |
| TCF1 | T cell factor 1 |
| $T_{cm}$ | Central memory T cell |
| TCR | T cell receptor |
| tdLN | Tumor-draining lymph node |
| $T_{emra}$ | Effector memory CD45RA$^+$ T cell |
| $T_{exh}$ | 'Exhausted-like' T cell |
| $T_{exh\text{-}int}$ | Intermediate 'exhausted-like' T cell |
| $T_{exh\text{-}prog}$ | 'Exhausted-like' progenitor or stem-like TCF1$^+$CD8$^+$ T cell |
| $T_{exh\text{-}term}$ | Terminal 'exhausted-like' T cell |
| TF | Transcription factor |
| TGF-β | Transforming growth factor beta |
| $T_h$ | T helper, CD4$^+$ helper T cell |

| | |
|---|---|
| TIGIT | T cell immunoreceptor with immunoglobulin and ITIM domain |
| TIM-3 | T cell immunoglobulin and mucin domain-containing protein 3 |
| TME | Tumor microenvironment |
| $T_{mem}$ | Memory T cell |
| $T_{mp}$ | Memory precursor T cell |
| TNF$\alpha$ | Tumor necrosis factor-$\alpha$ |
| TNFR1 | TNF receptor 1 |
| TOX | Thymocyte selection-associated high-mobility group box protein |
| $T_{reg}$ | Regulatory $CD4^+$ T cell |
| $T_{scm}$ | Stem cell memory T cell |
| U | Units |
| UMAP | Uniform manifold approximation and projection |
| UMI | Unique molecular identifier |
| VEGF | Vascular endothelial growth factor |
| VSV-G | Vesicular stomatitis virus-glycoprotein |
| WT | Wildtype |
| XCL1 | X-C motif chemokine ligand 1 |